

広島大学学位請求論文

**Molecular Recognition of Supramolecular
Assemblies Based on Calix[4]arenes**

カリックス[4]アレーンを基盤とした超分子集合体の特異な分子認識

2019 年

広島大学大学院理学研究科

化学専攻

山崎 祐太朗

目 次

1. 主論文

Molecular Recognition of Supramolecular Assemblies Based on Calix[4]arenes.

カリックス[4]アレーンを基盤とした超分子集合体の特異な分子認識

広島大学大学院理学研究科化学専攻 山崎 祐太郎

2. 公表論文

(1) Hexameric assembly of 5,17-di-substituted calix[4]arene in the solid state

Yutaro Yamasaki, Ryo Sekiya, and Takeharu Haino

CrystEngComm **2017**, *19*, 6744-6751.

(2) Majority-Rules Effect and Allostery in Molecular Recognition of Calix[4]arene-Based Triple-Stranded Metallohelicates

Yutaro Yamasaki, Hidemi Shio, Tomoko Amimoto, Ryo Sekiya, and Takeharu Haino

Chemistry – A European Journal **2018**, *24*, 8558-8568.

3. 参考論文

- (1) Head-to-tail polymeric columnar structure of calix[4]arene possessing catechol arms in the solid state

Ryo Sekiya, Yutaro Yamasaki, Susumu Katayama, Hidemi Shio, and Takeharu Haino

CrystEngComm **2013**, *15*, 8404-8407.

- (2) Guest induced head-to-tail columnar assembly of 5,17-difunctionalized calix[4]arene

Ryo Sekiya, Yutaro Yamasaki, Wataru Tada, Hidemi Shio, and Takeharu Haino

CrystEngComm **2014**, *16*, 6023-6032.

- (3) Induced-Fit Molecular Recognition of Alkyl Chains in *p*-*tert*-Butylcalix[5]arene in the Solid State

Yasunori Kajiki, Ryo Sekiya, Yutaro Yamasaki, Yuichiro Uemura, and Takeharu Haino

Bulletin of the Chemical Society of Japan **2016**, *89*, 220-225.

Contents

Chapter 1 General Introduction

1-1	Host-Guest Chemistry	...2
1-2	Calixarenes	
1-2-1	History of Calixarenes	...6
1-2-2	Molecular Recognition Properties of Calix[4]arene	...8
1-2-3	Supramolecular Capsules Based on Calix[4]arene and Its Derivatives	...14
1-3	Overview of the Present Thesis	...16
1-5	References	...18

Chapter 2 Molecular Recognition of Calix[4]arene Clathrate

2-1	Introduction	...22
2-2	Results and Discussion	
2-2-1	Synthesis of Calix[4]arene and Preparation of Single Crystals	...24
2-2-2	Crystal Structure of Hexameric Assembly	...26
2-2-3	Crystal Structure of (S,S)- 1 ·(Solvent) (Solvent = MeOH, 1-PrOH, CH ₃ CN)	...29
2-2-4	Crystal Structure of (S,S)- 1 ·(2-PrOH)	...31
2-2-5	Crystal Structure of Racemic Mixture	...32
2-2-6	Adsorption properties of 1 _{apo}	...34
2-3	Conclusion	...39
2-4	Experimental	...40
2-5	References	...46

Chapter 3 Calix[4]arene Helical Complexes with Multiple Binding Sites

3-1	Introduction	...48
3-2	Results and Discussion	
3-2-1	Synthesis of the Calix[4]arene Ligands	...51
3-2-2	Coordination-Driven Self-Assembly	...53
3-2-3	Guest Complexation	...63
3-2-4	Determination of Binding Constants	...65
3-2-5	Cooperativity in the Guest Binding	...69
3-2-6	Chiral Induction	...70
3-2-7	Majority-Rules Effect	...71
3-3	Conclusion	...73
3-4	Experimental	...74
3-5	References	...113
	Acknowledgements	...119

主論文

**Molecular Recognition of Supramolecular
Assemblies Based on Calix[4]arenes.**

Department of Chemistry, Graduate School of Science

Hiroshima University

January, 2019

Yutaro Yamasaki

Chapter 1

General Introduction

1-1 Host-Guest Chemistry

Host-guest chemistry is a central topic of supramolecular chemistry. J. W. Steed and J. L. Atwood introduce the terms ‘host’ and ‘guest’ in *Supramolecular Chemistry, Second Edition* stating that ”Commonly, the host is a large molecule or aggregate such as an enzyme or synthetic cyclic compound possessing a sizable, central hole or cavity, while the guest may be a monoatomic cation, a simple inorganic anion, an ion pair or a more sophisticated molecule such as a hormone, pheromone or neurotransmitter. More formally, the host is defined as the molecular entity possessing convergent binding sites, while the guest possesses divergent binding sites. In turn, a binding site is defined as a region of the host or guest capable of taking part in a noncovalent interaction.”^[1]

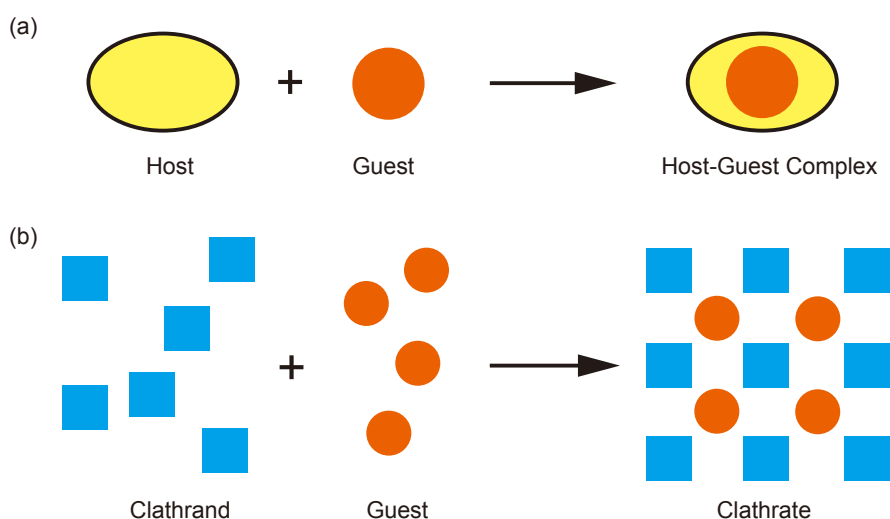


Figure 1-1-1. Schematic illustration of molecular recognition by a) a cavitand and b) a clathrand. A cavitand incorporates a guest to form a host-guest complex, while a clathrand traps a guest species in extramolecular space generated among clathrands arranged periodically, forming a clathrate.

Molecular recognition is found in a variety of fields.^[2-5] In supramolecular chemistry, a molecular host, which has a permanent intramolecular space with a volume of hundreds of cubic angstroms, can incorporate other chemical species of an appropriate shape and size to produce molecular complexes (Figure 1-1-1a). Alternatively, a molecular host that does not have an intramolecular space can trap other chemical species when an extramolecular space is created among hosts arranged periodically. In that case, guest species are trapped within the extramolecular space (Figure 1-1-1b).

The former hosts can be described as ‘*cavitands*’, and their complexes are ‘*cavities*’ or ‘*host-guest complexes*’ depending on the type of intermolecular interactions formed between a cavitand and a guest.^[6] The inner space available for guest binding is an intrinsic molecular property of cavitands and exists both in solution and in the solid-state. On the other hand, the latter hosts are defined as ‘*clathrands*’, and their molecular complexes are ‘*clathrates*’.^[7] Because the three-dimensional arrangement of clathrands is essential for the generation of the extramolecular space, clathrates are found only in the solid-state. The term ‘*clathrates*’ was originally defined by H. M. Powell of the University of Oxford in 1948 as a kind of inclusion compound in which two or more components are associated without ordinary covalent bonds, but instead through complete enclosure of one set of molecules in a suitable structure formed by another.^[1]

The importance of host-guest chemistry has been demonstrated by various applications. For example, Charles Pederson, who won the Nobel Prize for his finding of crown ethers in 1987, showed the entrapment of specific ions inside cyclic polyethers (Figure 1-1-2a).^[8] Crown ethers direct their lone pairs to the inside of the macrocycle and tightly bind ionic species of the appropriate size by multiple ion-dipole interactions. Later, this platform was applied for phase transfer catalysts,^[9] which enable the transfer of hydrophilic inorganic anions into organic solvents, accelerating chemical reactions such as oxidation.^[1] Jean-Marie Lehn^[10] and Donald Cram,^[11] who shared the Nobel Prize in Chemistry with Charles Pederson, developed cryptands and spherands, respectively (Figure 1-1-2b), both of which are important molecular hosts for ionic species. Urea is a simple molecule and lacks an intramolecular cavity. This naturally occurring species can function as a clathrand and form crystals possessing channels several angstroms in diameter. The extramolecular space in urea crystals selectively traps linear alkanes (Figure 1-1-2c).^[1] This selective molecular recognition is quite useful for the separation of linear alkanes from their branched counterparts with similar boiling points because these species are difficult to separate by conventional distillation techniques.

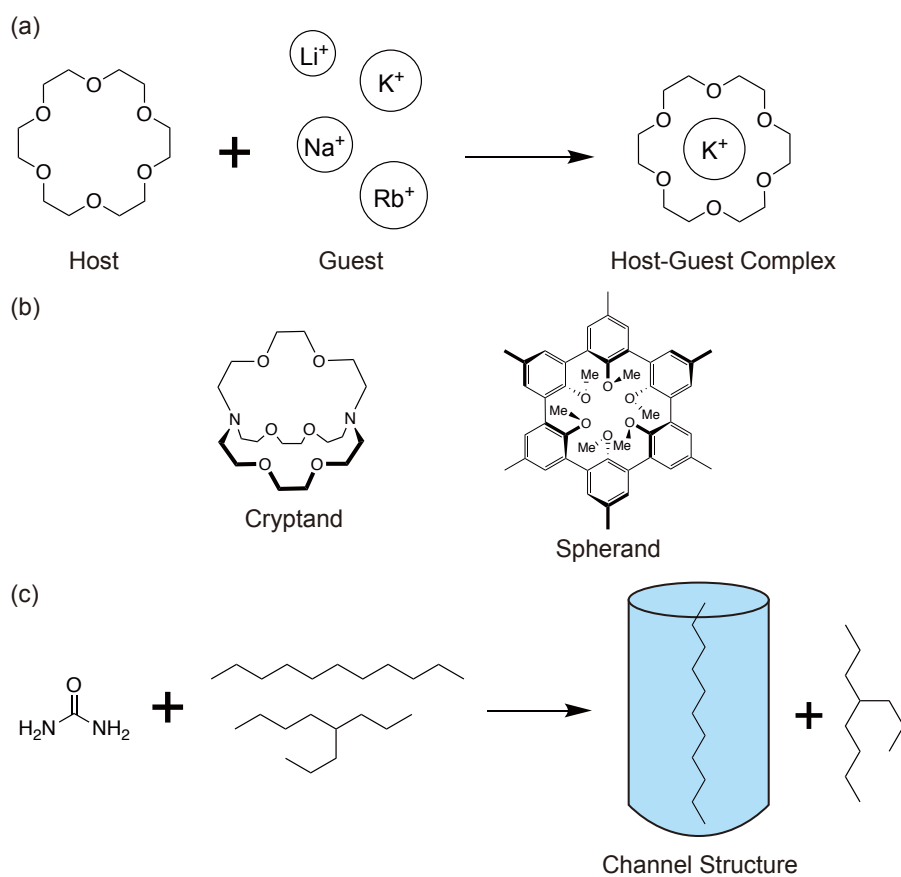


Figure 1-1-2. a) Molecular recognition by a crown ether. A cationic species of the appropriate size for the intramolecular space provided by the crown ether is selectively trapped to form a host-guest complex. b) (left) Cryptands developed by J.-M. Lehn and (right) spherands developed by D. Cram. c) Urea and the channel structure generated in urea crystals. The channel selectively incorporates linear alkyl chains. This molecular recognition is utilized for the separation of linear alkanes from their branched counterparts.

In recent years, a variety of cavitand hosts have been found or developed, such as cyclodextrins (Figure 1-1-3a), cucurbiturils (Figure 1-1-3b), calixpyrroles (Figure 1-1-3c), pillar[*n*]arenes (Figure 1-1-3d), and calix[*n*]arenes.

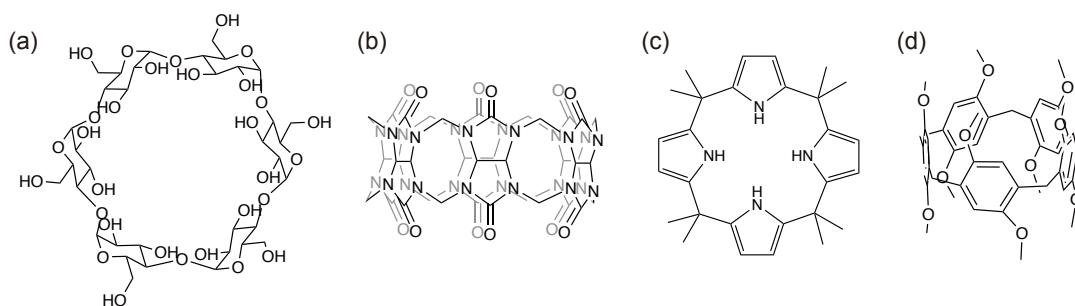


Figure 1-1-3. a) α -Cyclodextrin, b) cucurbit[6]uril, c) calix[4]pyrrole, and d) pillar[5]arene.

Cyclodextrins are cyclic oligosaccharides that possess an internal hydrophobic cavity that can bind organic cations and metal complexes.^[12] Cucurbiturils, the binding behavior of which was reported in 1981, have a cyclic array of glycoluril units linked with methylene bridges (Figure 1-1-3b).^[13] Cucurbiturils have relatively rigid structures and electronegative oxygen atoms at the termini of their inner cavity, which permits the binding of cationic guests such as alkylammonium cations via charge-dipole interactions. In contrast, calix[4]pyrrole, which is composed of four pyrrole rings, has an affinity for anionic guests due to the N–H bonds of the four pyrroles (Figure 1-1-3c),^[14] allowing the binding of anions by hydrogen bonding. Among halide anions, this macrocycle selectively binds fluoride anions. Pillararenes, which were reported by Ogoshi in 2008, are macrocycles composed of hydroquinone units.^[15] Pillararenes have attracted the attention of supramolecular scientists due to their highly symmetric structures and potential applications for interlocked species such as rotaxanes.^[16]

Our laboratory has paid considerable attention to *calixarenes*. In the following sections, I present a brief history of *calixarenes*, their molecular recognition properties, the background of my research topics, and an overview of this Ph.D. thesis.

1-2 Calixarenes

1-2-1 History of Calixarenes

Calixarenes are $[1n]$ metacyclophanes comprising cyclic arrays of n phenolic residues connected by methylene groups (Figure 1-2-1). These macrocycles possess an intramolecular cavity that varies with the number of phenolic groups. The cavity is surrounded by the aromatic rings, and therefore calix $[n]$ arenes recognize guests using their aromatic surfaces via intermolecular interactions including $\pi \cdots \pi$, cation $\cdots\pi$, and C–H $\cdots\pi$ interactions between the calix $[n]$ arenes and guests. Calix $[n]$ arene platforms have frequently been employed in the development of new host-guest systems^[17] and functional molecules such as enzyme mimics^[18] and chemo-sensors^[19] because of their ability to recognize organic molecules as well as their potential for structural modification.

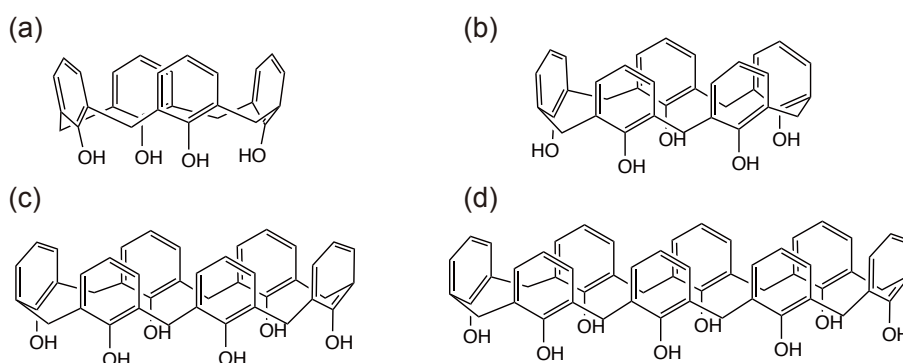


Figure 1-2-1. Molecular structures of members of the calix $[n]$ arene family. a) $n = 4$, b) $n = 5$, c) $n = 6$, and d) $n = 8$.

Calixarene chemistry can be traced back to the reaction products of phenols and formaldehyde. In 1872, Adolph von Baeyer found that a hard, resinous, amorphous product was generated by the reaction of aqueous formaldehyde with phenol in the presence of strong acids.^[20] This report set began the field of phenol-formaldehyde chemistry. In 1894, Lederer^[21] and Manasse^[22] independently reported base-induced reactions between formaldehyde and phenol. They isolated crystalline solids of *o*-hydroxymethylphenol and *p*-hydroxymethylphenol. Their reports advanced the field of phenol-formaldehyde chemistry. At that time, the chemical structure of Bayer's resinous products had not been determined due to the lack of suitable instrumental techniques, as the instruments commonly used in modern chemistry, such as NMR and IR, had not been

developed. In 1907, three decades after Baeyer's report, Leo Baekeland succeeded in making a robust and resilient resin using a small and controlled amount of base.^[23] He named the material bakelite and obtained over 400 patents based on the bakelite process (Figure 1-2-2). Although the bakelite process represents the first large-scale production of a synthetic plastic, the structure of bakelite was unknown at the time.

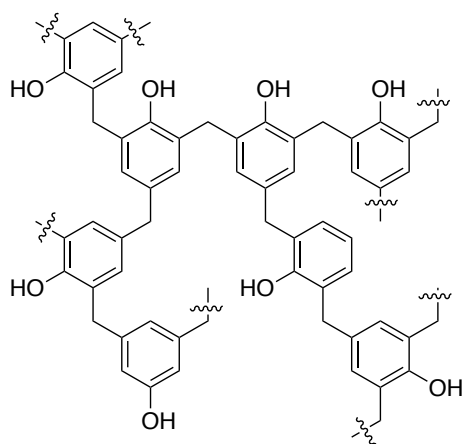


Figure 1-2-2. Schematic representation of the chemical structure of bakelite produced by the reaction of phenol with formaldehyde in the presence of an inorganic base.

In 1944, Alois Zinke condensed *p*-substituted phenols with formaldehyde to study the curing phase of the phenol-formaldehyde process.^[24] The reaction can only occur at the two ortho positions of a *p*-substituted phenol. Therefore, the reaction should give linear polymers. However, he obtained a crystalline product from the reaction. The acetate product obtained from Zinke's experiment was isolated as crystalline needles with a molecular weight of 876. The molecular weight was in good agreement with the calculated weight of the cyclic tetramers, i.e., calix[4]arene. The reports of Zinke's tetramers contributed to the beginning of calixarene chemistry.

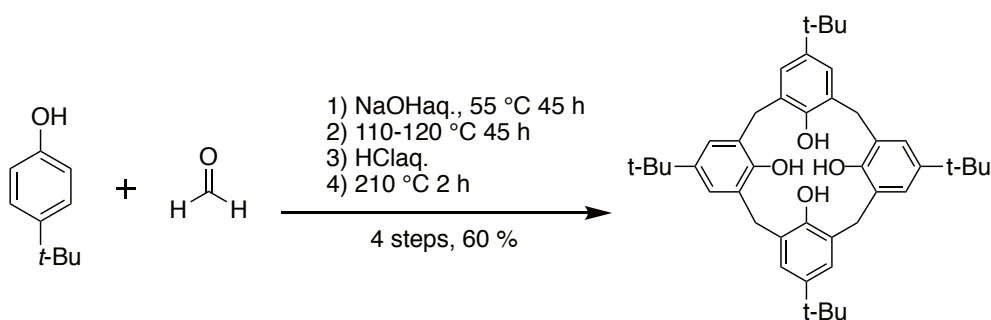


Figure 1-2-3. Modified synthesis procedure of *p-tert*-calix[4]arene. Under the given reaction conditions, *p-tert*-butylcalix[4]arene was obtained as a crystalline solid in 60 % yield.^[26]

In the early 1970s, David Gutsche took an interest in Zincke's cyclic tetramer as a potential candidate for preparing enzyme mimics. He considered that a crown ether, which was reported by Pedersen in 1967,^[8] did not have a large enough cavity to serve as an enzyme mimic, and he excluded cyclodextrins as they are more difficult than Zincke's cyclic tetramer to structurally modify. In 1978, he named the cyclic tetramer a '*calixarene*'.^[25] The name is derived from the Greek word 'calix', meaning vase or chalice. Gutsche reported a modified synthesis of this macrocyclic host using *p-tert*-butylphenol and formaldehyde (Figure 1-2-3). He succeeded in obtaining *p-tert*-butylcalix[4]arene in 60 % yield.^[26] He also reported the binding behavior of the host,^[27] and his reports became the basis of calix[*n*]arene chemistry.

1-2-2 Molecular Recognition Properties of Calix[4]arene

Among the calix[*n*]arene family, calix[4]arene has been widely employed due to its well-established synthetic procedure and conformational rigidity relative to larger calixarenes, such as calix[6]arene and calix[8]arene. Calix[4]arene has four conformations, cone, partial cone, 1,2-alternate, and 1,3-alternate (Figure 1-2-4).

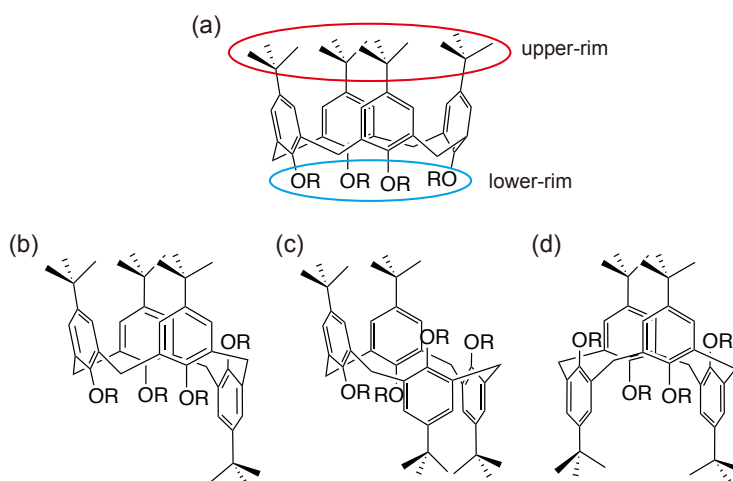


Figure 1-2-4. Four conformations of calix[4]arene; a) cone, b) partial cone, c) 1,2-alternate, and d) 1,3-alternate conformations.

Among the four conformers, the 1,3-alternate and cone conformations have been widely employed for the development of calix[4]arene-based functional molecules. The cone conformation has a wide rim and a narrow rim (Figure 1-2-4a), which are named the upper and lower rims, respectively. A variety of functional groups can be installed onto the rims; however, lower-rim functionalization is easier than upper-rim functionalization. For example, the deprotonation of calix[4]arene by an inorganic base followed by a reaction with an organic halide yields lower-rim functionalized calix[4]arenes. Indeed, lower-rim functionalized calix[4]arenes can be found in many reports.^[28-31]

In 1979, Andreotti reported the inclusion compound of *p*-*tert*-butylcalix[4]arene with toluene (Figure 1-2-5).^[32] He demonstrated that the methyl group of the toluene interacted with the surface of the cavity through C–H \cdots π interactions to form the host-guest complex with the 1:1 host-to-guest ratio. This paper demonstrated that the intramolecular cavity of calix[4]arene can be utilized for the molecular recognition of small organic molecules.

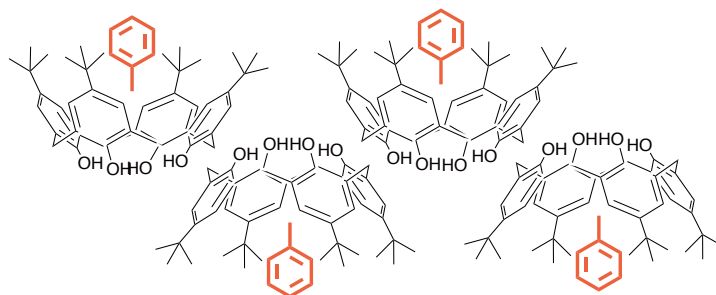


Figure 1-2-5. Schematic representation of the inclusion compound of *p-tert*-butylcalix[4]arene with toluene.^[32]

In 1983, Izatt and coworkers investigated the molecular recognition capability of *p-tert*-butylcalix[*n*]arenes ($n = 4, 6, \text{ and } 8$). They showed that these calixarenes can transport cations across a liquid membrane.^[33] This research was the first evidence of the complexing ability of calix[*n*]arenes in solutions. Ungaro, Andreetti, and coworkers designed calix[4]arene derivatives capped by pentaethylene glycol (Figure 1-2-6).^[28] This hybrid molecule can serve as a neutral receptor of alkali cations. They showed that this molecule can selectively extract potassium cations from a mixture of alkali metal cations and transport them through an organic liquid membrane.

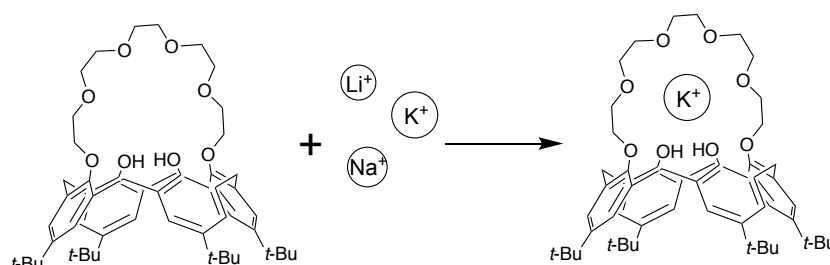


Figure 1-2-6. Extraction of a potassium cations from a mixture of alkali metal cations by pentaethylene glycol-capped *p-tert*-butylcalix[4]arene.^[28]

In 1993, Shinkai and coworkers reported the binding behavior of 25,26,27,28-tetrapropoxy-calix[4]arene (Figure 1-2-7a).^[29] They showed that the methyl group of the methylpyridinium cation is trapped in the cavity of calix[4]arene via cation $\cdots\pi$ interactions. In 1996, Pochini and coworkers synthesized conformationally rigid calix[4]arene by introducing diethylene glycols (Figure 1-2-7b).^[30] Their binding study revealed the formation of 1:1 host-guest complexes with guest species bearing acidic methyl groups. In the same year, Kubo and coworkers reported the chiral recognition

capability of calix[4]arene-based hosts (Figure 1-2-7c).^[31] The chirality is generated on the host by installing an (*S*)-binaphthyl moiety into the lower rim. They demonstrated that the host selectively recognized (*R*)-phenyl glycinol and forms a host-guest complex. The installed binaphthyl group informed the host-guest complexation and caused a color change upon uptake of the guest.

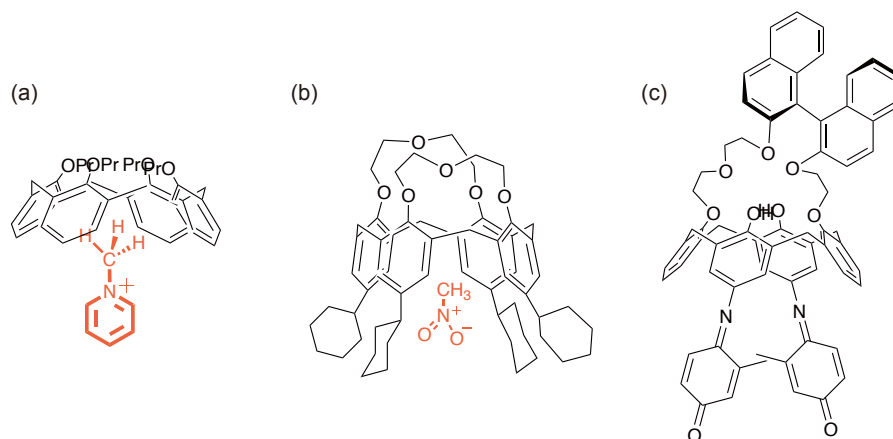


Figure 1-2-7. Schematic representation of molecular hosts reported by a) Sinkai et al.,^[29] b) Pochini et al.,^[30] and c) Kubo et al.^[31]

As demonstrated by the X-ray crystal structure of the inclusion compound of *p*-*tert*-butylcalix[4]arene and toluene reported by Andreetti, the intramolecular cavity of calix[4]arene can include at most one methyl group. When calix[4]arene crystallizes, it sometimes creates extramolecular space and traps a variety of guests in the extramolecular space to form clathrates. Since Andreetti's report in 1979,^[32] many examples of calix[4]arene clathrates have been reported. In 1983, Andreetti, Ungaro, and coworkers reported a *p*-(1,1,3,3-tetramethylbutyl)calix[4]arene clathrate.^[34] One-dimensional channels were formed among the hosts, and toluene could be accommodated in the channels (Figure 1-2-8). X-ray crystal structure analysis suggested that van der Waals interactions were expected to be present between the trapped guests and the aliphatic chains of the hosts.

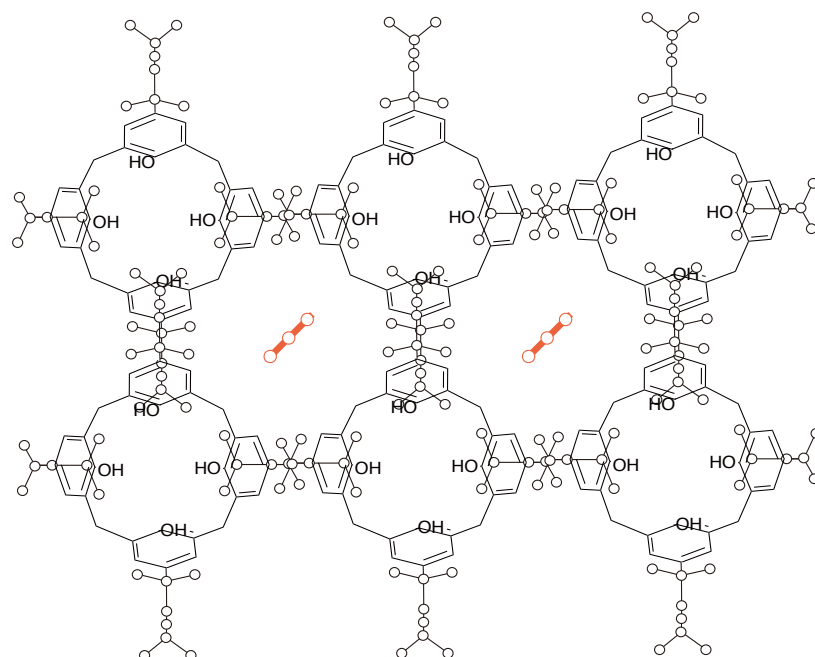


Figure 1-2-8. Schematic representation of the crystal structure of the clathrate of *p*-(1,1,3,3-tetramethylbutyl)calix[4]arene. Toluene was incorporated into the channels generated among the calix[4]arene host.^[34]

In recent years, some researchers have used weak intermolecular interactions such as van der Waals and C–H \cdots π interactions for the molecular recognition of alkanes. For example, in 2006, Ripmeester and coworkers reported the new inclusion motif of *p*-*tert*-butylcalix[4]arene (Figure 1-2-9).^[35] They demonstrated that the host recognizes the methyl group of amino alkanes. The amino group abstracted the proton from a hydroxy group, resulting in charge-assisted N–H \cdots O hydrogen bond. This type of molecular recognition rarely occurs in solutions because the solvation of the hosts and guests prevent them from forming the host-guest complex.

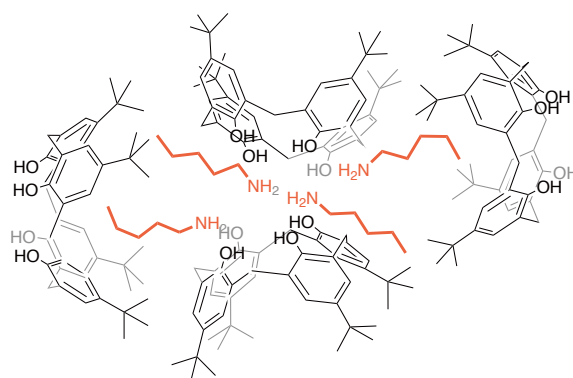


Figure 1-2-9. Schematic representation of the crystal structure of the *p-tert*-butylcalix[4]arene host with the amylamine guest.^[35]

In 1985, Ungaro, Andreetti, and coworkers reported an interesting example of a calix[4]arene assembly in the solid-state. Two molecules of *p-tert*-butylcalix[4]arene were arranged in a head-to-head manner to form a capsule-like assembly (Figure 1-2-10).^[36] One molecule of anisole was encapsulated in the inner space generated by the two *p-tert*-butylcalix[4]arene hosts. This capsule-like assembly provides an exciting platform for designing calix[4]arene-based hosts. Although the volume of the intramolecular space of the calix[4]arene is not large enough to incorporate entire guests, they can be incorporated into the capsule-like assembly because of its larger intramolecular pocket. This is well exemplified by supramolecular capsules based on calix[4]arene and its derivatives, such as calix[4]resorcinarenes.

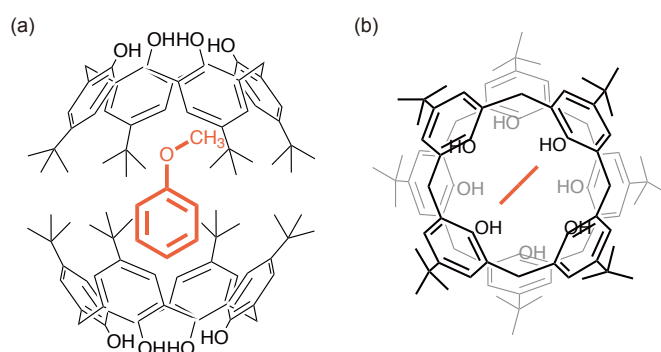


Figure 1-2-10. a) Front and b) top views of the capsule-like assembly of *p-tert*-butylcalix[4]arene in the solid-state.^[36] One molecule of anisole is trapped in the space generated by the two hosts.

1-2-3 Supramolecular Capsules Based on Calix[4]arene and Its Derivatives

The first example of molecular capsules is Cram's *carcerand* reported in 1985 (Figure 1-2-11a).^[37] The term '*carcerand*' is defined as a closed molecular container or capsule without portals of significant size through which guests can either enter or leave.

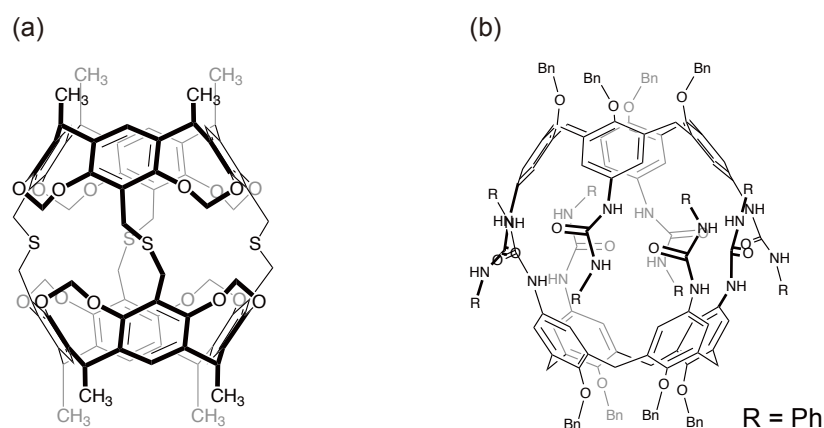


Figure 1-2-11. Schematic representations of a) a carcerand and b) Rebek's molecular capsule.

This molecular host is composed of two calix[4]resorcinarenes connected to each other by thioether linkages. The four methylene linkages on the upper rim rigidify the conformation. These modifications generate an inner cavity that permits encapsulation of a variety of neutral and charged guests, such as dimethylformamide, tetrahydrofuran, and cesium chloride, affording incarcerated host-guest complexes. The four thioether linkages prevent release of the encapsulated guests until decomposition of the carcerand shell, which means that the guests must be trapped during the formation of the carcerand.

In 1995, Rebek Jr. and Shimizu reported a dimeric calix[4]arene capsule (Figure 1-2-11b).^[38] The urea groups on the upper rim drives dimerization through the formation of multiple N-H \cdots O hydrogen bonds between the urea groups to afford highly symmetrical (S_8 point group) molecular capsules.

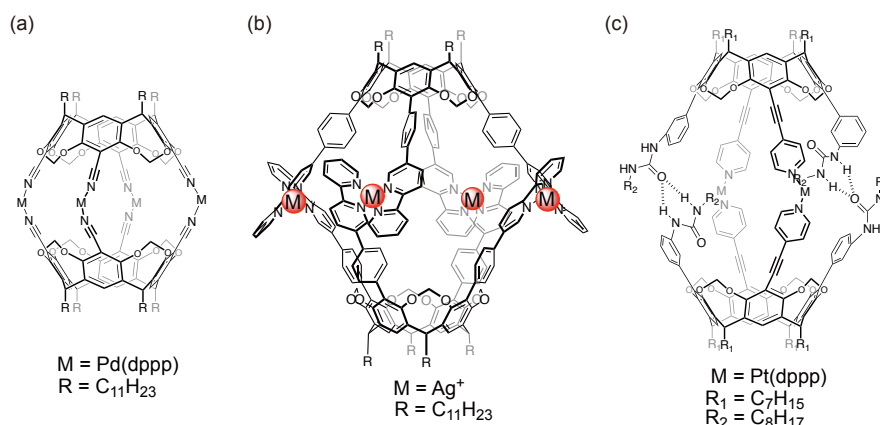


Figure 1-2-12. Schematic representations of the coordination capsules reported by a) Dalcanale's group,^[39] b) Haino's group,^[40] and c) Kobayashi's group.^[41]

Recently, the utilization of metal-ligand coordination for the formation of molecular capsules has attracted increasing attention. In 1997, Dalcanale et al. reported the quantitative self-assembly of organopalladium capsules (Figure 1-2-12a).^[39] This capsule is very stable and shows heat resistance because of the strong cyano- Pd^{2+} coordination bonds. Due to the comparatively large cavity, these capsules could not trap solvent molecules but could trap one of the eight triflate counterions. Treatment of this capsule with competing ligands, such as triethylamine, leads to complete disassembly of the capsule. In 2005, our group reported a self-assembled calix[4]resorcinarene-based coordination capsule (Figure 1-2-12b).^[40] This dimeric complex was produced in almost quantitative yield by metal-ligand coordination between 2,2'-bipyridyl arms and a metal cation with tetrahedral coordination geometry, such as Ag^+ or Cu^+ . The volume of the intramolecular space is approximately 580 \AA^3 , allowing it to encapsulate sizable molecules such as 4,4'-diacetoxybiphenyls and a heterodimer composed of acetic acid and 4-acetylbenzoic acid. Kobayashi et al. also reported calix[4]resorcinarene-based molecular capsules (Figure 1-2-12c).^[41] This complex used coordination bonds and hydrogen bonds for dimerization, and it encapsulates guests such as 4,4'-diiodobiphenyl with the assistance of an anion. The binding behavior can be tuned by controlling the amount and/or type of anion. The above examples nicely demonstrate that capsule-like assemblies can expand the scope of potential guests.

1-3 Overview of the Present Thesis

Our group has employed the calix[4]arene core for the development of new supramolecular systems. In recent years, our group reported the development of a calix[4]arene-based metallohelicate and investigations of their molecular recognition properties.^[42] We also reported the X-ray crystal structure analysis of 5,17-difunctionalized calix[4]arene, which forms a unique head-to-tail columnar structure in the solid-state and functions as a clathrand.^[43,44] Based on these previous works, the following are the main topics of my Ph.D. Thesis.

1. Installation of new functional groups into 25,26,27,28-tetrapropoxy-5,17-diaminocalix[4]arene to generate new clathrands and an investigation of the solid-state structures of the resulting clathrates. (Chapter 2)
2. Synthesis of dimeric and trimeric triple-stranded complexes as a proof-of-concept of calix[4]arene-based polymeric triple-stranded metallohelicates and an investigation of their molecular recognition properties. (Chapter 3)

In Chapter 2, the synthesis and solid-state structure of chiral mandelic acid-containing calix[4]arene clathrands are reported. I found that a difunctionalized calix[4]arene formed a head-to-tail columnar structure,^[43,44] and a unique hexagonal structure was found. The former result supports that the head-to-tail columnar structures can be utilized as a tool for the crystal engineering of 5,17-difunctionalized calix[4]arene-based clathrands, and the latter result demonstrates the generation of chiral space in the solid-state. The investigation of the adsorption properties of apohost provided by the clathrate crystals revealed selective adsorption for a specific molecule.

In Chapter 3, the synthesis of dimeric and trimeric calix[4]arene helical complexes is reported. The formation of the metallohelicates was carefully examined by UV-Vis absorption spectroscopy, NMR spectroscopy, and ESI-MS. The hollow space generated among the three calix[4]arene cores incorporated guests to afford the corresponding host-guest complexes. Since the two or three calix[4]arene cores in a strand are connected by covalent bonds, chirality on one monomer unit was expected to be transferred to another unit. Indeed, the guest-binding study revealed a majority-rules effect^[42] and positive

cooperativity,^[43] which were carefully assessed by circular dichroism spectroscopy.

1-4 References

- [1] J. W. Steed and J. L. Atwood, *Supramolecular Chemistry Second Edition*, John Wiley & Sons., Ltd. United Kingdom, **2009**.
- [2] S. Mann, *Nature* **1988**, *332*, 119-124.
- [3] J. Bernstein, R. E. Davis, L. Shimoni, and N.-L. Chang, *Angew. Chem. Int. Ed. Engl.* **1995**, *34*, 1555-1573.
- [4] D. P. Bartel, *Cell* **2004**, *116*, 281-294.
- [5] J. D. G. Jones and J. L. Dangl, *Nature* **2006**, *444*, 323-329.
- [6] J. R. Moran, S. Karbach, and D. J. Cram, *J. Am. Chem. Soc.* **1982**, *104*, 5826-5828.
- [7] H. M. Powell, *J. Chem. Soc.* **1948**, 61-73.
- [8] C. J. Pedersen, *J. Am. Chem. Soc.* **1967**, *89*, 7017-7036.
- [9] D. Landini, F. Montanari, and F. M. Pirisi, *J. Chem. Soc., Chem. Commun.* **1974**, 879-880.
- [10] B. Dietrich, J.-M. Lehn, and J.-P. Sauvage, *Tetrahedron Lett.* **1969**, *10*, 2885-2888.
- [11] D. J. Cram, T. Kaneda, R. C. Helgeson, and G. M. Lein, *J. Am. Chem. Soc.* **1979**, *101*, 6752-6754.
- [12] A. Harada, S. Takahashi, *J. Chem. Soc., Chem. Commun.* **1983**, 645-646.
- [13] W. A. Freeman, W. L. Mock, and N.-Y. Shih, *J. Am. Chem. Soc.* **1981**, *103*, 7367-7368.
- [14] P. A. Gale, J. L. Sessler, V. Král, and V. Lynch, *J. Am. Chem. Soc.* **1996**, *118*, 5140-5141.
- [15] T. Ogoshi, S. Kanai, S. Fujinami, T. Yamagishi, and Y. Nakamoto, *J. Am. Chem. Soc.* **2008**, *130*, 5022-5023.
- [16] S. Dong, C. Han, B. Zheng, M. Zhang, F. Huang, *Tetrahedron Lett.* **2012**, *53*, 3668-3671.
- [17] V. Böhmer, *Angew. Chem. Int. Ed. Engl.* **1995**, *34*, 713-745.
- [18] Zeyuan Dong, Quan Luo, and Junqiu Liu, *Chem. Soc. Rev.* **2012**, *41*, 7890-7908.
- [19] P. Linnane, T. D. James, and S. Shinkai, *J. Chem. Soc., Chem. Commun.* **1995**, 1997-1998.
- [20] A. von Baeyer, *Ber. Dtsch. Chem. Ges.* **1872**, *5*, 25-26.
- [21] L. Lederer, *J. Prakt. Chemie* **1894**, *50*, 223-226.
- [22] O. Manasse, *Ber. Dtsch. Chem. Ges.* **1894**, *27*, 2409-2413.

- [23] L. H. Baekeland, U.S. Patent 942,699; October **1908**.
- [24] A. Zinke and E. Ziegler, *Ber. Dtsch. Chem. Ges.*, **1944**, *77*, 264-272.
- [25] C. D. Gutsche and R. Muthukrishnan, *J. Org. Chem.* **1978**, *43*, 4905-4906.
- [26] C. D. Gutsche, M. Iqbal, and D. Stewart, *J. Org. Chem.* **1986**, *51*, 742-745.
- [27] L. J. Bauer and C. D. Gutsche, *J. Am. Chem. Soc.* **1985**, *107*, 6063-6069.
- [28] C. Alfieri, E. Dradi, A. Pochini, R. Ungaro, and G. D. Andreetti, *J. Chem. Soc. Chem. Comm.* **1983**, 1075-1077.
- [29] K. Araki, H. Shimizu, and S. Shinkai, *Chem. Lett.* **1993**, 205-208.
- [30] A. Arduini, W. M. McGregor, D. Paganuzzi, A. Pochini, A. Secchi, F. Ugozzoli, and R. Ungaro, *J. Chem. Soc., Perkin Trans. 2* **1996**, 839-846.
- [31] Y. Kubo, S. Maeda, S. Tokita, and M. Kubo, *Nature* **1996**, *382*, 522-524.
- [32] G. D. Andreetti, R. Ungaro, and A. Pochini, *J. Chem. Soc. Chem. Comm.* **1979**, 1005-1007.
- [33] R. M. Izatt, J. D. Lamb, R. T. Hawkins, P. R. Brown, S. R. Izatt, and J. J. Christensen, *J. Am. Chem. Soc.* **1983**, *105*, 1782-1785.
- [34] G. D. Andreetti, A. Pochini, and R. Ungaro, *J. Chem. Soc., Perkin Trans. 2* **1983**, 1773-1779.
- [35] P. O. Brown, K. A. Udachin, G. D. Enright, and J. A. Ripmeester, *Chem. - Eur. J.* **2006**, *12*, 8240-8252.
- [36] R. Ungaro, A. Pochini, G. D. Andreetti, and P. Domiano, *J. Chem. Soc., Perkin Trans. 2* **1985**, 197-201.
- [37] D. J. Cram, S. Karbach, Y. H. Kim, L. Baczyński, and G. W. Kallemeyn, *J. Am. Chem. Soc.* **1985**, *107*, 2575-2576.
- [38] K. D. Shimizu and J. Rebek Jr., *Proc. Natl. Acad. Sci. USA* **1995**, *92*, 12403-12407.
- [39] P. Jacopozzi and E. Dalcanale, *Angew. Chem. Int. Ed. Engl.* **1997**, *36*, 613-615.
- [40] T. Haino, M. Kobayashi, M. Chikaraishi, and Y. Fukazawa, *Chem. Commun.* **2005**, 2321-2323.
- [41] M. Yamanaka, N. Toyoda, and K. Kobayashi, *J. Am. Chem. Soc.* **2009**, *131*, 9880-9881.
- [42] T. Haino, H. Shio, R. Takano, and Y. Fukazawa, *Chem. Commun.* **2009**, 2481-2483.
- [43] R. Sekiya, Y. Yamasaki, S. Katayama, H. Shio, and T. Haino, *CrystEngComm*, **2013**, *15*, 8404-8407.
- [44] R. Sekiya, Y. Yamasaki, W. Tada, H. Shio, and T. Haino, *CrystEngComm*, **2014**, *16*,

6023-6032.

[45] M. M. Green, N. C. Peterson, T. Sato, A. Teramoto, R. Cook, S. Lifson, *Science* **1995**, 268, 1860-1866.

[46] J. Rebek Jr., *Acc. Chem. Res.* **1984**, 17, 258-264.

Chapter 2

Molecular Recognition of Calix[4]arene

Clathrates

The contents of this chapter have been published in a slightly modified form: Y. Yamasaki, R. Sekiya, and T. Haino, *CrystEngComm* **2017**, *19*, 6744-6751.

2-1 Introduction

Crystal engineering is the design and preparation of crystals based on the consideration of the molecular structure and noncovalent intermolecular interactions, such as hydrogen bonding, halogen bonding, and π -interactions. In fact, it is difficult to construct a targeted molecular arrangement in crystals because the structure of the crystals is affected by the conditions of crystallization.

Among the various arrangements of calix[4]arenes found in the solid state, columnar structures are attractive supramolecular organizations due to their positional adaptability toward entrapped guests and relatively controllable crystal packings. These features can be useful for molecular recognition and reversible gas adsorption and desorption. Although one-dimensional arrangements of calix[4]arene derivatives in the solid state have been reported by several groups such as *p*-benzylcalix[4]arene by Raston's group^[1] and mono-*O*-substituted calix[4]arene by Coleman's group,^[2] the number of examples remains small.

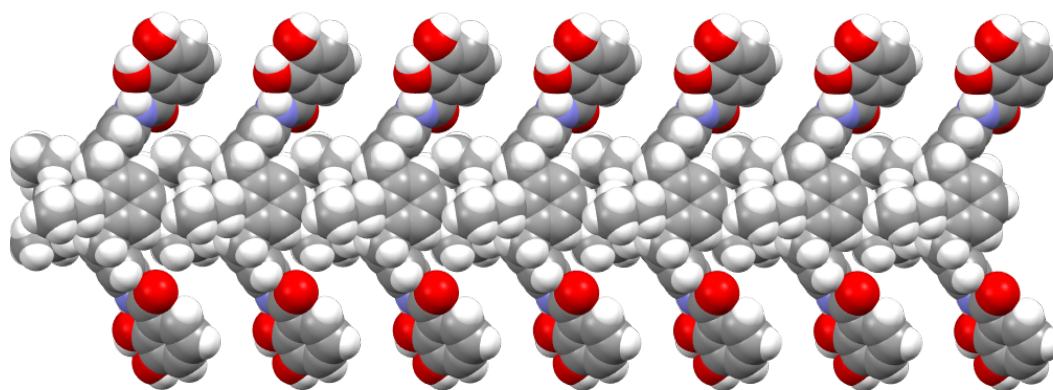


Figure 2-1-1. Space-filling illustration of the head-to-tail columnar structure of 5,17-difunctionalized 25,26,27,28-tetrapropoxy-calix[4]arene.^[4]

During our studies on calix[4,5]arenes,^[3] we found an unusual head-to-tail columnar structure of 25,26,27,28-tetrapropoxy-calix[4]arene possessing catechol arms at the 5,17-positions of the calix[4]arene core in cocrystals (Figure 2-1-1).^[4] This columnar structure was stabilized by multiple C–H \cdots π interactions between the terminal methyl group of the propoxy chain and the cavity of the neighboring calix[4]arene. This finding is true for the formation of the columnar structures irrespective of the types of guests.

This suggests that the interactions between the propyloxy chain and the cavity of the calix[4]arene core can be used as a supramolecular synthon^[5] driving 5,17-difunctionalized calix[4]arenes to form columnar structures. Inspired by this notion, my project focuses on assessing the versatility of this supramolecular structure for the crystal engineering of 5,17-difunctionalized calix[4]arenes.

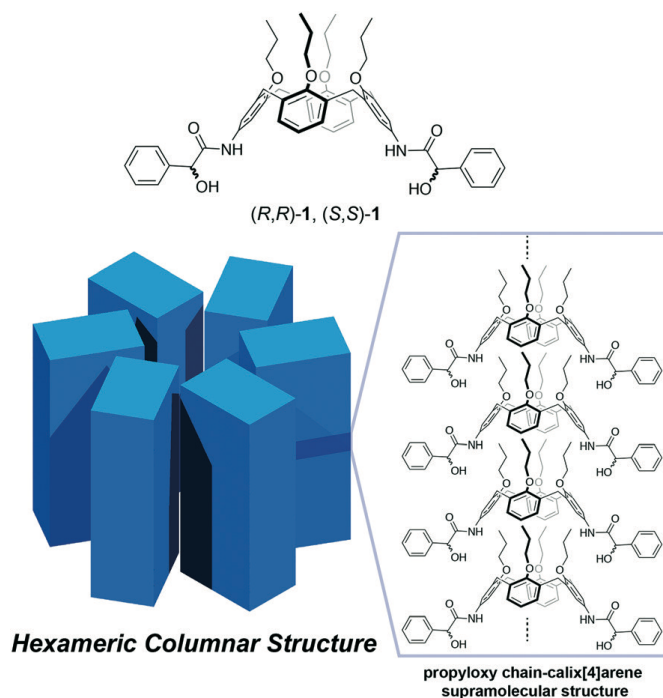


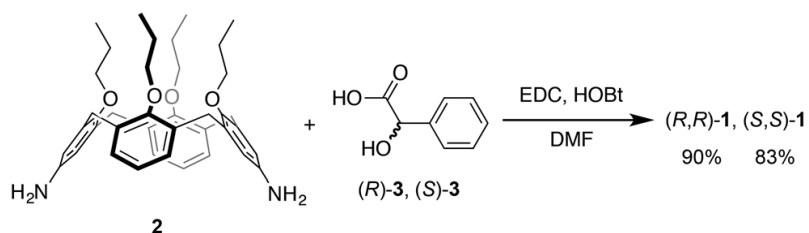
Figure 2-1-2. 5,17-difunctionalized calix[4]arenes (*R,R*)-**1** and (*S,S*)-**1** and schematic illustration of the columnar structures in the solid state.

In this chapter, I report the synthesis of a new 5,17-difunctionalized calix[4]arene **1** and its molecular recognition capability in the solid state (Figure 2-1-2). I found that calixarene **1** functions as a clathrand and affords clathrates with organic molecules. As expected, calixarene **1** formed a head-to-tail columnar structure, which demonstrates that the calix[4]arene core can be used for the crystal engineering of calix[4]arene-based clathrates. A unique chiral hexagonal arrangement for the columnar structures was found. Such a structure was formed only when linear molecules were used as guests. Finally, the guest release and the uptake of an apohost are discussed.

2-2 Results and Discussion

2-2-1 Synthesis of Calix[4]arene and Preparation of Single Crystals

Calixarenes (*R,R*)-**1** and (*S,S*)-**1** were synthesized by the coupling reaction of 5,17-diaminocalix[4]arene **2** with 2 equivalents of (*R*)- or (*S*)-mandelic acid **3** in excellent yield (Scheme 2-2-1). The characterization of the new host was accomplished by means of ¹H (Figure 2-2-1a), ¹³C (Figure 2-2-1b), and DQF-COSY spectra (Figure 2-2-2). One signal set of a mandelic group on the ¹H NMR spectrum indicates the C₂ symmetric structure of the product. Furthermore, the methylene group of calix[4]arene shows two doublet peaks on the ¹H NMR spectrum. This pattern implied that the conformation of calix[4]arene was maintained. All the signals were assigned by the DQF-COSY spectrum.



Scheme 2-2-1. Synthesis of (*R,R*)-**1** and (*S,S*)-**1**. Reaction conditions: **2**, 2 equiv. of (*R*)-**3** or (*S*)-**3**, 2 equiv. of EDC, 2 equiv. of HOBT, DMF, room temperature, 3 h.

We have prepared five cocrystals, namely, (*S,S*)-**1**·(MeOH), (*S,S*)-**1**·(EtOH), (*S,S*)-**1**·(1-PrOH), (*S,S*)-**1**·(2-PrOH), and (*S,S*)-**1**·(CH₃CN), and one racemic crystal, *rac*-**1**. The cocrystals of (*S,S*)-**1**·(MeOH) and (*S,S*)-**1**·(EtOH) were not very stable. They started releasing the entrapped guests just after harvesting the cocrystals and gradually became opaque.

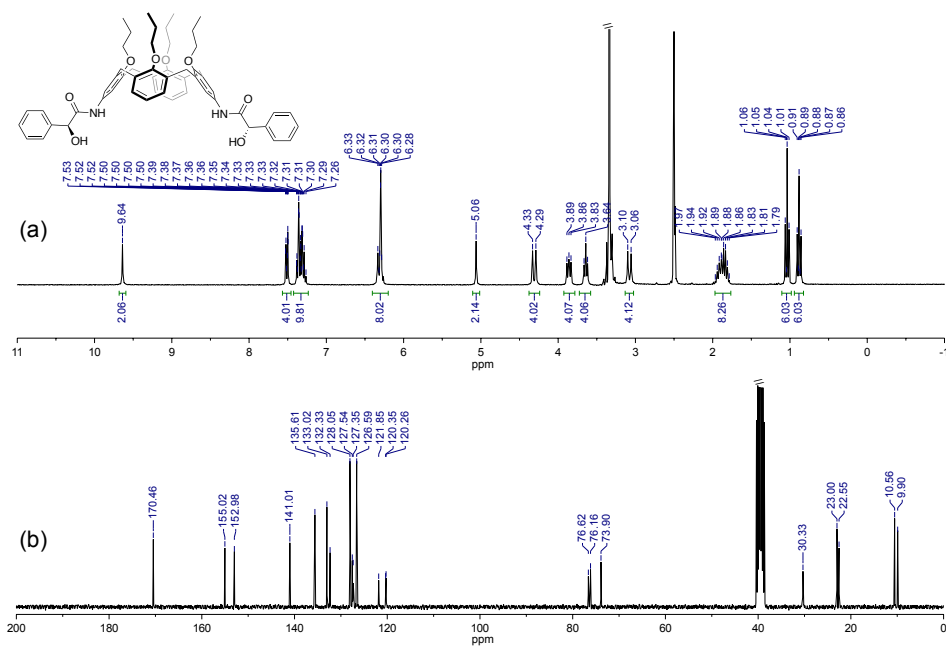


Figure 2-2-1. a) ^1H (500 MHz, $\text{DMSO-}d_6$, 293 K) and b) ^{13}C (125 MHz, $\text{DMSO-}d_6$, 293 K) NMR spectra of (*S,S*)-1.

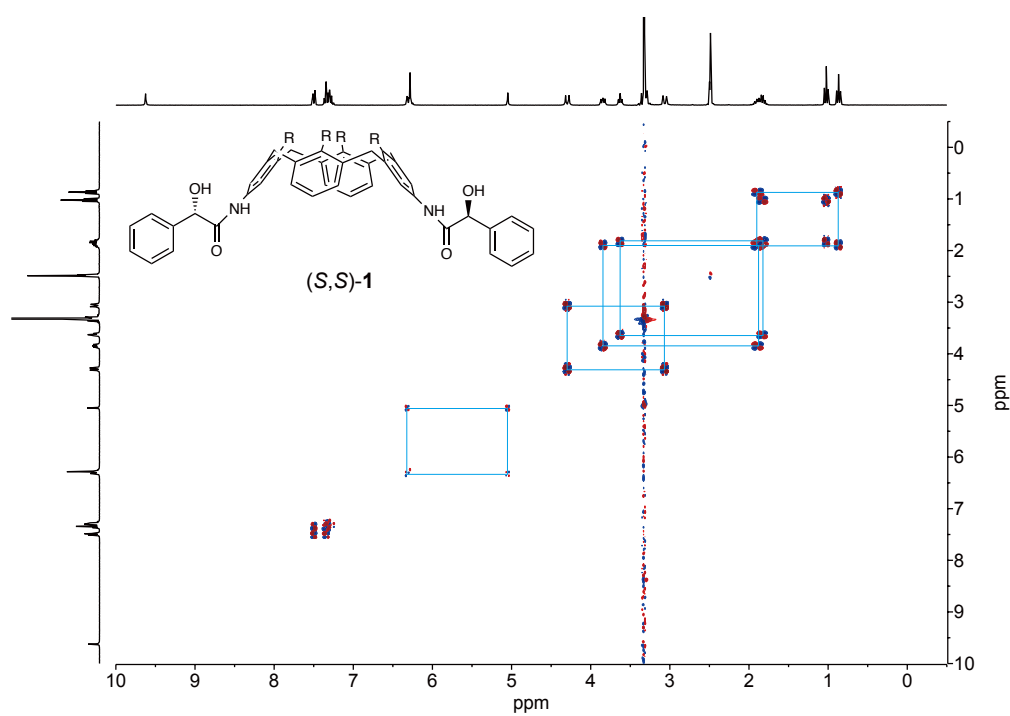


Figure 2-2-2. DQF-COSY spectrum (500 MHz, $\text{DMSO-}d_6$, 293 K) of (*S,S*)-1.

2-2-2 Crystal structure of hexameric assembly

(*S,S*)-**1**·(EtOH) crystallized in a trigonal crystal system with the space group *P*3(#143) (Figure 2-2-3a). The absolute structure was determined based on the chirality centers embedded in the mandelamide arms. The calixarene core adopted a pinched cone conformation. Both of the mandelamide arms flipped down, and as a result, (*S,S*)-**1** has a ‘U’-like conformation. They were stacked on top of each other along the *c* axis to form a head-to-tail columnar structure (Figure 2-2-3b). The stacking manner was very similar to that observed in previous studies;^[4] the terminal methyl groups of the two propyloxy chains at the 25 and 27 positions of the calix[4]arene core came into contact with the cavity of the neighboring core to form multiple C–H··· π interactions.

Each (*S,S*)-**1** molecule in the columnar structure came into contact with (*S,S*)-**1** molecules in the neighboring four columns to form an unusual hexameric arrangement on the *ab* plane (Figure 2-2-3c). The six calix[4]arene cores were arranged with a clockwise orientation when the crystal packing is seen from the *c* axis. O–H···O hydrogen bonds between the hydroxy group and the carbonyl group (red line in Figure 2-2-3c; O2···O4 = 2.711(6) Å; O1···O3 = 2.715(7) Å) and C–H··· π interactions between the phenyl rings of the arms (green line in Figure 2-2-3c; H5B···ring = 2.71(1) Å) were found in the hexameric structure and unite the six columns.

A hexagonal space was formed in the center of the six hosts, giving rise to a chiral one-dimensional hydrophobic channel penetrating along the *c* axis. The aromatic rings of the arms were found to be disordered over two positions, with a site occupancy factor (sof) of 0.60:0.40. This indicates that the crystal contained two diastereomeric channels with an approximately 1.5:1 ratio; the major channel contained clockwise C–H··· π interactions (Figure 2-2-3c, top), and the minor channel has counterclockwise C–H··· π interactions (Figure 2-2-3c, bottom).

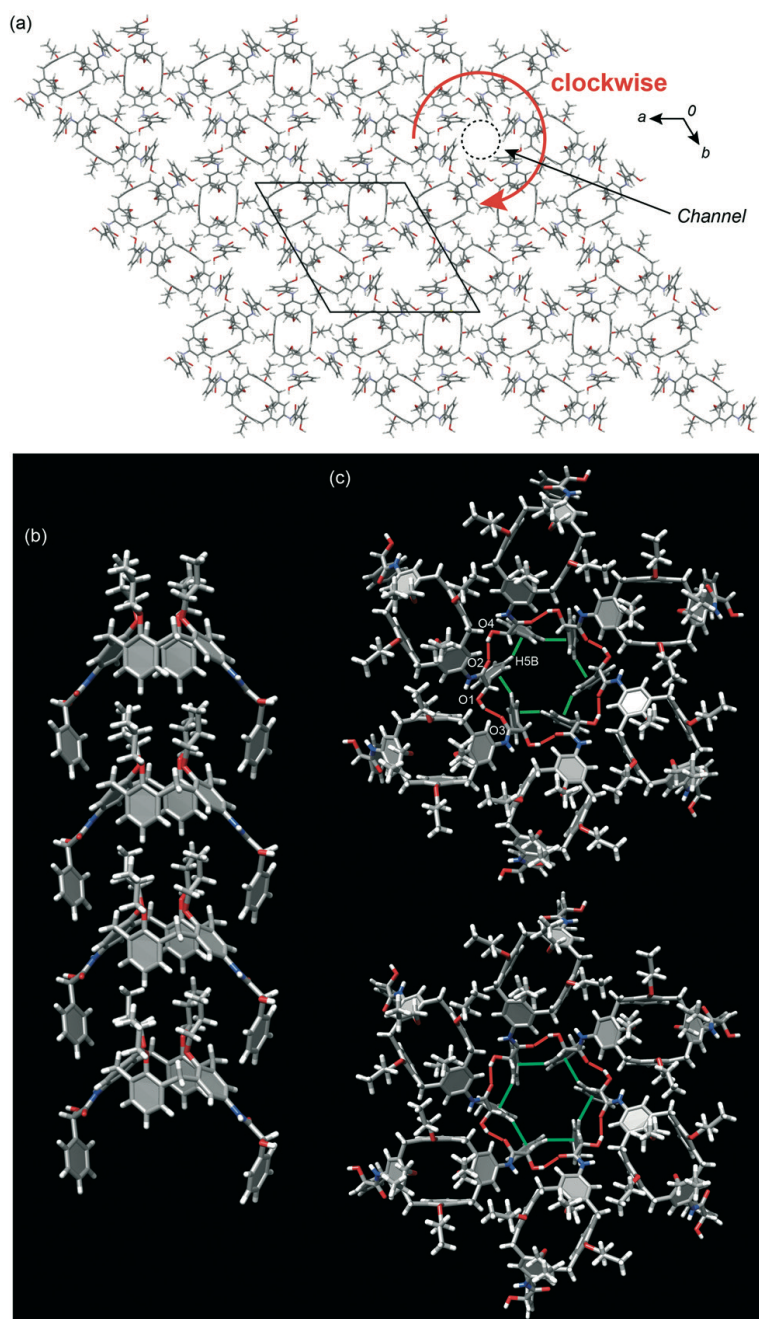


Figure 2-2-3. a) X-ray crystal structure of $(S,S)\text{-1}\cdot(\text{EtOH})$ viewed down the c axis. The EtOH guests are omitted for clarity. b) Head-to-tail columnar structure of $(S,S)\text{-1}$ and (c) hexameric assemblies of $(S,S)\text{-1}$ found in $(S,S)\text{-1}\cdot(\text{EtOH})$. In c), the top image is the predominant assembly and the bottom image is the minor assembly in the crystal. In c), the red lines denote hydrogen bonds, and the green lines denote $\text{C-H}\cdots\pi$ interactions.

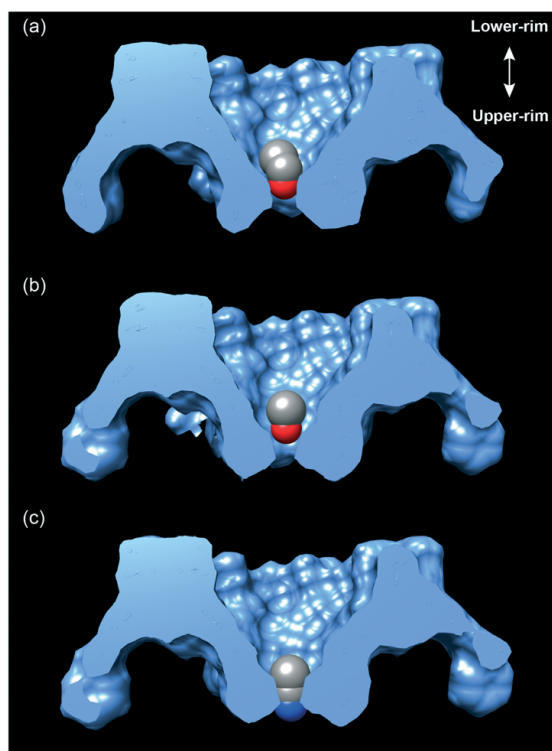


Figure 2-2-4. The guests inside the hexagonal channel: a) EtOH, b) MeOH, and c) CH₃CN. In a), one of the three disordered guests is shown for clarity.

The EtOH guest was on the three-fold rotational axis penetrating the center of the channel and came into contact with the aromatic rings of the mandelamide arms (Figure 2-2-4a). The hydroxy group pointed to the upper-rim side. No hydrogen bond between the guests or between the guest and the host was found, suggesting that the EtOH guest was entrapped in the channel by van der Waals interactions. This may relate to the facile release of the EtOH guest from the powdered cocrystal of (*S,S*)-**1**·(EtOH) (*vide infra*).

2-2-3 Crystal structure of (*S,S*)-**1**·(Solvent) (Solvent = MeOH, 1-PrOH, CH₃CN)

The crystal packings of (*S,S*)-**1**·(MeOH) (Figure 2-2-5), (*S,S*)-**1**·(1-PrOH) (Figure 2-2-6), and (*S,S*)-**1**·(CH₃CN) (Figure 2-2-7) were very similar to that of (*S,S*)-**1**·(EtOH). The MeOH and CH₃CN guests were entrapped in the channel similarly to the EtOH guest (Figures 2-2-4b and 2-2-4c). The CH₃CN guest penetrated more deeply into the channel than the EtOH and MeOH guests, probably because the C≡N group was sterically less hindered than the MeOH and EtOH guests. The 1-PrOH guest was not evaluated due to the disorder. The sof of the aromatic rings of (*S,S*)-**1**·(1-PrOH) and (*S,S*)-**1**·(CH₃CN) was similar to that of (*S,S*)-**1**·(EtOH), whereas that of (*S,S*)-**1**·(MeOH) was approximately 1:1.

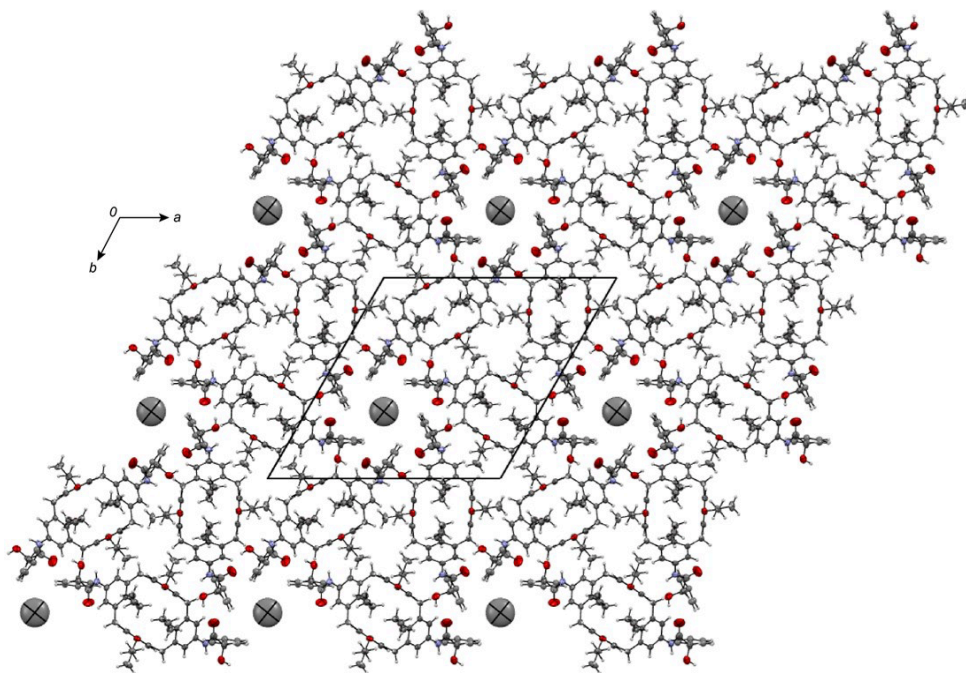


Figure 2-2-5. X-ray crystal structure of (*S,S*)-**1**·(MeOH) viewed down the crystallographic *c* axis. Color scheme: gray (carbon), white (hydrogen), blue (nitrogen), red (oxygen).

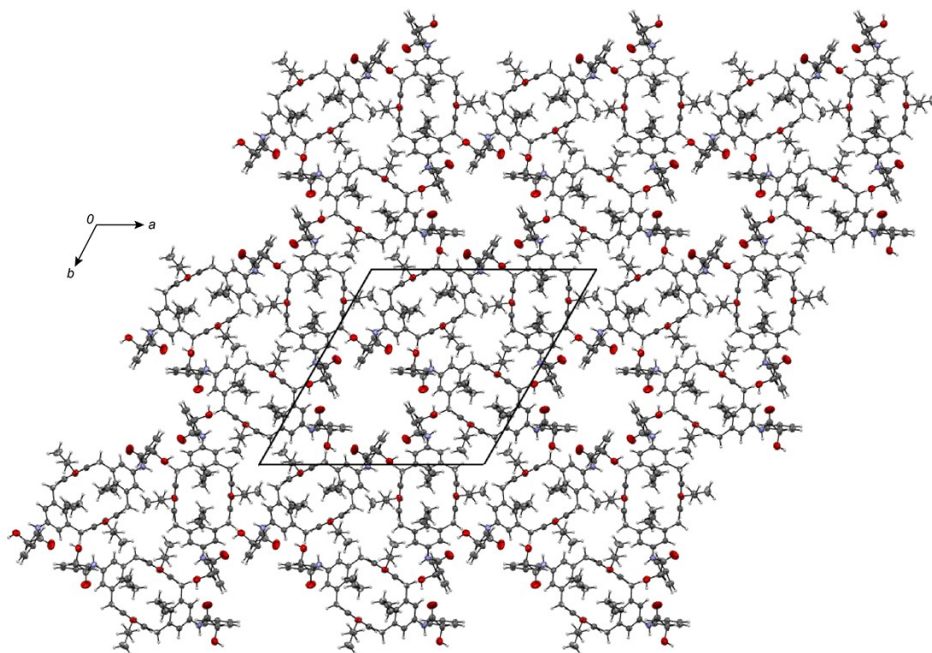


Figure 2-2-6. X-ray crystal structure of (S,S) -1·(1-PrOH) viewed down the crystallographic c axis. Color scheme: gray (carbon), white (hydrogen), blue (nitrogen), red (oxygen).

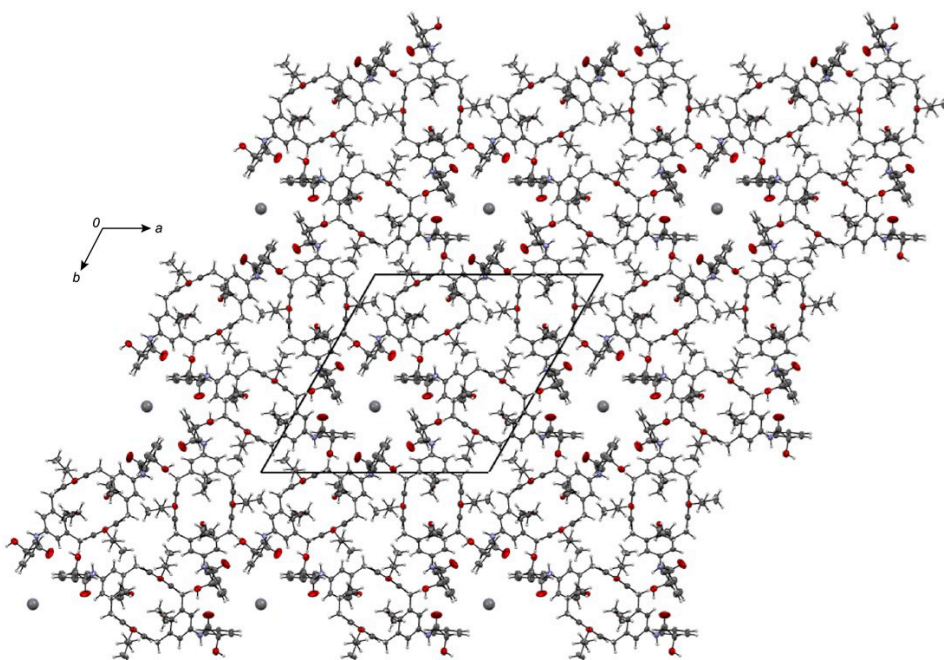


Figure 2-2-7. X-ray crystal structure of (S,S) -1·(CH₃CN) viewed down the crystallographic c axis. Color scheme: gray (carbon), white (hydrogen), blue (nitrogen), red (oxygen).

2-2-4 Crystal structure of (*S,S*)-1·(2-PrOH)

(*S,S*)-1·(2-PrOH) has a different crystal packing (Figure 2-2-8). It crystallized in a monoclinic crystal system with the space group $C2(\#5)$.

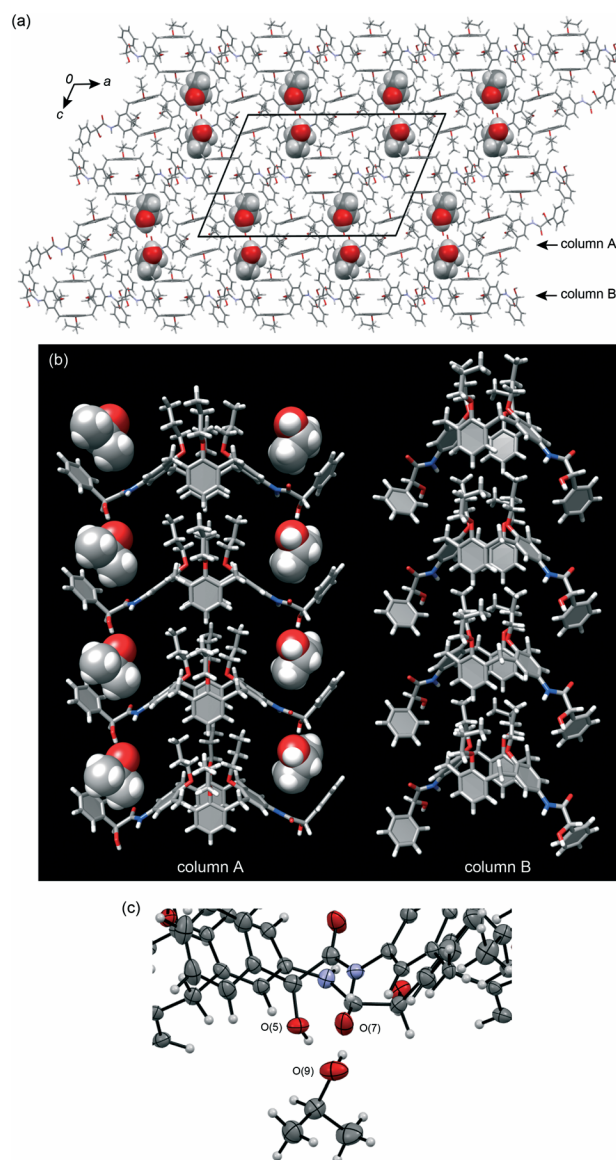


Figure 2-2-8. a) X-ray crystal structure of (*S,S*)-1·(2-PrOH) viewed down the *b*-axis. b) The two different head-to-tail columnar structures of (*S,S*)-1 (column A and column B) found in the crystal. c) The hydrogen bonds between the 2-PrOH guest and two (*S,S*)-1 molecules. The guest molecules in a) and b) are shown as space-filling for clarity.

Again, (*S,S*)-**1** formed the head-to-tail columnar structure. Two types of columnar structures were found in the cocrystal (column A and column B); column A consists of (*S,S*)-**1** with a ‘W’-like conformation wherein the mandelamide arms are flipped up, whereas in column B, (*S,S*)-**1** adopted a ‘U’-like conformation similar to that found in the four cocrystals (Figure 2-2-8b). Columns A and B were arranged alternately along the *c* axis, and their stacking directions were opposite to each other. The 2-PrOH guests were held between the mandelamide arms, and there was no channel penetrating the crystal. The 2-PrOH guest formed two hydrogen bonds with the hydroxy group of (*S,S*)-**1** in the same column with $O(5)\cdots O(9) = 2.665(4)$ Å and the carbonyl group of (*S,S*)-**1** in the neighboring column A with $O(9)\cdots O(7) = 2.757(4)$ Å (Figure 2-2-8c).

2-2-5 Crystal structure of racemic mixture

To clarify the relationship between the homochirality of the host and the hexameric assembly of the columnar structures, we prepared a cocrystal of (*S,S*)-**1** and (*R,R*)-**1**. The racemic mixture gave *rac*-**1**. It crystallized in a monoclinic crystal system with the space group *C2/c*(#15). The crystal packing was similar to that of (*S,S*)-**1**·(2-PrOH), as demonstrated by their similar cell parameters, and there was no hexameric structure of the columns (Figure 2-2-9). This result shows the importance of the homochirality of the host for the formation of the hexameric structure. Both (*S,S*)-**1** and (*R,R*)-**1** adopted a ‘W’-like conformation, and each enantiomer formed homochiral head-to-tail columnar structures ((*S,S*)-**1** and (*R,R*)-**1** columns, Figure 2-2-9). They were stacked antiparallel and arranged alternately along the *c* axis. In contrast to (*S,S*)-**1**·(2-PrOH) and the other chiral cocrystals, there was no space available for the inclusion of a guest. This means that the racemic mixture can form a dense crystal packing by itself. Indeed, the calculated density of *rac*-**1** is 1.26 g cm^{-3} , which is slightly denser than that of (*S,S*)-**1**·(2-PrOH) (1.21 g cm^{-3}). The space between the mandelamide arms, which was occupied by the 2-PrOH guests in (*S,S*)-**1**·(2-PrOH), was occupied by the propyloxy chain of the neighboring column.

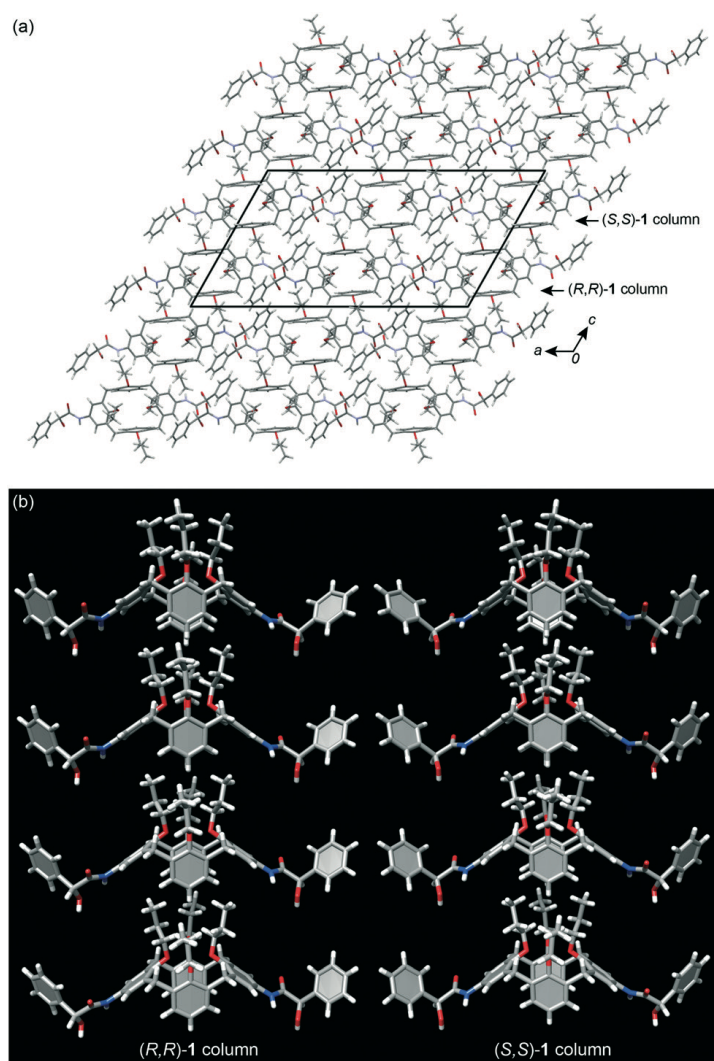


Figure 2-2-9. a) X-ray crystal structure of *rac-1* viewed down the *b*-axis. b) The columnar structures of (*R,R*)-**1** (left) and (*S,S*)-**1** (right) found in *rac-1*.

The above six crystal structures demonstrate that the interactions between the propyloxy chain and the hydrophobic cavity of the calix[4]arene core can be used to arrange (*S,S*)-**1** one-dimensionally with and without the presence of the guest. This result supports the versatility of the propyloxy chains···calix[4]arene supramolecular structure for the crystal engineering of 5,17-difunctionalized calix[4]arenes. The various conformations of the mandelamide arms of (*S,S*)-**1** indicate that it works as a regulator for adapting the columnar structures to the guests.

The crystal packings of the chiral cocrystals were influenced by the guests; the linear molecules (MeOH, EtOH, 1-PrOH and CH₃CN) afforded trigonal crystals, whereas the monoclinic crystal was selected when the branched guest (2-PrOH) was included. These

results show that linear guests are a suitable template for directing the columnar structures to form the hexameric assembly. This result is reasonable, as the guests were entrapped in the narrow part of the channel (Figure 2-2-4), and the steric requirement of the guest becomes severe.

2-2-6 Adsorption properties of 1_{apo}

An adsorption–desorption study was performed using $(S,S)\text{-1}\cdot(\text{EtOH})$ as a starting crystal phase. Figure 2-2-12a and b show the simulated XRD patterns of $(S,S)\text{-1}\cdot(\text{EtOH})^\ddagger$ and rac-1 at 123 K and Figure 2-2-12c shows the observed XRD pattern of the powdered $(S,S)\text{-1}\cdot(\text{EtOH})$ after it was left to stand for a few minutes at room temperature (*ca.* 20 °C).

The XRD pattern of $(S,S)\text{-1}\cdot(\text{EtOH})$ completely disappeared and became broad in a particular high-angle region ($2\theta = 16\text{--}27^\circ$), demonstrating that the EtOH guests were quickly released from the channel and the crystallinity became lower, likely due to the change of the crystal packing. The complete removal of the guests was confirmed by the ^1H NMR spectrum of $(S,S)\text{-1}_{\text{apo}}$ dissolved in $\text{DMSO-}d_6$, which showed no peaks assignable to ethanol (Figure 2-2-10). The crystal packing of $(S,S)\text{-1}_{\text{apo}}$ is unclear, but its XRD pattern, with diffractions at $2\theta = 10.1^\circ$ and 19.6° , is similar to that of rac-1 . This similarity suggests that $(S,S)\text{-1}_{\text{apo}}$ has a crystal packing similar to that of rac-1 .

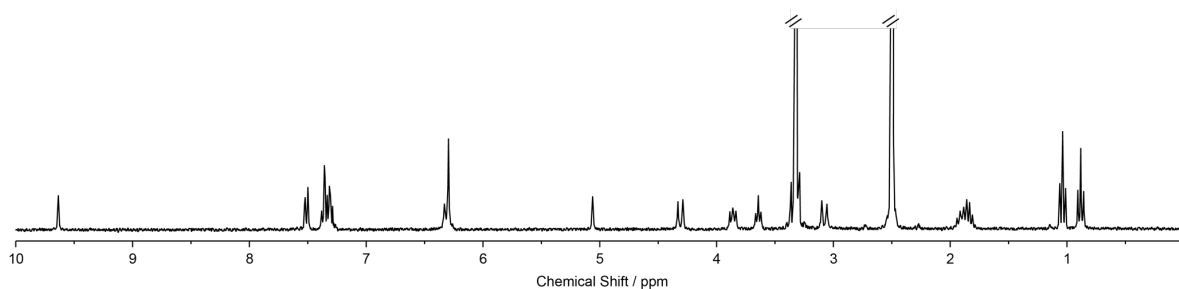


Figure 2-2-10. ^1H NMR spectrum (300 MHz, $\text{DMSO-}d_6$, 293 K) of $(S,S)\text{-1}_{\text{apo}}$.

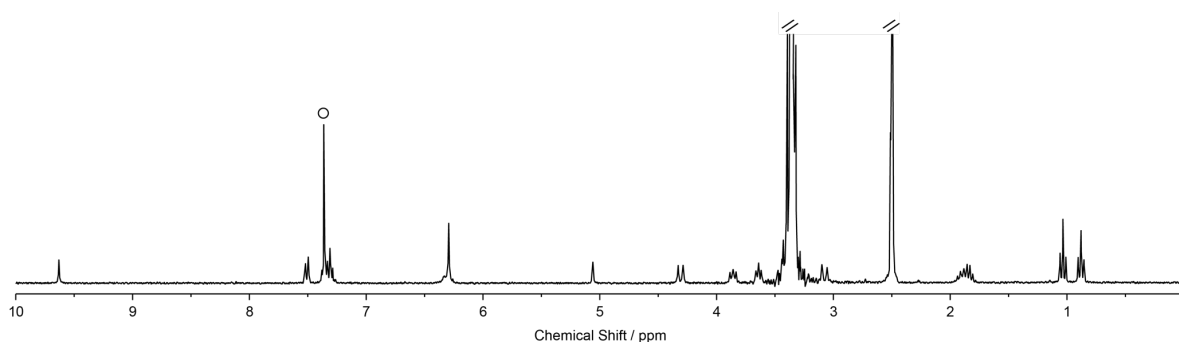


Figure 2-2-11. ^1H NMR spectrum (300 MHz, $\text{DMSO-}d_6$, 293 K) of $(S,S)\text{-1}_{\text{apo}}$ after contacting benzene vapor with $(S,S)\text{-1}_{\text{apo}}$ for 3 days at room temperature. Open circle denotes the signal of benzene.

The adsorption capability of $(S,S)\text{-1}_{\text{apo}}$ was investigated by bringing finely powdered $(S,S)\text{-1}_{\text{apo}}$ into contact with the vapors of 10 different organic solvents at room temperature (Table 2-2-1). Unexpectedly, $(S,S)\text{-1}_{\text{apo}}$ did not adsorb EtOH at all; no change of the XRD pattern resulted after the powder of $(S,S)\text{-1}_{\text{apo}}$ came into contact with the EtOH vapor for over 3 days at room temperature. The lack of readsorption suggests that the hexameric structure no longer exists after the release of the guest. Interestingly, benzene was absorbed in $(S,S)\text{-1}_{\text{apo}}$ to form $(S,S)\text{-1}_{\text{apo}}\cdot(\text{benzene})$ cocrystals (Figure 2-2-12d, red line). The host–guest stoichiometric ratio of $(S,S)\text{-1}_{\text{apo}}\cdot(\text{benzene})$ was determined to be 1:4 using the relative signal intensities of $(S,S)\text{-1}$ and benzene in the ^1H NMR spectrum (Figure 2-2-11). The guest selectivity is interesting, because the difference between benzene and toluene is only one methyl group. This result implies that $(S,S)\text{-1}_{\text{apo}}$ can recognize the steric difference between benzene and the other compounds.

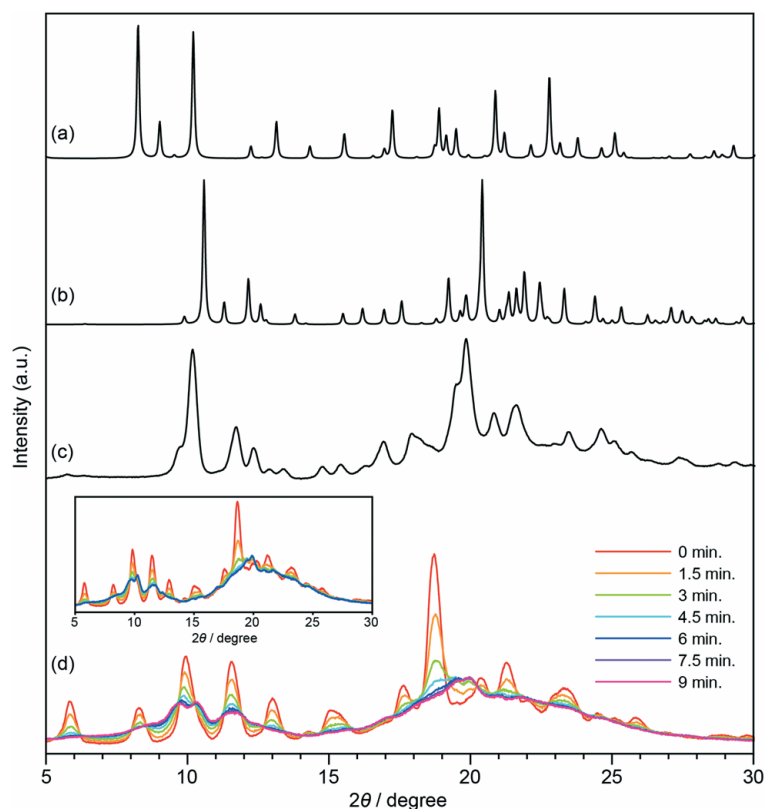


Figure 2-2-12. Simulated XRD patterns of a) (S,S) -**1**·(EtOH) and b) *rac*-**1** at $-150\text{ }^{\circ}\text{C}$ and the observed XRD pattern of c) (S,S) -**1**_{apo}. Change of XRD patterns of d) (S,S) -**1**_{apo}·(benzene). Inset: second cycle of adsorption and desorption of benzene.

Table 2-2-1. Molecular recognition of (S,S) -**1**_{apo} in the solid state.

Vapor	Result	H–G ratio ^a	Vapor	Result	H–G ratio
MeOH	N. D. ^b	—	Ethyl acetate	N. D.	—
EtOH	N. D.	—	Acetonitrile	N. D.	—
1-PrOH	N. D.	—	Benzene	Changed ^c	1:4
2-BuOH	N. D.	—	Toluene	N. D.	—
Acetone	N. D.	—	Benzyl alcohol	N. D.	—

^a Host–guest stoichiometric ratio. The host–guest ratio was determined by ¹H NMR. ^b The XRD pattern did not change after the vapor came into contact with (S,S) -**1**_{apo} for 3 days. ^c The XRD pattern was changed.

The adsorption–desorption of benzene could be repeated several times. The change of the crystal structure was monitored by the XRD analysis, and half of the benzene guest was released from the cocrystal after 1.2 min (Figure 2-2-13). Although the 2θ of the diffractions did not change, they became broader. After the readsorption of benzene, the powder again showed well-defined diffractions (inset in Figure 2-2-13). During the adsorption–desorption process, no melting of the powder was observed.

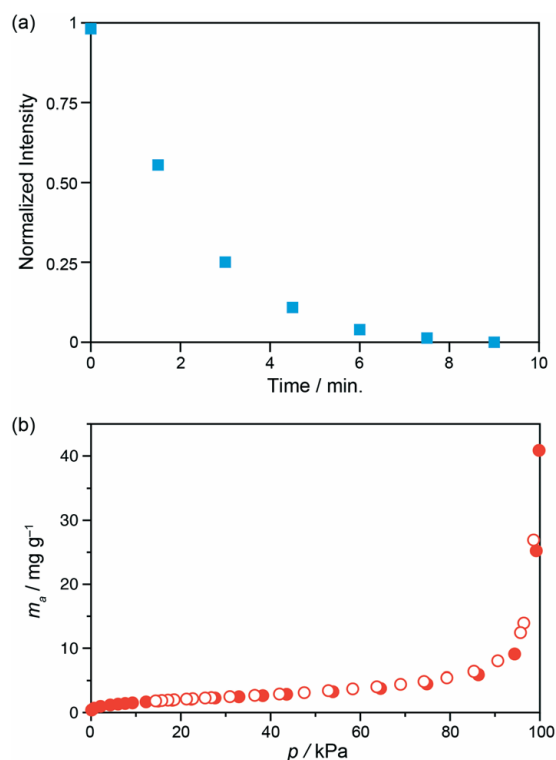


Figure 2-2-13. a) Time course of the change of the diffraction intensity of $(S,S)\text{-1}_{\text{apo}}\cdot(\text{benzene})$. The peak at $2\theta = 18.7^\circ$ was monitored. b) N_2 adsorption–desorption isotherm of $(S,S)\text{-1}_{\text{apo}}$ at 77 K. Filled circles denote the adsorption of N_2 gas, and open circles denote the desorption of N_2 gas.

The N_2 adsorption–desorption isotherm of $(S,S)\text{-1}_{\text{apo}}$ is shown in Figure 2-2-13. The sorption curves were analyzed using the Brunauer–Emmett–Teller (BET) method. The estimated BET surface area of $(S,S)\text{-1}_{\text{apo}}$ was *ca.* $6.2 \text{ m}^2 \text{ g}^{-1}$ and the average pore size was 3.2 \AA , demonstrating that after releasing the EtOH guests from $(S,S)\text{-1}\cdot(\text{EtOH})$, the crystal shrank, and only a small space remained in $(S,S)\text{-1}_{\text{apo}}$. The adsorption and desorption of benzene indicate that when the surface of $(S,S)\text{-1}_{\text{apo}}$ came into contact with the vapor of

benzene, the pores opened and adsorbed benzene, and after releasing the benzene, the pores closed again. This cycle showed the sponge-like character of (S,S) -**1**_{apo}.

The observed selectivity can be useful for the separation of benzene from other compounds. For example, when (S,S) -**1**_{apo} came into contact with mixed vapors of benzene and acetone or ethyl acetate, it selectively adsorbed the benzene (Figures 2-2-14 and 2-2-15).

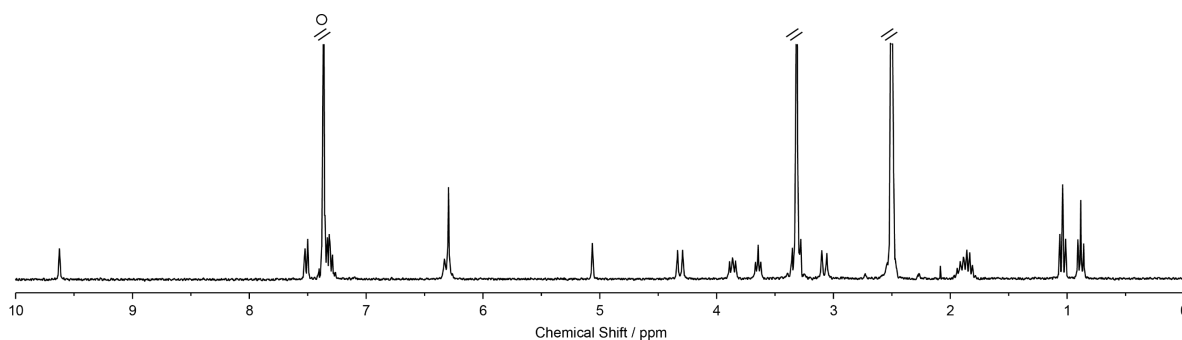


Figure 2-2-14. ^1H NMR spectrum (300 MHz, $\text{DMSO-}d_6$, 293 K) of (S,S) -**1**_{apo} after contacting a mixed vapor of benzene and acetone for 3 days at room temperature. Open circle denotes the signal of benzene.

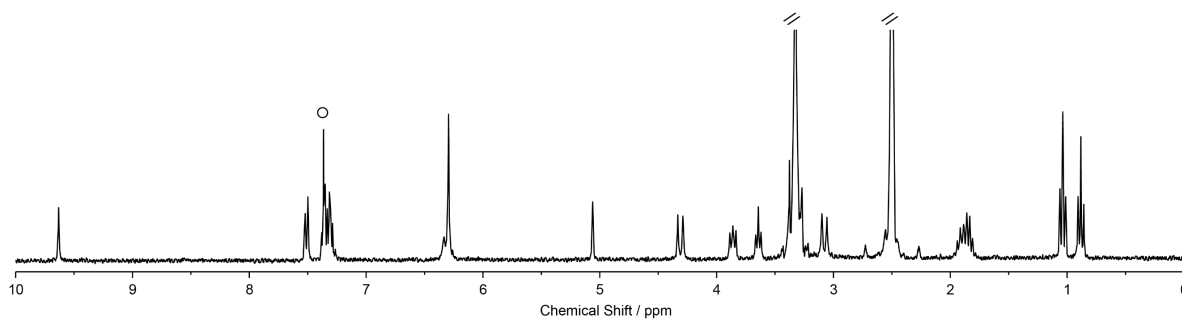


Figure 2-2-15. ^1H NMR spectrum (300 MHz, $\text{DMSO-}d_6$, 293 K) of (S,S) -**1**_{apo} after contacting a mixed vapor of benzene and ethyl acetate for 3 days at room temperature. Open circle denotes the signal of benzene.

2-3 Conclusions

In conclusion, the new chiral 5,17-difunctionalized calix[4]arene (*S,S*)-**1** and the racemic mixture formed head-to-tail columnar structures in the solid state, irrespective of both the crystal packing and the types of entrapped guests, confirming the versatility of the propyloxy chains···calix[4]arene supramolecular structure for the crystal engineering of 5,17-difunctionalized calix[4]arenes. The linear molecules afforded a hexameric assembly of the head-to-tail columnar structure, unlike the branched guest and the racemic mixture of the host, demonstrating that both the linearity of the guest and the homochirality of the host are prerequisites for the formation of the unusual crystal packing. The apohost prepared from (*S,S*)-**1**·(EtOH) showed selective molecular adsorption for benzene, and the desorption–adsorption study showed the sponge-like character of the apohost.

2-4 Experimental

2-4-1 Materials and methods

All chemicals and solvents were purchased from Kanto Chemical Co., Ltd., Wako Pure Chemical Co., Ltd., Tokyo Kasei Kogyo Co., Ltd., and Sigma-Aldrich Co., Ltd. and were used as received without further purification. ^1H and ^{13}C NMR spectra were recorded on VARIAN 300 MHz and JEOL 500 MHz spectrometers. Chemical shifts are quoted in parts per million (ppm) relative to dimethylsulfoxide (dimethylsulfoxide- d_6 , $\delta = 2.50$ ppm for ^1H and 39.52 ppm for ^{13}C). IR spectrum was recorded on a JASCO FT/IR-4600 spectrometer equipped with an attenuated total reflectance (ATR) apparatus. High-resolution mass spectrum (HRMS) was recorded on a Thermo Fisher Scientific LTQ Orbitrap XL by electron spray ionization (ESI) method. Melting point was measured with a Yanagimoto micro melting point apparatus and uncorrected. Elemental analysis was performed using a Perkin-Elmer 2400CHN elemental analyzer.

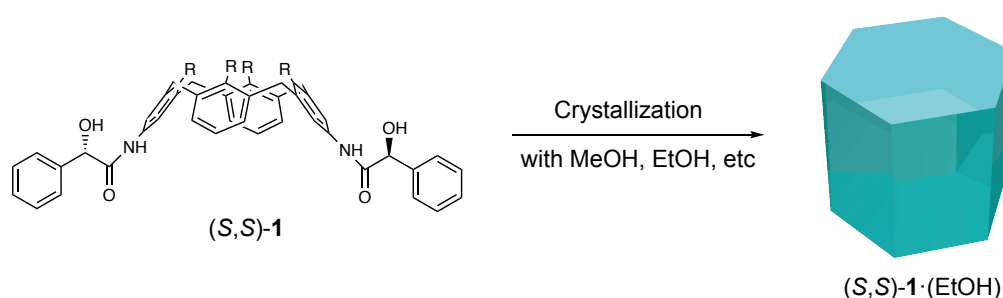
2-4-2 Synthesis of (*R,R*)-1 and (*S,S*)-1

(*R,R*)-1 and (*S,S*)-1 were synthesized as shown in Scheme 2-2-1. To a solution of (*R*)-mandelic acid (172 mg, 1.12 mmol) in dry *N,N*-dimethylformamide (20 ml), hydroxybenzotriazole (153 mg, 1.12 mmol), 1-(3-dimethylaminopropyl)-3-ethylcarbodiimide hydrochloride (217 mg, 1.12 mmol), and 5,17-diamino-25,26,27,28-tetrapropylloxycalix[4]arene (350 mg, 0.562 mmol) were added. The mixture was stirred for 3 hours at room temperature. The reaction was quenched with 1N aqueous hydrochloric acid. The organic layer was extracted with ethyl acetate, neutralized with aqueous sodium hydrogen carbonate, washed with brine and dried over anhydrous sodium sulfate. The solvent was removed under reduced pressure. The organic residue was crystallized from an ethyl acetate/toluene = 9:1 solution (15 mL) to give (*R,R*)-1 (452 mg, 0.507 mmol) as a white solid in 90% yield. (*S,S*)-1 was prepared by the same method in 83% yield.

M.P. >300 °C; ^1H NMR (500 MHz, DMSO- d_6): δ 9.64 (s, 2H), 7.51 (d, 4H, $J = 7.7$ Hz), 7.22–7.41 (m, 10H), 6.24–6.37 (m, 8H), 5.06 (d, 2H, $J = 4.8$ Hz), 4.31 (d, 4H, $J = 12.8$ Hz), 3.86 (t, 4H, $J = 7.6$ Hz), 3.64 (t, 4H, $J = 6.8$ Hz), 3.08 (d, 4H, $J = 12.8$ Hz), 1.90 (sext, 4H, $J = 7.6$ Hz), 1.84 (sext, 4H, $J = 7.2$ Hz), 1.04 (t, 6H, $J = 7.5$ Hz), 0.88 (t, 6H, J

= 7.4 Hz); ^{13}C NMR (125 MHz, $\text{DMSO-}d_6$): δ 170.5, 155.0, 153.0, 141.0, 135.6, 133.0, 132.3, 128.1, 127.5, 127.4, 126.6, 121.9, 120.4, 120.3, 76.6, 76.1, 73.9, 30.3, 23.0, 22.5, 10.5, 9.9; IR (ATR): ν 3372, 2960, 2933, 2873, 1662, 1602, 1531, 1453, 1387, 1248, 1215, 1195, 1139, 1083, 1062, 1037, 1003, 965, 877, 757, 696 cm^{-1} ; HRMS (ESI+) calcd. for $\text{C}_{56}\text{H}_{62}\text{N}_2\text{O}_8$ m/z 913.43984 $[\text{M} + \text{Na}]^+$, found m/z 913.44043; elemental analysis calcd. for $\text{C}_{56}\text{H}_{62}\text{N}_2\text{O}_8(\text{H}_2\text{O})_{0.3}$: C 75.02, H 7.04, N 3.12; found C 75.10, H 7.11, N 3.18.

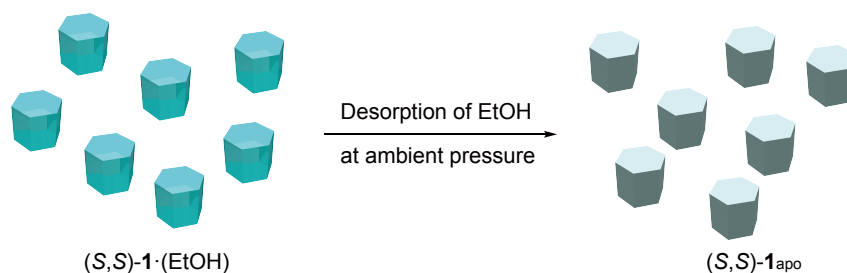
2-4-3 Preparation of cocrystals



Scheme 2-4-1. Preparation of single crystals of cocrystals. Single crystals of X-ray quality were obtained by evaporation of the solvent at room temperature. Crystals were harvested, dried and subjected to X-ray diffraction analysis.

Cocrystals of $(S,S)\text{-1}\cdot(\text{MeOH})$, $(S,S)\text{-1}\cdot(\text{EtOH})$, $(S,S)\text{-1}\cdot(1\text{-PrOH})$, $(S,S)\text{-1}\cdot(2\text{-PrOH})$, and $(S,S)\text{-1}\cdot(\text{CH}_3\text{CN})$ were obtained by crystallization of $(S,S)\text{-1}$ from methanol, ethanol, 1-propanol, 2-propanol, and acetonitrile, respectively. We also prepared *rac*-1 by crystallization of the racemic mixture of $(S,S)\text{-1}$ and $(R,R)\text{-1}$ from ethanol. The cocrystals were harvested, dried under room temperature, and subjected to single-crystal X-ray diffraction analysis at $-150\text{ }^\circ\text{C}$. The crystallographic parameters are listed in Table 2-4-1 and 2-4-2. We tried to prepare single crystals of $(R,R)\text{-1}\cdot(\text{EtOH})$ several times, but only powder was obtained. Hence, we were not able to conduct X-ray crystal structure analysis.

2-4-4 Preparation of Apohost



Scheme 2-4-2. Preparation of apohost. Finely powdered cocrystals of $(S,S)\text{-1}\cdot(\text{EtOH})$ were used.

Apohost $(S,S)\text{-1}_{\text{apo}}$ was prepared by adsorption of the entrapped EtOH guests from finely powdered cocrystals of $(S,S)\text{-1}\cdot(\text{EtOH})$ under ambient pressure at room temperature. $(S,S)\text{-1}_{\text{apo}}$ was stored in a desiccator under a N_2 atmosphere.

2-4-5 Single-crystal X-ray diffraction analysis

The X-ray crystallographic data were collected on a Bruker SMART APEX-II ULTRA CCD diffractometer using graphite-monochromatized Mo $K\alpha$ radiation ($\lambda = 0.71073 \text{ \AA}$) at $-150 \text{ }^\circ\text{C}$. Due to the low quality of the single crystals, the quality of the diffraction data except for $(S,S)\text{-1}\cdot(2\text{-PrOH})$ was not good. The diffraction data were solved with the SHELXS-2013 program and was refined by successive differential Fourier synthesis and full-matrix least-squares procedures with the SHELXL-2013 program.^[7] The absolute structures were determined based on the chirality embedded in the arms. Two of the four propyloxy chains and the phenyl ring of the mandelamide arms of $(S,S)\text{-1}$ in the cocrystals were disordered over two positions. The site occupancy factors were determined using the SHELXL-2013 program. Anisotropic thermal factors were applied to all non-hydrogen atoms except for those of the disordered guests. The hydrogen atoms on $(S,S)\text{-1}$ and $(R,R)\text{-1}$ were generated geometrically. The hydrogen atoms on all guests except 2-PrOH were not generated.

Diffuse electron densities arising from the disordered solvents in $(S,S)\text{-1}\cdot(\text{MeOH})$, $(S,S)\text{-1}\cdot(\text{EtOH})$, $(S,S)\text{-1}\cdot(1\text{-PrOH})$, and $(S,S)\text{-1}\cdot(\text{CH}_3\text{CN})$ were treated with the SQUEEZE routine in the PLATON program.^[8] The unit cells of $(S,S)\text{-1}\cdot(\text{MeOH})$, $(S,S)\text{-1}\cdot(\text{EtOH})$, $(S,S)\text{-1}\cdot(1\text{-PrOH})$, and $(S,S)\text{-1}\cdot(\text{CH}_3\text{CN})$ maintained the possible solvent accessible volume of 304, 282, 380, and 290 \AA^3 , respectively. The removed electron densities originated from disordered solvent molecules. The formula, formula weight, and density

of these crystals were known contents only. Crystallographic parameters are listed in Tables 2-4-1 and 2-4-2.

Table 2-4-1. Crystallographic parameters of (*S,S*)-1·(MeOH), (*S,S*)-1·(EtOH), and (*S,S*)-1·(1-PrOH).

Crystal	(<i>S,S</i>)-1·(MeOH)	(<i>S,S</i>)-1·(EtOH)	(<i>S,S</i>)-1·(1-PrOH)
Formula	C ₅₆ H ₆₂ N ₂ O ₈ (CH ₄ O) _{0.33}	C ₅₆ H ₆₂ N ₂ O ₈ (C ₂ H ₆ O) _{0.33}	C ₅₆ H ₆₂ N ₂ O ₈
Formula weight	901.75	906.43	891.07
Crystal system	Trigonal	Trigonal	Trigonal
Space group	<i>P</i> 3(#143)	<i>P</i> 3(#143)	<i>P</i> 3(#143)
<i>a</i> /Å	21.411(3)	21.411(2)	21.430(3)
<i>b</i> /Å	21.411(3)	21.411(2)	21.430(3)
<i>c</i> /Å	9.7370(13)	9.7990(8)	9.6863(13)
α /°	90	90	90
β /°	90	90	90
γ /°	120	120	120
<i>V</i> /Å ³	3865.57(9)	3890.47(6)	3852.38(9)
<i>Z</i>	3	3	3
<i>d</i> /g cm ⁻³	1.16	1.16	1.15
μ /mm ⁻¹	0.077	0.077	0.076
Temperature/°C	-150	-150	-150
Crystal size/mm ³	0.23 × 0.09 × 0.06	0.29 × 0.22 × 0.10	0.21 × 0.10 × 0.06
Crystal	Needle/colorless	Block/colorless	Block/colorless
Total reflections	15155	16561	13315
2 θ range/°	2.2 ≤ 2 θ ≤ 44.8	2.2 ≤ 2 θ ≤ 46.8	3.8 ≤ 2 θ ≤ 42.8
<i>h</i> range	-22 ≤ <i>h</i> ≤ 16	-23 ≤ <i>h</i> ≤ 17	-22 ≤ <i>h</i> ≤ 20
<i>k</i> range	-21 ≤ <i>k</i> ≤ 22	-23 ≤ <i>k</i> ≤ 23	-10 ≤ <i>k</i> ≤ 22
<i>l</i> range	-10 ≤ <i>l</i> ≤ 10	-10 ≤ <i>l</i> ≤ 10	-9 ≤ <i>l</i> ≤ 9
Unique	6646	7517	5749
R_{int}	0.023	0.028	0.025
Obs. reflections	5948	7005	5201
<i>R</i> ₁	0.0440	0.0460	0.0370
w <i>R</i> ₂	0.1186	0.1246	0.0920
G.O.F	1.055	1.050	1.062
Parameters used	600	670	526
$\Delta\rho_{\text{max}}/e \text{ \AA}^{-3}$	+0.577	+0.566	+0.201
$\Delta\rho_{\text{min}}/e \text{ \AA}^{-3}$	-0.209	-0.354	-0.137
CCDC	1569410	1569412	1569413

Table 2-4-2. Crystallographic parameters of (*S,S*)-**1**·(2-PrOH), (*S,S*)-**1**·(CH₃CN), and *rac*-**1**.

Crystal	(<i>S,S</i>)- 1 ·(2-PrOH)	(<i>S,S</i>)- 1 ·(CH ₃ CN)	<i>rac</i> - 1
Formula	C ₅₆ H ₆₂ N ₂ O ₈ (C ₃ H ₈ O)	C ₅₆ H ₆₂ N ₂ O ₈ (C ₂ H ₃ N) _{0.33}	C ₅₆ H ₆₂ N ₂ O ₈
Formula weight	951.17	904.76	891.07
Crystal system	Monoclinic	Trigonal	Monoclinic
Space group	<i>C2</i> (#5)	<i>P3</i> (#143)	<i>C2/c</i> (#15)
<i>a</i> /Å	30.557(2)	21.4358(15)	31.802(11)
<i>b</i> /Å	9.5507(8)	21.4358(15)	9.443(3)
<i>c</i> /Å	19.5075(15)	9.7080(8)	17.980(6)
α /°	90	90	90
β /°	113.560(1)	90	119.438(3)
γ /°	90	120	90
<i>V</i> /Å ³	5223.6(3)	3863.14(5)	4702(1)
<i>Z</i>	4	3	4
<i>d</i> /g cm ⁻³	1.21	1.17	1.26
μ /mm ⁻¹	0.081	0.077	0.083
Temperature/°C	-150	-150	-150
Crystal size/mm ³	0.30 × 0.10 × 0.05	0.11 × 0.10 × 0.10	0.07 × 0.06 × 0.03
Crystal	Platelet/colorless	Block/colorless	Platelet/colorless
Total reflections	15902	17120	6808
2θ range/°	4.4 ≤ 2θ ≤ 58.2	2.2 ≤ 2θ ≤ 46.8	4.6 ≤ 2θ ≤ 41.4
<i>h</i> range	-35 ≤ <i>h</i> ≤ 41	-17 ≤ <i>h</i> ≤ 24	-24 ≤ <i>h</i> ≤ 31
<i>k</i> range	-12 ≤ <i>k</i> ≤ 13	-17 ≤ <i>k</i> ≤ 24	-9 ≤ <i>k</i> ≤ 9
<i>l</i> range	-25 ≤ <i>l</i> ≤ 22	-9 ≤ <i>l</i> ≤ 10	-7 ≤ <i>l</i> ≤ 9
Unique	10913	7148	2418
R_{int}	0.017	0.024	0.034
Obs. reflections	9273	6615	1840
R_1	0.0456	0.0363	0.0424
wR_2	0.01123	0.0945	0.1056
G.O.F	1.049	1.044	1.072
Parameters used	667	676	301
$\Delta\rho_{\text{max}}/e \text{ \AA}^{-3}$	+0.473	+0.224	+0.266
$\Delta\rho_{\text{min}}/e \text{ \AA}^{-3}$	-0.343	-0.383	-0.201
CCDC	1569414	1569411	1569415

2-4-6 Powder X-ray diffraction analysis

X-ray powder diffraction (XRD) data were collected on a Rigaku Rint-2000 X-ray diffractometer using graphite-monochromatized Cu K α radiation ($\lambda = 1.5418 \text{ \AA}$) at room temperature with a scanning rate of $20^\circ \text{ min}^{-1}$. XRD patterns were calculated with Mercury Program ver. 3.9.

2-4-7 BET surface analysis

The surface area of (*S,S*)-**1**_{apo} was calculated by means of the N₂ adsorption–desorption isotherm at 77 K using a Belsorp max 12 N-VP-LTC MicrotracBEL. The sample was stored on a probe and heated at 50 °C for 1 h before measurement.

2-5 References

- [1] M. Makha and C. L. Raston, *Chem. Commun.* **2001**, 2470-2471.
- [2] S. Cecillon, A. Lazar, O. Danylyuk, K. Suwinska, B. Rather, M. J. Zaworotko, and A. W. Coleman, *Chem. Commun.* **2005**, 2442-2444.
- [3] a) Y. Tsunoda, M. Takatsuka, R. Sekiya, and T. Haino, *Angew. Chem. Int. Ed.* **2017**, *56*, 2613-2618. b) D. Shimoyama, H. Yamada, T. Ikeda, R. Sekiya, and T. Haino, *Eur. J. Org. Chem.* **2016**, 3300-3303. c) T. Imamura, T. Maehara, R. Sekiya, and T. Haino, *Chem. Eur. J.* **2016**, *22*, 3250-3254. d) M. Kobayashi, M. Takatsuka, R. Sekiya, and T. Haino, *Org. Biomol. Chem.* **2015**, *13*, 1647-1653. e) Y. Tsunoda, K. Fukuta, T. Imamura, R. Sekiya, T. Furuyama, N. Kobayashi, and T. Haino, *Angew. Chem. Int. Ed.* **2014**, *53*, 7243-7247. f) T. Hirao, M. Tosaka, S. Yamago, and T. Haino, *Chem. Eur. J.* **2014**, *20*, 16138-16146. g) H. Yamada, T. Ikeda, T. Mizuta, and T. Haino, *Org. Lett.* **2012**, *14*, 4510-4513. h) T. Haino, E. Hirai, Y. Fujiwara, and K. Kashihara, *Angew. Chem. Int. Ed.* **2010**, *49*, 7899-7903. i) T. Haino, H. Shio, R. Takano, and Y. Fukazawa, *Chem. Commun.* **2009**, 2481-2483.
- [4] a) R. Sekiya, Y. Yamasaki, S. Katayama, H. Shio, and T. Haino, *CrystEngComm* **2013**, *15*, 8404-8407. b) R. Sekiya, Y. Yamasaki, W. Tada, H. Shio, and T. Haino, *CrystEngComm* **2014**, *16*, 6023-6032.
- [5] G. R. Desiraju, *Angew. Chem. Int. Ed. Engl.* **1995**, *34*, 2311-2327.
- [6] T. Gruber, F. Eißmann, M. Gruner, L. G. Heinz, W. Seichter, and E. Weber, *CrystEngComm* **2014**, *16*, 3730-3736.
- [7] G. M. Sheldrick, *Acta Crystallogr. Sect. A* **2008**, *64*, 112-122.
- [8] A. L. Spek, *Acta Crystallogr. Sect. D* **2009**, *65*, 148-155.

Chapter 3

Calix[4]arene Helical Complexes with Multiple Binding Sites

The contents of this chapter have been published in slightly modified form: Y. Yamasaki, H. Shio, T. Amimoto, R. Sekiya, and T. Haino, *Chem. Eur. J.* **2018**, *24*, 8558-8568.

3-1 Introduction

Helical structures are ubiquitous in nature.^[1] The tobacco mosaic virus,^[2] F-actin,^[3] DNA,^[4] and the α -helix peptide sequence^[5] are typical examples of helical organization in a range of sizes extending from the nanometer to the micron scale. These helical structures are key structural motifs that play a crucial role in the regulation of physiological functions.^[6] Much effort has been devoted to mimicking the helical structures of biopolymers with artificial supramolecules and macromolecules to obtain unique photochemical and catalytic properties.^[7] Compared to single-chain helical structures,^[8] multistranded helical structures have been studied to a lesser extent due to the difficulties in their synthesis. Therefore, additional noncovalent interactions, such as hydrogen-bonding interactions, π - π stacking interactions, and dipole-dipole interactions, are required to direct multistranded helical organizations.^[9]

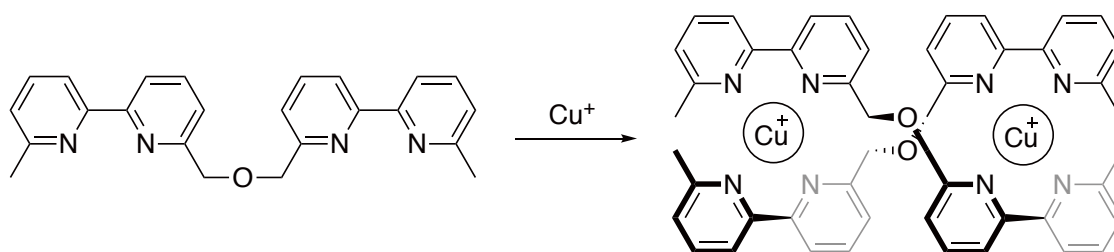


Figure 3-1-1. Schematic illustration of a metallohelicite formed through the self-organization of bipyridine ligands and copper cations.^[10]

A coordination-driven self-assembly has become an alternative approach for the construction of multistranded helical structures, the so-called “*metallohelicite*.” In a seminal work, Lehn and coworkers reported on a structurally characterized double-stranded metallohelicite using a bipyridine copper(I) coordination bond (Figure 3-1-1).^[10]

Since then, metallohelicates have been actively investigated.^[11,12] The groups of Raymond,^[13] Stack,^[14] Albrecht,^[15] and Hahn^[16] synthesized triple-stranded metallohelicates formed through the self-assembly of catechol ligands with metal ions. The labile coordination bonds permit the dynamic interconversion between the left-handed (*M*) and right-handed (*P*) forms, which can be biased by chiral guest complexation to the exterior of the helicates.^[17]

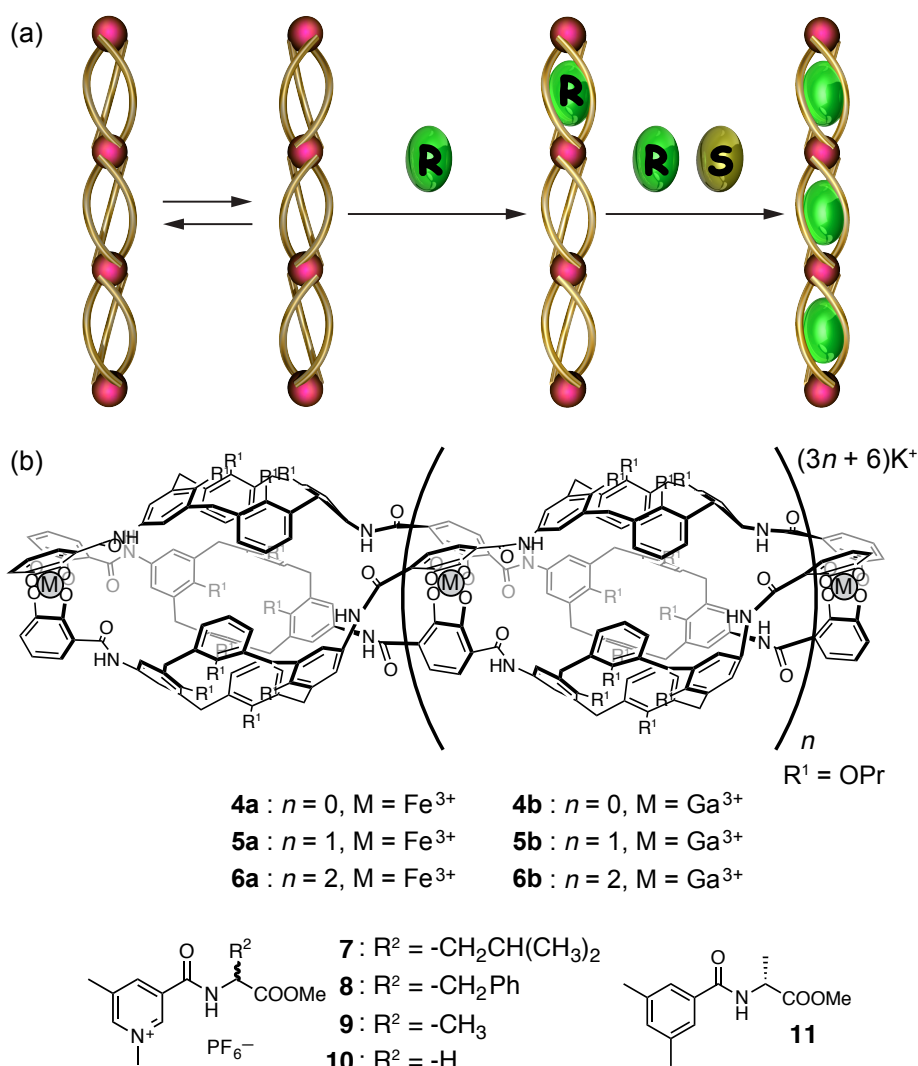


Figure 3-1-2. a) Schematic representation of the preorganization of conformationally coupled guest-binding cavities through guest encapsulation. b) Structures of the triple-stranded metallohelicates **4a**, **4b**, **5a**, **5b**, **6a**, and **6b** and the guests **7–11**.

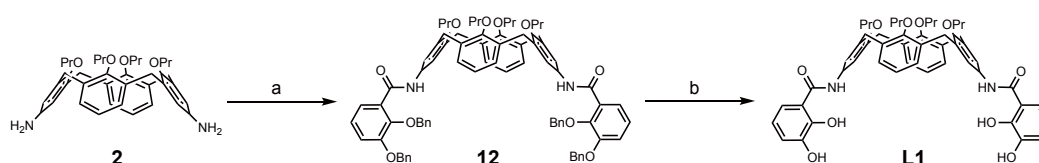
Despite the many examples of self-assembled multinuclear metallohelicates possessing conformationally coupled metal cores,^[18] a limited number of majority-rules and allosteric effects have been demonstrated in the molecular recognition of multinuclear metallohelicates due to the lack of binding cavities large enough to encapsulate the sizable chiral guests.^[19] Extended helicates possessing multiple guest-binding cavities are of particular interest (Figure 3-1-2a). The encapsulation of chiral guests in one of the cavities can bias the handedness of the helicates and simultaneously regulate the rest of the cavities to drive the positive cooperativity for the inclusion of another guest.

In this chapter, I report the synthesis and the molecular recognition of the multinuclear triple-stranded supramolecular helicates **4a**, **4b**, **5a**, **5b**, **6a**, and **6b** possessing one, two, and three guest-binding cavities (Figure 3-1-2b). The *N*-methyl pyridinium guests **7–10** bearing chiral amino acids were captured into the cavities. The conformationally coupled multiple cavities of **5a** and **6a** displayed strong cooperativity in the guest binding. The guest chirality was effectively transferred to the helical senses of the helicates through the steric interaction between the cavities and the stereogenic centers of the guests. Majority-rules effects were found in the guest binding for the helicates **5a** and **6a**.

3-2 Results and Discussion

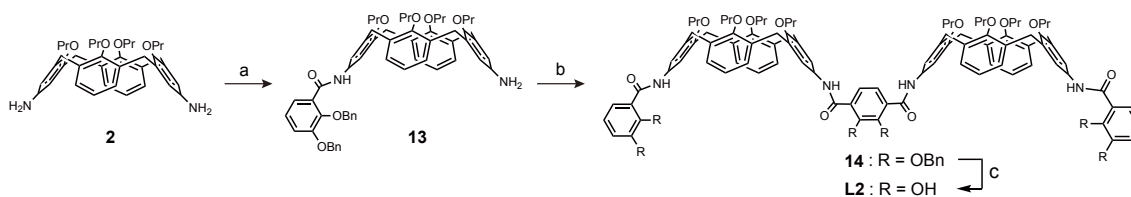
3-2-1 Synthesis of the calix[4]arene ligands

The syntheses of ligands **L1**–**L3** are outlined in the following schemes. Ligand **L1** was prepared from 5,17-diaminocalix[4]arene (**2**)^[21] in accordance with our previously reported method.^[20] The condensation reaction of **2** and 2,3-bis(benzyloxy)benzoic acid gave the protected calix[4]arene **12**, which was deprotected to afford the monomeric ligand **L1** in good yield (Scheme 3-2-1).



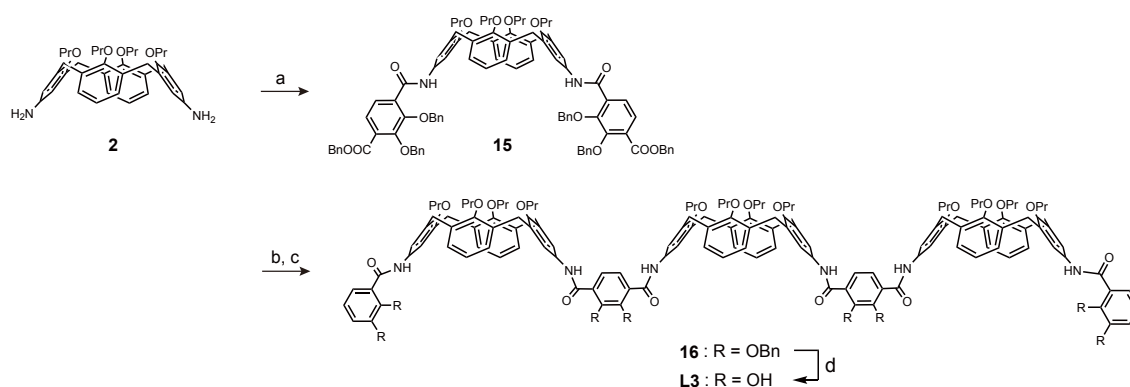
Scheme 3-2-1. Synthesis of **L1**. Reagents and conditions: a) 2,3-bis(benzyloxy)benzoic acid, *N*'-(3-dimethylaminopropyl)-*N*-ethylcarbodiimide (EDC), 1-hydroxybenzotriazole (HOBt), DMF, 85 %; b) H_2 , Pd/C, 25 % AcOEt–THF, 89 %.

Ligand **L2** was also synthesized from **13** (Scheme 3-2-2). The mono-substituted calix[4]arene **13** was produced through the condensation of **2** with one equivalent of 2,3-bis(benzyloxy)benzoic acid. The treatment of **13** with 0.5 equivalents of 2,3-bis(benzyloxy)terephthalic acid gave bis(calix[4]arene) **14**, which was subjected to hydrogenolysis in the presence of Pd/C under a hydrogen atmosphere to furnish **L2** in good yield.



Scheme 3-2-2. Synthesis of **L2**. Reagents and conditions: a) 2,3-bis(benzyloxy)benzoic acid, EDC, HOBt, DMF, 21 %; b) 2,3-bis-(benzyloxy)terephthalic acid, EDC, HOBt, DMF, 77 %; c) H_2 , Pd/C, 25 % AcOEt–THF, 88 %;

Ligand **L3** was also prepared from compound **2** (Scheme 3-2-3). The condensation reaction of **2** with two equivalents of 2,3-bis(benzyloxy)telephthalic acid monobenzyl ester afforded the disubstituted calix[4]arene **15** in a 63 % yield. The hydrolysis of **15** with LiOH and the following condensation reaction with two equivalents of **13** resulted in the triscalix[4]arene **16** in a 60 % yield. The hydrogenolysis of **16** in the presence of Pd/C under a hydrogen atmosphere afforded **L3** in a 67 % yield.



Scheme 3-2-3. Synthesis of ligand **L3**. Reagents and conditions: a) 2,3-bis(benzyloxy)telephthalic acid monobenzyl ester, EDC, HOBT, DMF, 63 %; b) LiOH, 30 % H₂O–THF, 69 %; c) **13**, EDC, HOBT, DMF, 87 %; d) H₂, Pd/C, THF, 67 %. Bn = benzyl.

The characterization of the new molecules were carried out by ¹H, ¹³C, and 2D NMR spectroscopy, IR spectroscopy, and high-resolution mass spectrometry. Elemental analysis confirmed their purity. These data are shown in **Section 3-4, Experimental Section**.

3-2-2 Coordination-driven self-assembly

The deprotonation of **L1**, **L2**, and **L3** by KOH in methanol gave the anionic ligands L1^{2-} , L2^{3-} , and L3^{4-} , which were treated with $[\text{Fe}(\text{acac})_3]$ (acac=acetylacetonate) or $[\text{Ga}(\text{acac})_3]$. The absorptions of $\text{K}_2\text{L1}$, $\text{K}_3\text{L2}$, and $\text{K}_4\text{L3}$ appeared approximately at $\lambda = 290$ nm (Figures 3-2-1a,b,c).

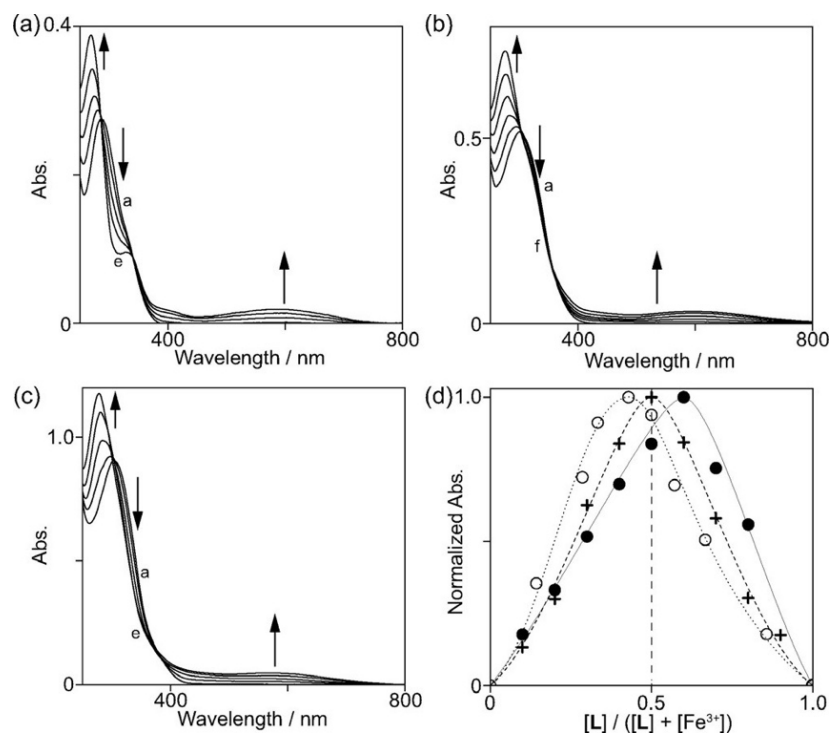


Figure 3-2-1. Changes in the UV/Vis absorption spectra of a) $\text{K}_2\text{L1}$ ($2.0 \times 10^{-5} \text{ mol L}^{-1}$) with $[\text{Fe}(\text{acac})_3]$ (a–e: 0.0, 0.34, 0.68, 1.02, $1.34 \times 10^{-5} \text{ mol L}^{-1}$), b) $\text{K}_3\text{L2}$ ($2.0 \times 10^{-5} \text{ mol L}^{-1}$) with $[\text{Fe}(\text{acac})_3]$ (a–f: 0.0, 0.4, 0.8, 1.2, 1.6, $2.0 \times 10^{-5} \text{ mol L}^{-1}$), and c) $\text{K}_4\text{L3}$ ($2.0 \times 10^{-5} \text{ mol L}^{-1}$) with $[\text{Fe}(\text{acac})_3]$ (a–e: 0.0, 0.67, 1.3, 2.0, $2.7 \times 10^{-5} \text{ mol L}^{-1}$) in methanol at 298 K. d) Job plots of $\text{K}_2\text{L1}$ (filled circles), $\text{K}_3\text{L2}$ (crosses), and $\text{K}_4\text{L3}$ (open circles) with $[\text{Fe}(\text{acac})_3]$ in methanol. The total concentration of the ligands and $[\text{Fe}(\text{acac})_3]$ was maintained at $2 \times 10^{-5} \text{ mol L}^{-1}$.

The addition of $[\text{Fe}(\text{acac})_3]$ decreased the intensity of the absorption bands, and new absorption bands emerged in the ranges of $\lambda = 270\text{--}280$ and $520\text{--}600$ nm with isosbestic points for L1^{2-} , L2^{3-} , and L3^{4-} . The visible absorption bands correspond to ligand-to-metal charge transfer (LMCT) in the $[\text{tris}(\text{catecholato})\text{iron}(\text{III})]^{3-}$ complexes, which is responsible for the formation of the self-assembled metallohelicates.^[22] The metal–ligand stoichiometric ratios for **4a**, **5a**, and **6a** were determined by Job plots (Figure 3-2-1d).

The plots showed peaks appearing at mole ratios of 3:2, 1:1, and 3:4 for K_2L1 , K_3L2 , and K_4L3 , respectively, confirming the formation of the triple-stranded helicates **4a**, **5a**, and **6a**.

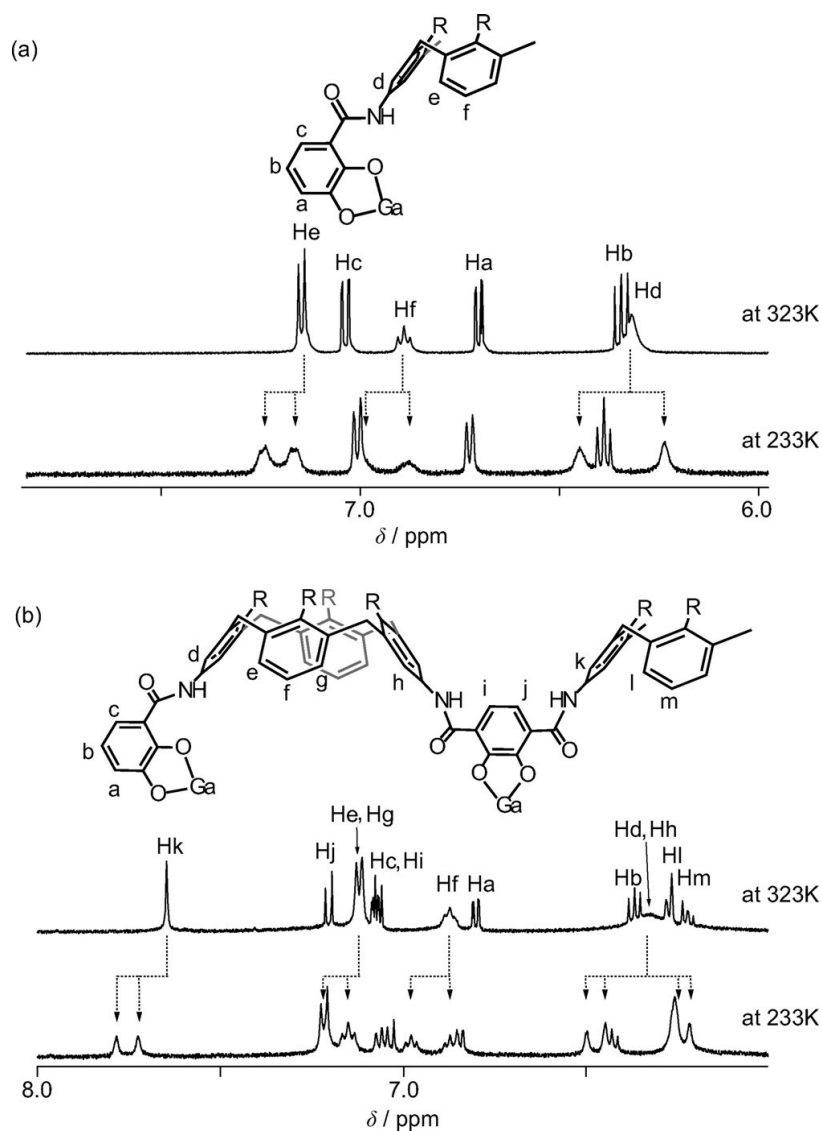


Figure 3-2-2. ^1H NMR spectra of a) **4b** and b) **6b** in methanol- d_4 .

To gain detailed structural insights into the metallohelicates **4a–6a** by using ^1H NMR spectroscopy, the Ga^{3+} ion was employed instead of the Fe^{3+} ion to avoid paramagnetic line broadening. Figure 3-2-2 displays the sharp ^1H NMR spectra of helicates **4b** and **6b** at 323 K, whereas **5b** gave rise to an ill-defined broad NMR spectrum (Figure 3-2-4). The ^1H NMR spectrum of **4b** showed the presence of a single compound in the solution. The aromatic protons Ha–Hf appeared as fairly sharp signals, showing the signatures of a D_{3h} -

symmetric structure due to the rapid exchange between the Δ,Δ -form and the Λ,Λ -form.^[16a]

The ^1H NMR spectrum was temperature-dependent. Upon cooling the solution, the interconversion of the Δ,Δ - and Λ,Λ -forms became slow on the NMR timescale, and they coalesce at $T_c = 273$ K. **4b** exhibited two sets of the aromatic calixarene protons Hd–Hf at 233 K. The energetic barrier of interconversion was calculated formula (1).^[13c]

$$\Delta G^\ddagger = 19.13 \times T_c \left(9.62 + \log \left(\frac{T}{\Delta\delta} \right) \right) \quad \dots (1)$$

The energetic barrier of **4b** was 52.3 kJ mol^{-1} , determined at the coalescence temperature (T_c) of 273 K, and $\Delta\delta = 110$ Hz at 233 K for Hd (Figure 3-2-3).

The ^1H NMR spectrum of the metallohelicate **6b** at 323 K also suggests the D_{3h} symmetry of the structure. Although the signals of the catechol protons Ha–Hc, Hi, and Hj were well resolved and sharp at 323 K, the signals of the aromatic calixarene protons Hd, Hf, and Hh were fairly broadened, implying that the interconversion process between the helical $\Delta,\Delta,\Delta,\Delta$ -form and the $\Lambda,\Lambda,\Lambda,\Lambda$ -form is slower than that of **4b**. Cooling the solution led to two sets of aromatic calixarene protons Hd–Hh and Hk–Hm below 300 K. The energetic barrier of 57.2 kJ mol^{-1} with $\Delta\delta = 75$ Hz at 233 K was determined at a T_c of 293 K for Hd (Figure 3-2-5).

The activation energy of **6b** is only 1.1 times as large as that of **4b**, although the number of the metal cores for **6b** is double that of **4b**. These findings suggest that each tris(catecholato)gallium(III) core in **6b** may be fairly independent in the interconversion process between the Δ -form and the Λ -form, as reported by Raymond and coworkers.^[13d]

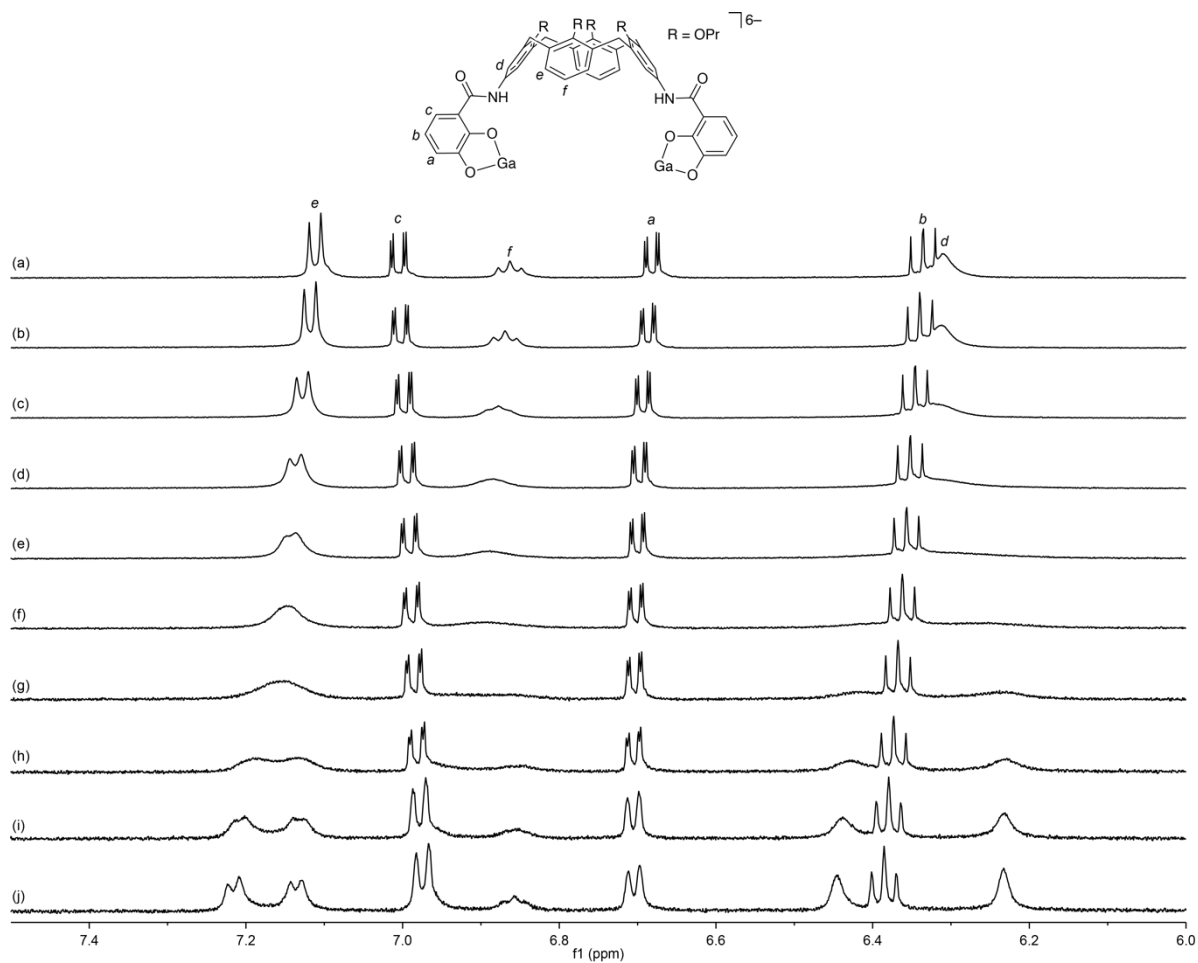


Figure 3-2-3. Variable temperature ^1H NMR spectra (methanol- d_4 , 500 MHz) of **4b** at a) 323, b) 313, c) 297, d) 283, e) 273, f) 263, g) 253, h) 243, i) 233, and j) 223 K.

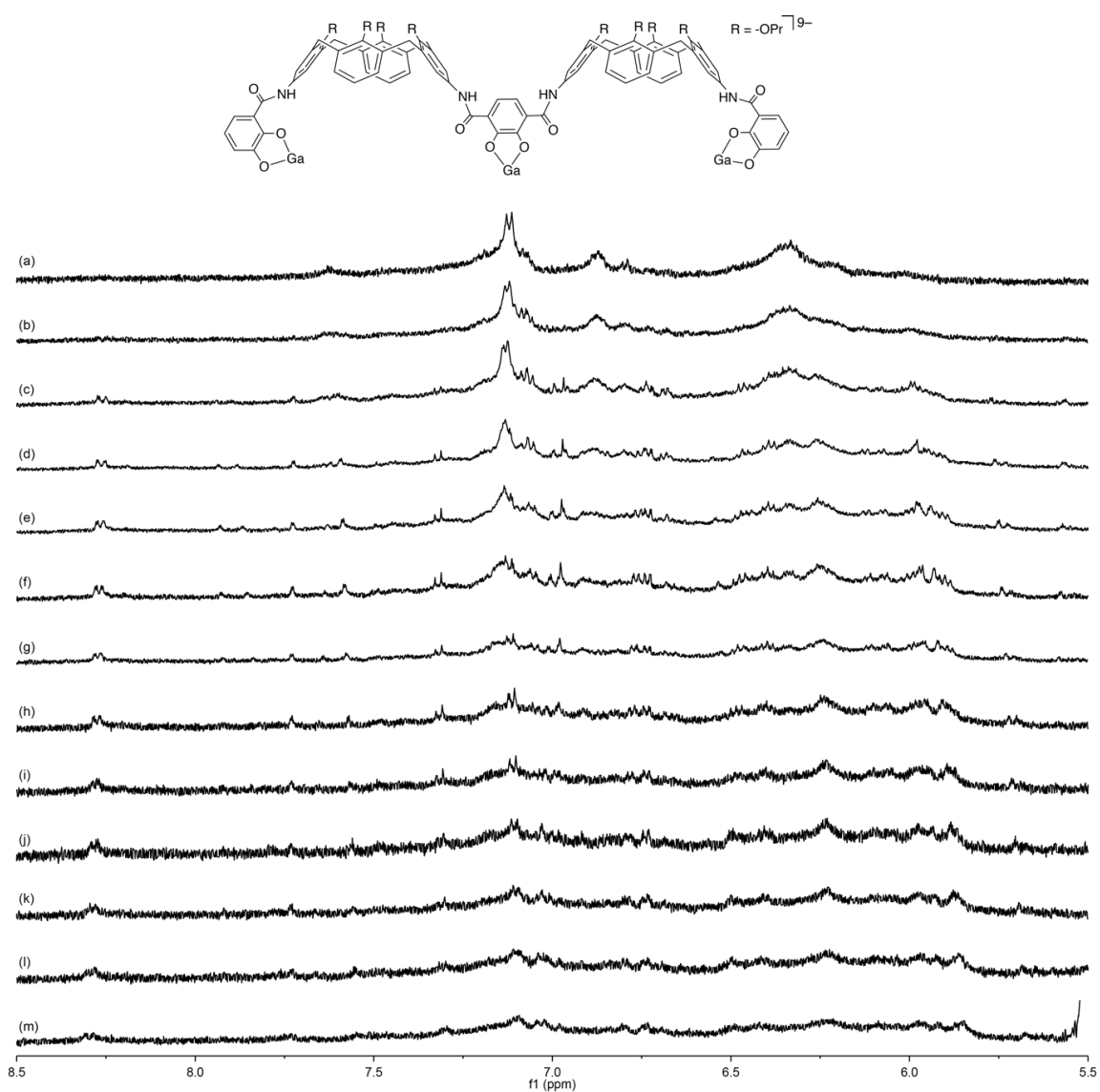


Figure 3-2-4. Variable temperature ^1H NMR spectra (methanol- d_4 , 500 MHz) of **5b** at a) 333, b) 323, c) 313, d) 303, e) 293, f) 283, g) 273, h) 263, i) 253, j) 243, k) 233, l) 223, and m) 213 K.

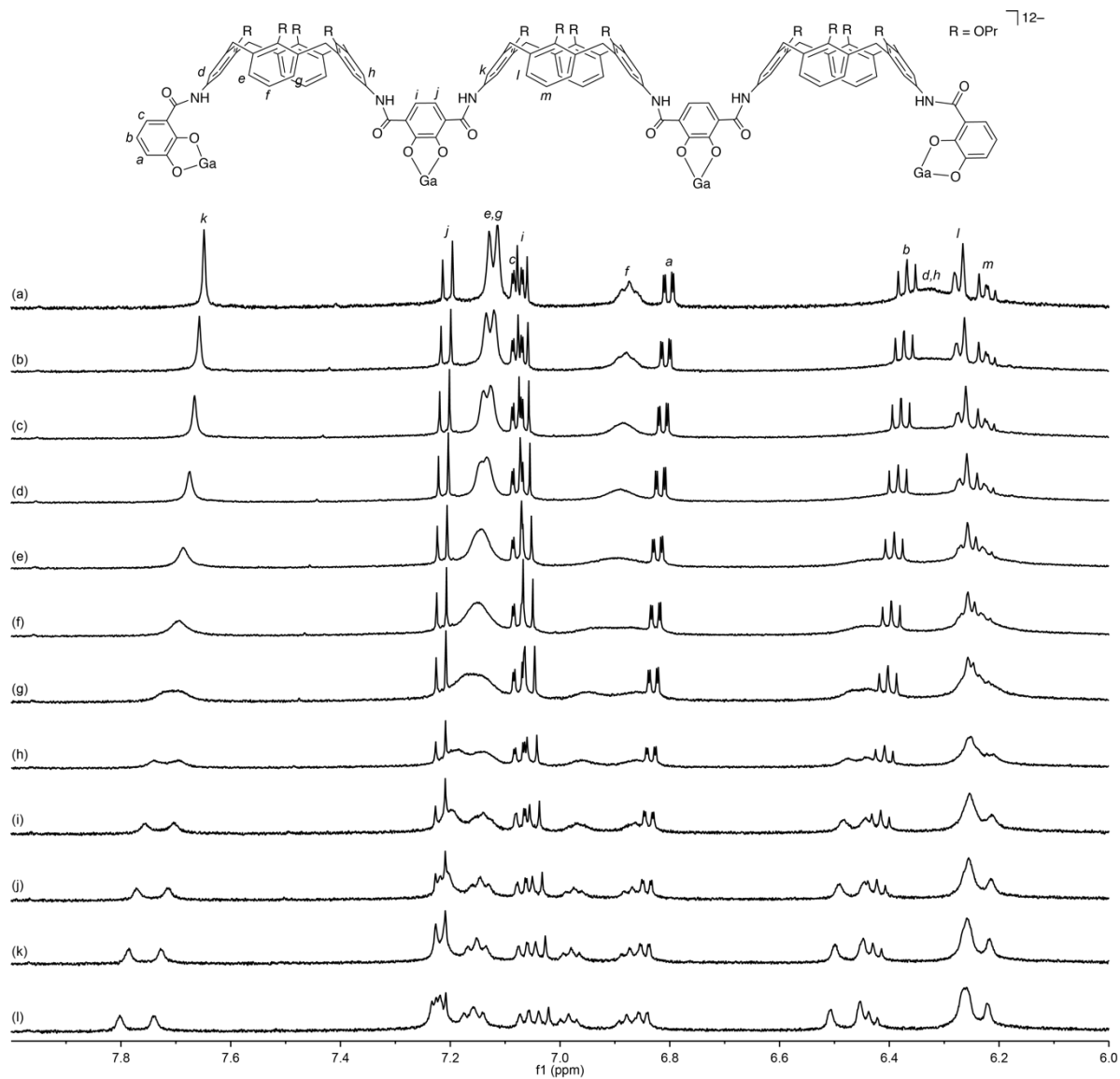


Figure 3-2-5. Variable temperature ^1H NMR spectra (methanol- d_4 , 500 MHz) of **6b** at a) 323, b) 313, c) 303, d) 293, e) 283, f) 273, g) 263, h) 253, i) 243, j) 233, k) 223, and l) 213 K.

Diffusion-ordered NMR spectroscopy (DOSY) is known to be useful for the examination of the size of molecular assemblies in solution. The use of the DOSY technique allows us to obtain molecular diffusion coefficients that estimate the hydrodynamic radius of either a molecule or a molecular assembly.^[23] Figure 3-2-6 shows the 2D DOSY spectra of ligands **L1–L3** and the metallohelicates **4b–6b**. One sets of signals was observed, showing that the self-assembly of the ligands with the Ga³⁺ ions resulted in uniform complexes without any polymeric aggregates.

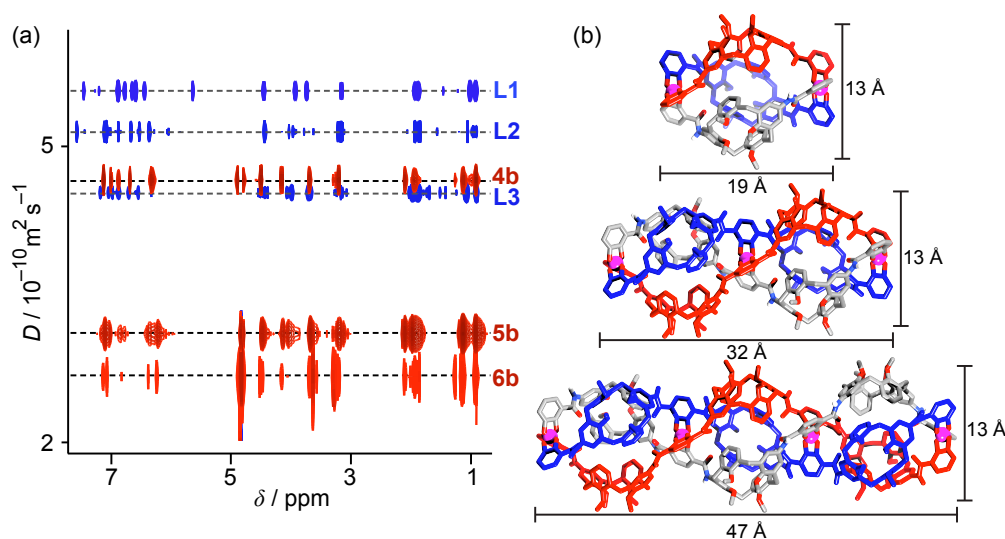


Figure 3-2-6. a) 2D DOSY spectra of **L1**, **L2**, **L3**, **4b**, **5b**, and **6b** in methanol-*d*₄ at ambient temperature. b) Energy-minimized structures of (*M*)-**4b**, (*M*)-**5b**, and (*M*)-**6b**. Hydrogen atoms are omitted for clarity.

The diffusion coefficients of $4.07(2) \times 10^{-10}$, $3.06(3) \times 10^{-10}$, and $2.366(6) \times 10^{-10} \text{ m}^2 \text{ s}^{-1}$ calculated for **4b**, **5b**, and **6b** at 293K, respectively, are obviously smaller than those of $6.64(6) \times 10^{-10}$, $5.82(8) \times 10^{-10}$, and $3.95(6) \times 10^{-10} \text{ m}^2 \text{ s}^{-1}$ found for **L1**, **L2**, and **L3**, respectively. These findings confirm that the metallohelicates **4b**, **5b**, and **6b** are large compared to the corresponding ligands. Assuming that all helicates are spherical, the hydrodynamic radii (r_h) of the metallohelicates **4b**, **5b**, and **6b** were calculated from the diffusion coefficients by the Stokes–Einstein equation, (2),

$$D = \frac{k_B T}{6\pi\eta r_h} \quad \dots (2)$$

where k_B is the Boltzmann constant and η is the viscosity of methanol at 293 K. However, the hard-sphere approximation may be valid only for the helicate **4b**, whereas helicates **5b** and **6b** are obviously nonspherical. The modified Stokes–Einstein equation, (3),

$$D = \frac{k_B T}{cf(p)\pi\eta r_h^X} \quad \dots (3)$$

where c is a size correlation factor and $f(p)$ is a shape correlation factor, takes into account the deviations from the hard-sphere approximation.^[24] These factors predict equation (4) semiempirically, as improved by Chen.^[25a]

$$cf(p) = \frac{6}{\left(1 + 0.695 \left(\frac{r_{solv}}{r_h^X}\right)^{2.234}\right)} \quad \dots (4)$$

r_h^X is the corrected hydrodynamic radii of the helicates, and r_{solv} is the hydrodynamic radius of the solvent. Equation (3) is combined with equation (4) to yield equation (5) that gives rise to r_h^X .

$$D = \left(\frac{k_B T}{6\pi\eta r_h^X}\right) \left(1 + 0.695 \left(\frac{r_{solv}}{r_h^X}\right)^{2.234}\right) \quad \dots (5)$$

The values obtained are listed in Table 3-2-1. When the helicates are considered as prolate ellipsoids, their diffusion coefficients can provide the ellipsoidal dimensions with the shape correction factors $f(p)$, resulting in the geometric factor p , which is a ratio of the semimajor axis a to the semiminor axis b .^[25]

Table 3-2-1. Diffusion coefficients (D), corrected hydrodynamic radii (r_h^X), equivalent radii (r_{eq}), shape factors [$f(p)$], geometric factors (p), and ratios of the semimajor axes (a) and the semiminor axes (b) of the optimized structures of **4b**, **5b**, and **6b**.

Helicate	D [$10^{-10} \text{ m}^2 \text{ s}^{-1}$]	r_h^X [\AA]	r_{eq} [\AA]	$f(p)$	p	a/b
4b	4.07(2)	9.08	8.98	0.99	1.4	1.5
5b	3.06(3)	12.0	11.1	0.93	2.4	2.5
6b	2.366(6)	15.4	12.7	0.83	4.4	3.6

Molecular mechanics calculations of a supramolecular complex enable the visualization of its size, shape, and dimensions. For greater insight, the structures of the metallohelicates **4b**, **5b**, and **6b** were calculated by MacroModel V9.1 by using the AMBER* force field.^[26] Figure 3-2-6b displays the energy-minimized structures of **4b**,

5b, and **6b**, which are obviously cigar-like ellipsoids. The stable structures of the triple-stranded metallohelicates possess three-fold rotational axes through the Ga^{3+} centers. Each monomer unit was twisted with an angle of approximately 155° , giving rise to pseudo D_3 -symmetric triple-stranded structures. Each metal ion adopts the Δ configuration in the (*P*) conformers and the Λ configuration in the (*M*) conformers. To compare the corrected hydrodynamic radii, the spherical equivalent radii (r_{eq}) were calculated based on the molecular volumes of the optimized structures (Table 3-2-1). The calculated structures of the helicates are used for the Connolly volume V estimated by SwissPDBViewer, which is built with a solvent-accessible surface.^[*] The spherical equivalent radii (r_{eq}) were calculated by using equation (6).

$$r_{\text{eq}} = \sqrt[3]{\frac{3V}{4\pi}} \quad \dots (6)$$

The r_{h}^{X} and r_{eq} values are related by the shape correlation factor $f(p)$ (equation (7)) for nonspherical molecules.^[25b]

$$f(p) = \frac{r_{\text{eq}}}{r_{\text{h}}^{\text{X}}} \quad \dots (7)$$

When the helicates are considered as prolate ellipsoids, they characterized by the geometrical factor $p = a/b$, whereby a is the semimajor axis and b is the semiminor axis of the ellipsoid. The final geometrical factors $f(p)$ were determined by fitting equation, (7),

$$f(p) = p^{\frac{1}{3}}(p^2 - 1)^{-\frac{1}{2}} \ln \left[p + (p^2 - 1)^{\frac{1}{2}} \right] \quad \dots (8)$$

and the values are shown in Table 3-2-1. For all helicates, the r_{eq} values are slightly smaller than the r_{h}^{X} values, which yields shape factors $[f(p)]$ of 0.99–0.83 and geometric factors (p) of 1.4–4.4 for **4b**, **5b**, and **6b**. The molecular dimensions of **4b**, **5b**, and **6b** are shown in Figure 3-2-6b. The ratios between the semimajor and semiminor axes for the optimized structures are in fair agreement with the geometric factors. Accordingly, helicates **4b**, **5b**, and **6b** behave in solution as cigar-like ellipsoids with dimensions very similar to those found in the optimized structures.

Mass spectrometry provides evidence for the formation of the metallohelicates in the gas phase.^[27] The metallohelicates **4a**, **4b**, **5a**, **5b**, **6a**, and **6b** can be negatively charged upon being infused into the mass analyzer. The ESI-MS spectra of **4a** and **4b** gave rise to

the most abundant peaks of 1394.02 and 1408.01, corresponding to $[4a - 6K^+ + 4H^+]^{2-}$ and $[4b - 6K^+ + 4H^+]^{2-}$, respectively (Figure 3-2-7).

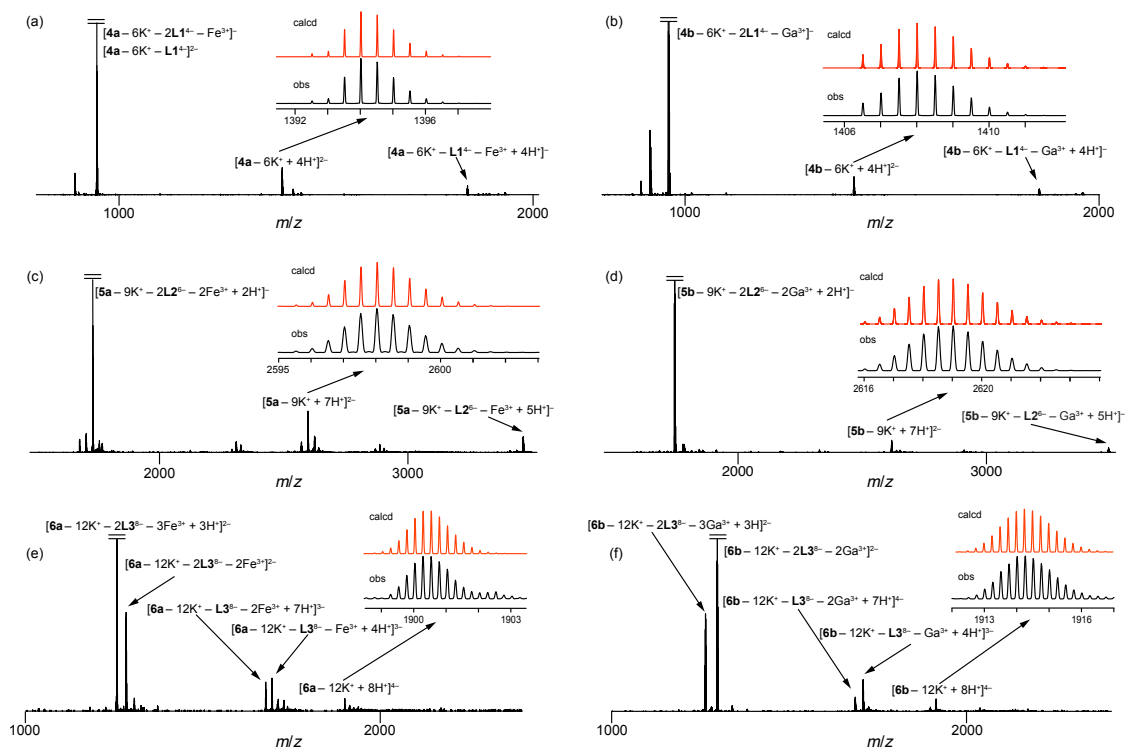


Figure 3-2-7. ESI-MS spectra of a) **4a**, b) **4b**, c) **5a**, d) **5b**, e) **6a**, and f) **6b**. Insets indicate the calculated (red) and observed (black) isotopic distributions.

The ligand fragmentation occurred easily in the gas phase, resulting in $[4a/4b - 6K^+ - L1^4 - M^{3+} + 4H^+]^-$ and $[4a/4b - 6K^+ - 2L1^4 - M^{3+}]^-$. The helicates **5a** and **5b** were successfully ionized to produce the divalent molecular ions $[5a - 9K^+ + 7H^+]^{2-}$ and $[5b - 9K^+ + 7H^+]^{2-}$, emerging at 2598.03 and 2619.02, respectively, with a certain amount of the fragment ions $[5a/5b - 9K^+ - L2^{6-} - M^{3+} + 5H^+]^-$ and $[5a/5b - 9K^+ - 2L2^{6-} - 2M^{3+} + 2H^+]^-$. In the ESI-MS spectra of **6a** and **6b**, the tetravalent molecular ions of **6a** and **6b** were successfully detected as weak peaks of 1900.52 and 1914.26, corresponding to $[6a - 12K^+ + 8H^+]^{4-}$ and $[6b - 12K^+ + 8H^+]^{4-}$, respectively. However, the ligand-fragmented ions $[6a/6b - 12K^+ - L3^{8-} - M^{3+} + 4H^+]^{3-}$, $[6a/6b - 12K^+ - L3^{8-} - 2M^{3+} + 7H^+]^{3-}$, $[6a/6b - 12K^+ - 2L3^{8-} - 2M^{3+}]^{2-}$, and $[6a/6b - 12K^+ - 2L3^{8-} - 3M^{3+} + 3H^+]^{2-}$ were simultaneously detected, most likely due to the highly charged nature of the molecular ions. All ESI-MS measurements provided well-resolved peaks of the molecular ions and their ligand-fragmented ions, which was in good agreement with their calculated isotope

distributions, confirming the formation of the metallohelicates in the gas phase. The ligand-fragmented ions observed in all MS spectra suggest that the metallohelicates are most likely labile due to the reversible coordination bonds of the tris(catecholato)iron or the gallium complex.

3-2-3 Guest complexation

To examine the formation of host–guest complexes, methyl pyridinium guests **7–10** bearing amino acid esters were employed. A ^1H NMR titration experiment of (*R*)-**4** was carried out with **4b** (Figure 3-2-8a). Upon the addition of **4b**, the signals of the aromatic protons Hb, Hc, and He and the two methyl protons Ha and Hd of the pyridine ring exhibited upfield shifts, whereas no upfield shift of the signal of the methyl ester group was observed (Table 3-2-2). These results indicate that the N-methyl pyridinium ring was selectively accommodated within the cavity of **4b**, providing a shielding effect to the aromatic rings of the three calix[4]arene units, and the ester methyl group remained outside the cavity. The acidic $\text{N}^+\text{-CH}_3$ protons of (*R*)-**7** should participate in the host–guest complexation through intermolecular CH/π interactions in the π -basic cavity. To confirm the contribution of the CH/π interaction, the reference guest **11**, which does not possess any positively charged methyl moieties on the aromatic ring, was titrated with **4b** instead of the guest (*R*)-**7**. No change was observed in the chemical shifts of the protons; therefore, the intermolecular CH/π interaction of the acidic $\text{N}^+\text{-CH}_3$ protons within the cavity of **4b** primarily drives the host–guest complexation. The multiple guest-binding cavities of **5b** and **6b** encapsulated the methyl pyridinium ring of (*R*)-**7** (Figure 3-2-8b). The pyridinium signals of the protons Hb and Hc shifted upfield in the presence of **4b**, **5b**, and **6b**, whereas the upfield shifts for the signal of the methyl ester proton Hf were negligible.

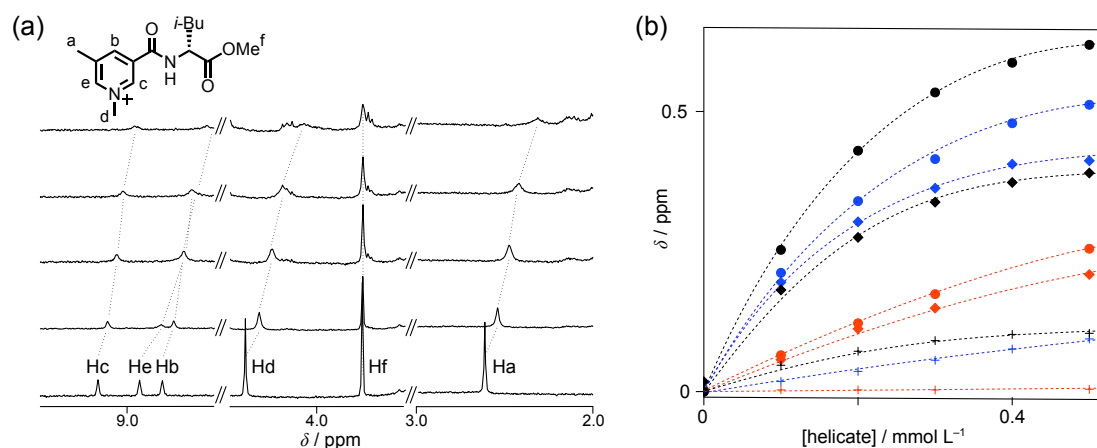


Figure 3-2-8. a) ^1H NMR spectra of the guest (*R*)-**7** ($1.0 \times 10^{-3} \text{ mol L}^{-1}$) in the presence of **4b** (from bottom to top: 0, 1.0, 2.0, 3.0, $5.0 \times 10^{-4} \text{ mol L}^{-1}$) at 298 K in methanol- d_4 . b) Chemical shift changes of the protons Hb (filled circles), Hc (filled rhombuses), and Hf (crosses) of (*R*)-**7** ($1.0 \times 10^{-3} \text{ mol L}^{-1}$) in the presence of helicites **4b** (red), **5b** (blue), and **6b** (black).

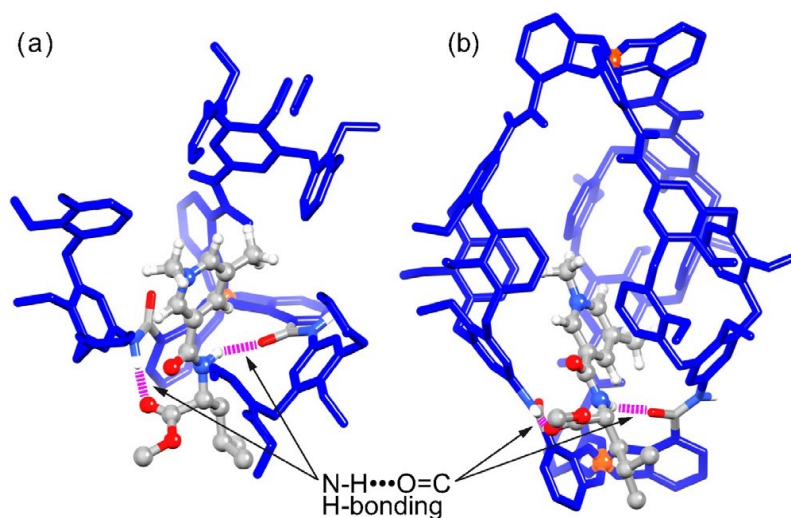


Figure 3-2-9. a) Top view and b) side view of the calculated structure of the host-guest complex (*R*)-**7C4b** by MacroModel Ver. 9.1 using the AMBER* force field.

Table 3-2-2. Chemical shift changes of protons (H_a - H_f) on (*R*)-**7** after the addition of 0.5 equiv. of the metallohelicates.

Helicate	H_a	H_b	H_c	H_d	H_e	H_f
4b	-0.306	-0.255	-0.209	-0.336	-0.525	-0.004
5b	-0.864	-0.512	-0.412	-0.721	- [a]	-0.094
6b	- [a]	-0.619	-0.616	- [a]	- [a]	-0.104

[a] The signal was not detected due to the overlapping with the signal of the metallohelicate.

Molecular mechanics calculations are helpful for understanding the intermolecular association of the host-guest complex (*R*)-**7**⋅**4b**. A conformational search was carried out using a low-mode search algorithm^[28] to generate 1000 initial geometries, which were then optimized using the AMBER* force field. Two low-energy host-guest structures with similar characteristics are found to be within 12 kJ mol⁻¹ of each other.

The most stable conformation is shown in Figure 3-2-9. The *N*-methyl group stays in one of the calixarene cavities, which evidences the presence of CH/ π interactions. The guest amide N-H group is hydrogen-bonded to one of the amide carbonyl groups of the host, and the ester carbonyl group of the guest is directed to the N-H proton of the host to form a hydrogen bond. These attractive intermolecular CH/ π and hydrogen-bonding interactions most likely drive the intermolecular association between **4b** and the cationic guests. In addition, the stereogenic carbon atom of the guest is located on the catechol ring. This close contact of the stereogenic carbon atom to the stereogenic metal center of **4b** most likely drives the one-handed helical structure of **4b**.

3-2-4 Determination of binding constants

To discuss the cooperative effects of the conformationally coupled multiple cavities, the guest binding abilities of **4a**, **5a**, and **6a** were evaluated using UV/Vis absorption spectroscopy. The tris(catecholato)iron(III) cores provide an LMCT band in the visible region, which was quite sensitive to guest binding (Figures 3-2-10a,b,c).

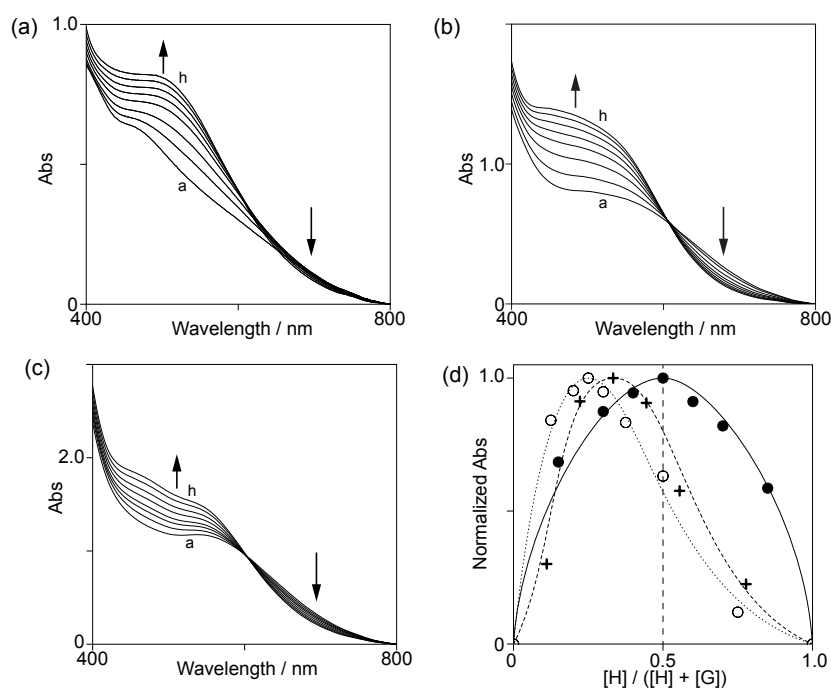


Figure 3-2-10. UV/Vis absorption spectra of a) **4a** (1.0×10^{-4} mol L $^{-1}$), b) **5a** (1.0×10^{-4} mol L $^{-1}$), and c) **6a** (1.0×10^{-4} mol L $^{-1}$) upon the addition of (*R*)-**7** (a–h: a) 0.0, 0.98, 1.9, 3.3, 4.6, 6.1, 8.0, 10.0×10^{-4} mol L $^{-1}$; b) 0.0, 0.98, 1.9, 2.8, 3.7, 5.0, 6.9, 10.0×10^{-4} mol L $^{-1}$; c) 0.0, 1.9, 3.2, 4.1, 5.3, 6.5, 8.0, 10.0×10^{-4} mol L $^{-1}$) in methanol at 298 K. d) Job plots of **4a** (filled circles), **5a** (crosses), and **6a** (open circles) with (*R*)-**7** in methanol. The total concentration of the helicates and (*R*)-**7** was maintained to be 1.0×10^{-4} mol L $^{-1}$.

When (*R*)-**7** was added into solutions of **4a**, **5a**, and **6a**, the broad band at approximately $\lambda = 700$ nm gradually decreased, and new bands at approximately $\lambda = 500$ nm emerged with isosbestic points at approximately $\lambda = 600$ nm. The stoichiometries for the host–guest complexes of **4a**, **5a**, and **6a** with (*R*)-**7** were determined using Job plots (Figure 3-2-10d). The host–guest ratios of 1:1, 1:2, and 1:3 for **4a**, **5a**, and **6a**, respectively, are perfectly matched with the number of guest binding cavities of the helicates; thereby, all cavities of the metallohelicates are capable of encapsulating guest molecules. For guests **8-10**, the host-guest ratios are also matched (Figure 3-2-11).

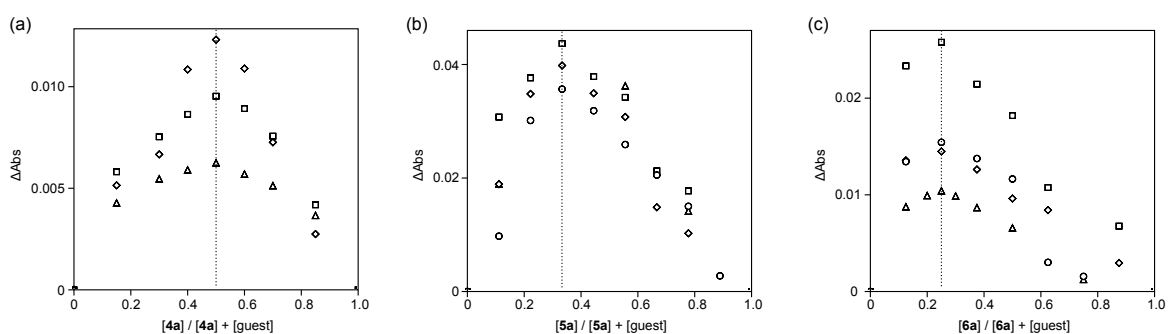


Figure 3-2-11. Job plots of a) **4a**, b) **5a**, and c) **6a** with (*R*)-**7** (open triangle), (*R*)-**8** (open square), (*R*)-**9** (open rhombus), and **10** (open circle).

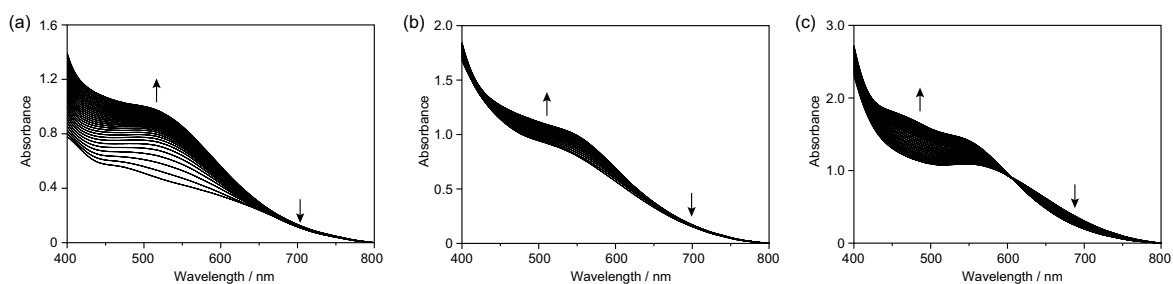


Figure 3-2-12. UV/vis titration experiments of a) **4a**, b) **5a**, and c) **6a** in the presence of (*R*)-**8** in methanol at 298 K. The concentrations of **4a**, **5a**, and **6a** were maintained to be 1.0×10^{-4} mol L⁻¹.

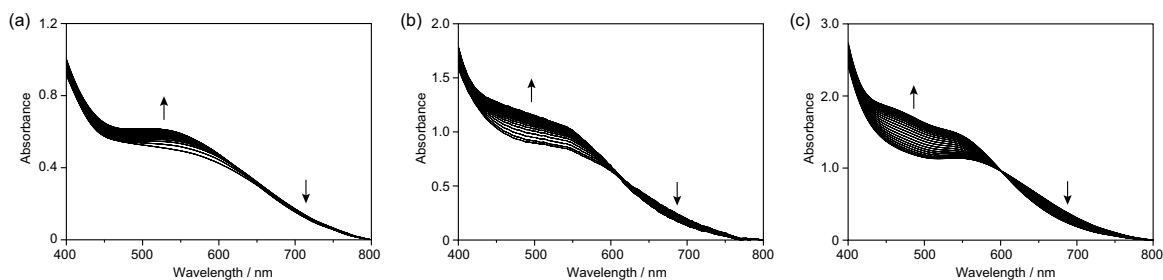


Figure 3-2-13. UV/vis titration experiments of a) **4a**, b) **5a**, and c) **6a** in the presence of (*R*)-**9** in methanol at 298 K. The concentrations of **4a**, **5a**, and **6a** were maintained to be 1.0×10^{-4} mol L⁻¹.

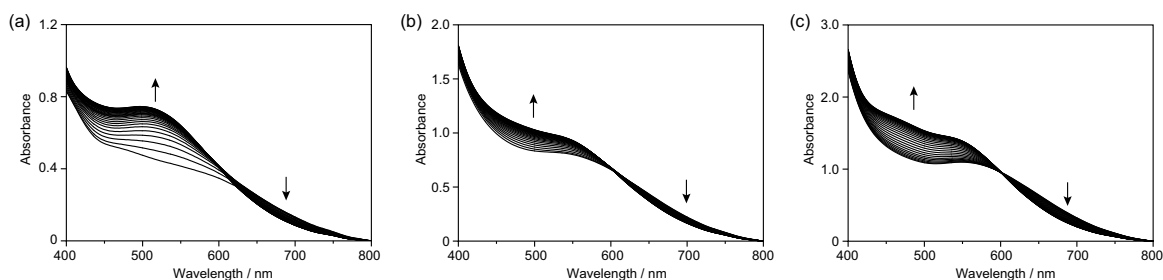


Figure 3-2-14. UV/vis titration experiments of a) **4a**, b) **5a**, and c) **6a** in the presence of **10** in methanol at 298 K. The concentrations of **4a**, **5a**, and **6a** were maintained to be $1.0 \times 10^{-4} \text{ mol L}^{-1}$.

The experimental spectra were elaborated with the HypSpec program^[29] and subjected to a nonlinear global analysis by applying 1:1 and 1:2 host–guest models of binding to determine the association constants for **4a** and **5a**. The binding constants of **4a** and **5a** for guests **7–10** are shown in Table 3-2-3. Upon the application of a 1:3 host–guest model of binding for **6a**, the binding constants (K_1 – K_3) were not directly obtained. A nonlinear global analysis was repeatedly carried out with arbitrary K_1 values estimated based on the results for **4a** and **5a** until the residual errors reached the smallest possible values.

The metallohelicates **4a**, **5a**, and **6a** encapsulate guests **7–10** bearing amino acid side chains with large binding constants in the range of 10^3 – 10^4 L mol^{-1} . The first guest binding into the cavities of the helicates was gradually facilitated from **4a** to **6a**, most likely implying that the cavities become structurally preorganized as the number of metal centers increases. The alkyl substituents of the amino acid side chains strongly influenced the guest binding. The steric interaction of the benzyl group of **8** is likely to be repulsive to the exterior of the cavities (Table 3-2-3, entries 7 and 10 vs. entry 4; entries 8 and 11 vs. entry 5; entries 9 and 12 vs. entry 6). By contrast, the isobutyl group may result in an attractive interaction to the aromatic exterior of the helicates (Table 3-2-3, entry 2 vs. entries 8 and 11; entry 3 vs. entries 9 and 12).

Table 3-2-3. Binding constants of metallohelicates **4a**, **5a**, and **6a** with (*R*)-**7**, (*R*)-**8**, (*R*)-**9**, and **10**.

Entry	Guest	Host	K_1 [L mol ⁻¹]	K_2 [L mol ⁻¹]	K_3 [L mol ⁻¹]
1	(<i>R</i>)- 7	4a	$2.99(2) \times 10^3$	—	—
2		5a	$7.48(8) \times 10^3$	$8.4(1) \times 10^3$	—
3		6a	$7.94 \times 10^{3[a]}$	$9.15(5) \times 10^3$	$5.04(3) \times 10^3$
4	(<i>R</i>)- 8	4a	$1.32(1) \times 10^3$	—	—
5		5a	$1.72(3) \times 10^3$	$2.45(5) \times 10^3$	—
6		6a	$2.34 \times 10^{3[a]}$	$5.1(1) \times 10^3$	$5.8(1) \times 10^3$
7	(<i>R</i>)- 9	4a	$3.58(4) \times 10^3$	—	—
8		5a	$4.00(5) \times 10^3$	$6.9(1) \times 10^3$	—
9		6a	$4.12 \times 10^{3[a]}$	$4.6(1) \times 10^3$	$1.4(1) \times 10^4$
10	10	4a	$5.11(3) \times 10^3$	—	—
11		5a	$3.10(7) \times 10^3$	$2.70(8) \times 10^3$	—
12		6a	$6.31 \times 10^{3[a]}$	$5.1(1) \times 10^3$	$2.31(6) \times 10^4$

[a] Estimated based on standard errors given by the analysis.

3-2-5 Cooperativity in the guest binding

The conformationally coupled multiple guest binding sites of a multitopic host molecule often show cooperativity in their multiple guest association.^[30] At the molecular level, the cooperativity in the multiple guest binding is described by the interaction parameters α defined by the equations $\alpha_{12} = 4K_2/K_1$, with $\alpha_{12} = 3K_2/K_1$ and $\alpha_{23} = 3K_3/K_2$ for a 1:2 host–guest system and a 1:3 host–guest system, respectively. To evaluate the cooperative effect in the multiple host–guest complexations of the helicates **5a** and **6a**, the interaction parameters α for the multiple guest binding were calculated (Table 3-2-4). The interaction parameters α_{12} and α_{23} of **5a** and **6a** are greater than unity, indicating that positive cooperative effects are present in the encapsulation of the second and third guests. Therefore, the conformationally coupled two or three binding sites sterically communicate with each other through the tris(catecholato)iron(III) cores, that is, the first or second guest binding information is effectively transferred and preorganizes the remaining binding sites. Then, the successive guests are facilitated to become accessible for encapsulation into the remaining cavities.

Table 3-2-4. Interaction parameter α of helicates **5a** and **6a** for (*R*)-**7**, (*R*)-**8**, (*R*)-**9**, and **10**.

Guests	5a	6a	α_{23}
	α_{12}	α_{12}	
(<i>R</i>)- 7	4.5	3.5	1.7
(<i>R</i>)- 8	5.7	6.5	3.4
(<i>R</i>)- 9	6.9	3.4	9.0
10	3.5	2.4	13.7

3-2-6 Chiral induction

The helicates **4a**, **5a**, and **6a** are D_3 symmetric due to the lack of a mirror plane. The (*P*)- and (*M*)-helical forms exist as racemic mixtures in solution. The labile nature of the tris(catecholato)iron(III) cores permits a dynamic interconversion between the (*P*)- and (*M*)-enantiomeric forms. When a chiral guest is encapsulated, the chiral cavities recognize the shape of the chiral guest, giving rise to an energy difference between the diastereomeric complexes. Circular dichroism (CD) spectroscopy was informative for gaining insight into the stereoselection of the diastereomeric complexes with chiral guests **7–9** (Figure 3-2-15).

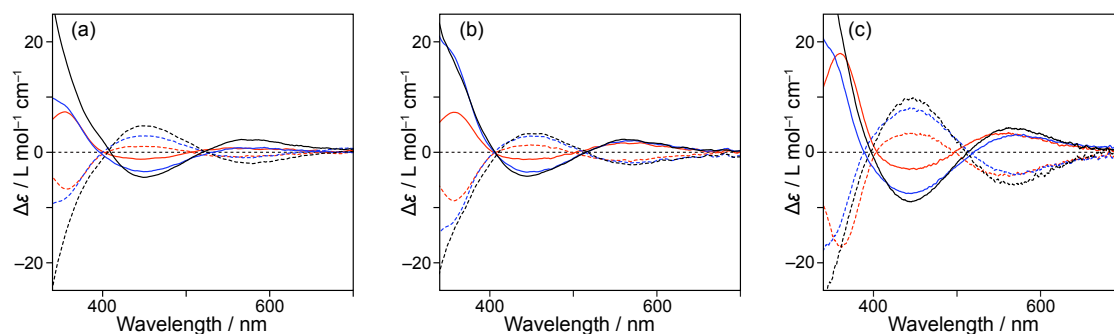


Figure 3-2-15. CD spectra of **4a** (red), **5a** (blue), and **6a** (black) with a) (*R*)-**7** (solid line) and (*S*)-**7** (dashed line), b) (*R*)-**8** (solid line) and (*S*)-**8** (dashed line), and c) (*R*)-**9** (solid line) and (*S*)-**9** (dashed line) in methanol at 298 K; [helicates] = 3.0×10^{-5} mol L⁻¹ and [guests] = 3.0×10^{-3} mol L⁻¹.

The induced CD emerged when the optically active guests (*R*)-**7** and (*S*)-**7** were encapsulated within the cavities into the solution of the metallohelicates (Figure 3-2-15a). The addition of (*R*)-**7** to a solution of **4a** resulted in induced plus-to-minus bisignate CD

signals at $\lambda = 574$ and at 446 nm, corresponding to the LMCT band of the tris(catecholato)iron(III) core. The CD spectra with (*R*)-**7** and (*S*)-**7** show a mirror-image relationship with respect to the line of $\Delta\epsilon = 0$. The signal intensities at approximately $\lambda = 446$ nm were dependent on the number of guest-binding cavities, indicating that the chiral guest complexation within the dissymmetric cavities resulted in an energy difference between the (*P*)- and (*M*)-conformations and biased the population. Raymond and coworkers reported that the absolute stereochemistry of tris(catecholato)iron(III) was determined using CD spectroscopy.^[31] The plus-to-minus Cotton effects at the LMCT band correspond to the Λ -configuration of the metal cores in the helicates possessing the (*M*)-conformation. The guests (*R*)-**8** and (*R*)-**9** also induced plus-to-minus Cotton effects of **4a**, **5a** and **6a** (Figures 3-2-15b,c); therefore, the stereogenic centers of the amino acid groups determined the left-handed helical sense of the host-guest complexes.

3-2-7 Majority-rules effect

Two chiral amplification mechanisms are possible in supramolecular assemblies: the first is the sergeants-and-soldiers principle, and the second is the majority-rules principle.^[32] The latter characterizes a nonlinear response in the chirality for assemblies consisting of both enantiomers of chiral monomers. A small excess of one of the enantiomers results in a chiral response in a nonlinear fashion.^[33,34] The cooperativity of the conformationally coupled guest binding cavities of **5a** and **6a** is already established in the guest binding; therefore, the majority-rules principle can be operative in the chiral guest recognition for **5a** and **6a**. Figure 3-2-16a shows the CD spectra of **5a** upon the variation of the enantiomeric excess (*ee*) of **9**. To confirm the cooperative effect on the molecular recognition, the induced circular dichroism (ICD) intensities at the LMCT bands versus the *ee* of the guests **7–9** were plotted (Figures 3-16b,c,d). The complexation of **4a** with chiral guests **7–9** gave rise to a good linear correlation between the ICD intensities and the *ee* of the guests. In contrast, the complexation of chiral guests **7–9** to the multiple guest binding cavities of **5a** and **6a** showed a remarkable deviation from linearity, indicating that the enantiomers in excess had a disproportionate impact on the helicity of the metallohelicates.^[19] The deviation was maximized when the guests were encapsulated within **6a** over **5a**, suggesting that the cavities of **6a** are more preorganized in a helical manner than those of **5a**. The majority-rules effects are influenced by the steric bulkiness of the amino acid side chains. The complexation of **7** to **5a** and **6a** showed

smaller deviations than the complexation of **8** and **9**. Accordingly, the amino acid side chains most likely generate a steric interaction with the stereogenic metal centers, thereby determining the absolute helical sense of the metallohelicates.

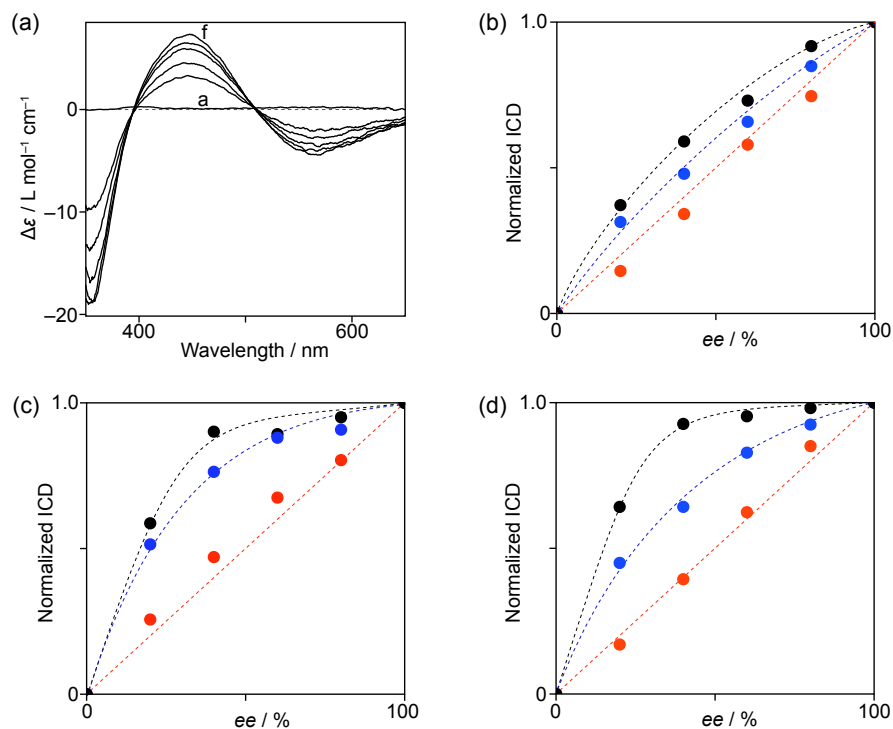


Figure 3-2-16. a) CD spectra of **5a** (1.0×10^{-4} mol L⁻¹) in the presence of mixtures [(*S*)-**9**]_x + [(*R*)-**9**]_{1-x} (1.0×10^{-2} mol L⁻¹) (a–f: $x = 0.5, 0.60, 0.70, 0.80, 0.90, 1.00$) in methanol at 298 K. b)–d) Plots of the normalized ICD intensities at the LMCT bands of **4a** (red circle), **5a** (blue circle), and **6a** (black circle) versus the *ee* of b) **7**, c) **8**, and d) **9**; [helicates] = 1.0×10^{-4} mol L⁻¹ and [guests] = 1.0×10^{-2} mol L⁻¹.

3-3 Conclusion

We have demonstrated that triple-stranded metallohelicates can be developed through the self-organization of trivalent metal ions and multidentate bridging ligands. Multiple guest-binding cavities are conformationally coupled; therefore, the first guest binding preorganizes the rest of the binding cavities in the multiple cavities, and as a result, large positive cooperative effects are manifested in the guest binding. The chiral guest complexation within the multiple guest-binding cavities determines the helical sense of the metallohelicates, directed by the stereogenic center of the amino acid. The chiral guest complexation to the metallohelicates gives rise to nonlinear relationships in the stereoselection for the helical direction, which are the so-called majority-rules effects. Accordingly, the induced chirality on a monomer unit is communicated to the other units through the strands, modulating the internal spaces in such a way that the second and third guests are easily accessible for the remaining cavities. These findings offer a facile synthetic strategy for readily preparing optically active multiple-stranded organizations with controlled helicity.

3-4 Experimental

3-4-1 General

All chemicals and solvents were purchased from Kanto Chemical Co., Ltd., Wako Pure Chemical Co., Ltd., Tokyo Kasei Kogyo Co., Ltd., and Sigma-Aldrich Co., Ltd., and were used as received without further purification. ^1H (300 MHz), ^{13}C NMR (75 MHz), and ^{19}F NMR (282 MHz) spectra were recorded on a Varian Mercury-300 spectrometer. Diffusion ordered spectroscopy (DOSY) and variable temperature ^1H NMR (500 MHz) spectra were recorded on a JEOL ECA-500 spectrometer. Chemical shifts are quoted as parts per million (ppm) relative to chloroform (chloroform- d_1 , $\delta = 7.26$ ppm for ^1H and 77.16 ppm for ^{13}C), methanol (methanol- d_4 , $\delta = 3.31$ ppm for ^1H and 49.00 ppm for ^{13}C), acetone (acetone- d_6 , $\delta = 2.05$ ppm for ^1H and 29.84 ppm for ^{13}C), DMSO (DMSO- d_6 , $\delta = 2.50$ ppm for ^1H and 34.52 ppm for ^{13}C), THF (THF- d_8 , $\delta = 1.72$ ppm for ^1H and 25.37 ppm for ^{13}C) and hexafluorobenzene ($\delta = -164.90$ ppm for ^{19}F). IR spectra were recorded on a HORIBA FT-720 spectrometer. UV/vis absorption spectra were recorded on a JASCO V-560 spectrometer. Circular dichroism (CD) spectra were recorded on a JASCO J-1500 spectrophotometer. High-resolution mass spectra (HRMS) were reported with a Thermo Fisher Scientific LTQ Orbitrap XL spectrophotometer by electrospray ionization (ESI) method or a JEOL JMS-SX102 spectrophotometer by fast atom bombardment (FAB) method. Melting points were measured with a Yanagimoto micro melting point apparatus and uncorrected. Elemental analyses were performed on a Perkin-Elmer 2400CHN elemental analyzer.

3-4-2 Computational methods

The geometrical calculations of **4**, **5**, and **6** were carried out by MacroModel Ver. 9.1 using AMBER* force field. The force field parameters for the hexa-coordinated metal centers were not available in AMBER* force field; therefore, a dummy atom was used to calculate the metal complex structures instead of the Ga and Fe metal centers. Tetramethyl ammonium were located in the cavities of the helicates to avoid the shrinkage of the cavities during the calculations. The conformational search for the host-guest complex (*R*)-**7C4** was performed using the Low-Mode Search option in MacroModel. A total of 1000 initial geometries were generated, and optimized to obtain in the most stable structure.

3-4-3 Diffusion-ordered NMR spectroscopy

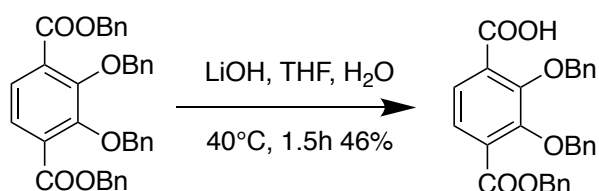
Helicates **4b**, **5b**, and **6b** were dissolved in methanol- d_4 , and were placed in a 3 mm NMR sample tube. The pulse-field gradient diffusion NMR spectra were recorded using a bipolar pulse pair stimulated echo (BPP-STE) pulse sequence on a JEOL Delta 500 spectrometer with a 3 mm inverse H3X/FG probe. The pulsed-field gradient strength was arrayed from ~ 0.003 to $\sim 0.653 \text{ T m}^{-1}$ with a pulse gradient time of 1 ms and a diffusion time of 200 ms. Both gradient strength and diffusion time were adjusted such that the peak heights in the final spectrum in the array were $\sim 5\text{--}10\%$ of the peak heights in the first spectrum. The peak intensities of the arrayed decay spectra were plotted against the gradient strengths, which were processed using Bayesian DOSY transformation in Mnova program.

3-4-4 UV/vis titration experiment

A standard titration technique was applied for the determination of the association constants for the host-guest complexes of the metallohelicates and the cationic guests in methanol. A titration was performed wherein the concentration of a host solution ($1.0 \times 10^{-4} \text{ mol L}^{-1}$) was fixed while varying the concentration of its guest. During the course of the titration, UV/vis absorption changes were measured from 400 nm to 800 nm. The experimental spectra were elaborated with the HypSpec program and subjected to a non-linear global analysis to determine the association constants.

3-4-5 Synthetic details

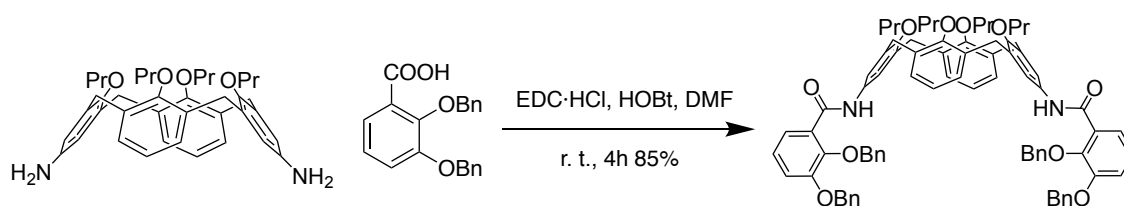
Synthesis of 2,3-bis(benzyloxy)telephthalic acid monobenzyl ester



2,3-bis(benzyloxy)telephthalic acid monobenzyl ester was synthesized by the following procedure (Scheme 3-4-1). To a solution of 2,3-bis(benzyloxy)telephthalic acid dibenzyl ester (1.69 g, 3.03 mmol) in dry THF (23 mL) was added lithium hydroxide (89 mg, 0.21 mmol) in water (10 mL). After being stirred at 40 °C for 1.5 h, the reaction mixture was diluted with water. The aqueous solution was washed with ethyl acetate, and acidified

with 1N aqueous hydrochloric acid. The resultant aqueous layer was extracted three times with chloroform. The combined organic layer was washed with brine, dried over anhydrous sodium sulfate, and concentrated in *vacuo*. The crude product was purified by column chromatography on silica gel (ethyl acetate) to give the desired compound as a white powder (0.809 g, 1.40 mmol) in 46% yield. M.p. 99–101 °C; ^1H NMR (300 MHz, chloroform-*d*): δ 7.89 (d, 1H, $J = 8.3$ Hz), 7.65 (d, 1H, $J = 8.3$ Hz), 7.27–7.46 (m, 15H), 5.35 (s, 2H), 5.27 (s, 2H), 5.11 (s, 2H); ^{13}C NMR (75 MHz, chloroform-*d*): δ 164.6, 164.5, 151.9, 151.7, 136.1, 135.3, 134.1, 131.7, 129.5 \times 2, 129.0, 128.7, 128.6 \times 2, 128.5, 127.3, 126.6 \times 2, 78.0, 76.97, 67.5; IR (ATR): ν 3031, 1728, 1228 cm^{-1} ; HRMS (ESI+): m/z $[\text{M} + \text{Na}]^+$ calcd for $\text{C}_{29}\text{H}_{24}\text{O}_6\text{Na}$ 491.14651, found 491.14655; Anal. calcd. for $\text{C}_{29}\text{H}_{24}\text{O}_6$: C 74.35, H 5.16. Found: C 74.60, H 5.22.

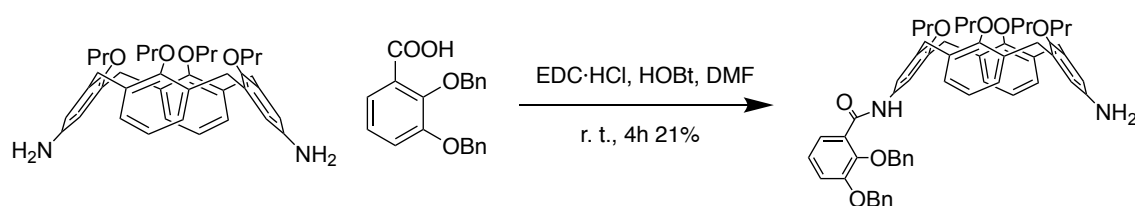
Synthesis of 12



To a solution of the benzoic acid (540 mg, 1.6 mmol), ethyl-3-(3-dimethylaminopropyl)carbodiimide hydrochloride (310 mg, 1.6 mmol), and 1-hydroxybenzotriazole (220 mg, 1.6 mmol) in dry DMF (30 ml) was added the diaminocalix[4]arene **2** (500 mg, 0.8 mmol). After stirred at room temperature for 4 h, the reaction mixture was poured into 1N hydrochloric acid and extracted with EtOAc. The organic layer was washed with aqueous sodium bicarbonate, dried over sodium sulfate, and concentrated in *vacuo*. The residue was purified by column chromatography on silica gel (methylene chloride) to give **12** as a white solid (850 mg, 85%). M.p. 259–261 °C; ^1H NMR (300 MHz, chloroform-*d*): δ 9.98 (s, 2H), 7.87–7.93 (m, 2H), 7.50–7.56 (m, 4H), 7.40–7.49 (m, 10 H), 7.32–7.37 (m, 6H), 7.20–7.24 (m, 4H), 7.08 (s, 4H), 6.32 (m, 2H), 6.21 (d, 4H, $J = 7.5$ Hz), 5.22 (s, 8H), 4.41 (d, 4H, $J = 13.2$ Hz), 3.99 (m, 4H), 3.71 (t, 4H, $J = 6.8$ Hz), 3.05 (d, 4H, $J = 13.2$ Hz), 1.98 (sext, 4H, $J = 7.4$ Hz), 1.92 (sext, 4H, $J = 7.4$ Hz), 2.04–1.84 (m, 8H), 1.13 (t, 6H, $J = 7.4$ Hz), 0.91 (t, 6H, $J = 7.4$ Hz).

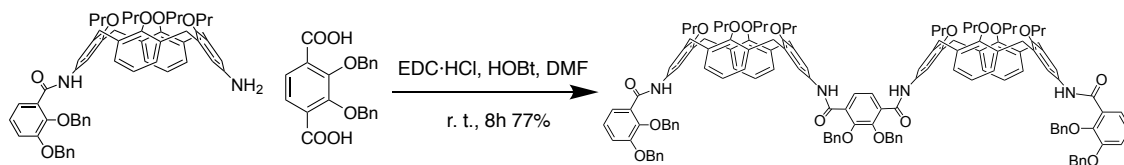
Hz); ^{13}C NMR (75 MHz, chloroform-*d*): δ 162.5, 155.2, 154.4, 151.9, 146.6, 137.1, 136.5, 136.1, 133.2, 132.2, 129.4, 129.1, 128.9, 128.8, 128.4, 127.8, 127.6 \times 2, 124.7, 123.7, 122.1, 120.6, 117.4, 77.1, 76.7, 76.6, 71.5, 31.0, 23.6, 23.0, 10.9, 10.0; IR (ATR): ν 3332, 1664, 1540 cm^{-1} ; HRMS (FAB+): m/z $[\text{M} + \text{H}]^+$ calcd for $\text{C}_{82}\text{H}_{83}\text{N}_2\text{O}_{10}$ 1255.6047, found 1255.6031; Anal. calcd. for $\text{C}_{82}\text{H}_{82}\text{N}_2\text{O}_{10} \cdot 0.5\text{H}_2\text{O}$: C 77.88, H 6.62, N 2.22. Found: C 77.86, H 6.54, N 2.21.

Synthesis of 13



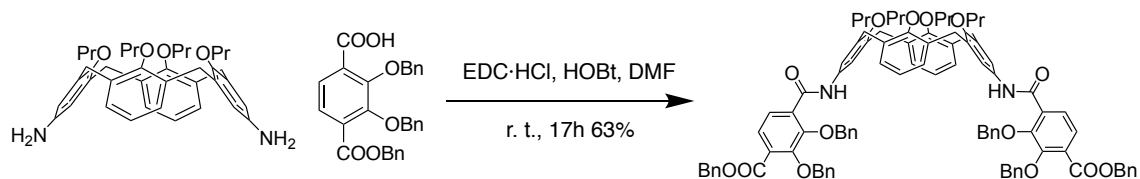
To a solution of 2,3-bis(benzyloxy)benzoic acid (154 mg, 0.462 mmol), ethyl-3-(3-dimethylaminopropyl)carbodiimide hydrochloride (147 mg, 0.770 mmol), and 1-hydroxybenzotriazole (104 mg, 0.770 mmol) in dry DMF (100 mL) was added **2** (962 mg, 1.54 mmol). After being stirred at room temperature for 4 h, the resultant mixture was poured in 1N aqueous hydrochloric acid. The aqueous layer was extracted with ethyl acetate. The organic layer was washed with brine, dried over anhydrous sodium sulfate, and concentrated in *vacuo*. The crude product was purified by column chromatography on silica gel (5% ethyl acetate–toluene) to give **13** as a white solid (0.297 g, 0.316 mmol) in 21% yield. M.p. 116–118 °C; ^1H NMR (300 MHz, chloroform-*d*₁): δ 9.72 (s, 1H), 7.72 (m, 1H), 7.29–7.52 (m, 10H), 7.14–7.18 (m, 2H), 6.67 (s, 2H), 6.48–6.63 (m, 6H), 5.94 (s, 2H), 5.16 (s, 2H), 5.10 (s, 2H), 4.40 (d, 2H, $J = 13.4$ Hz), 4.36 (d, 2H, $J = 13.4$ Hz), 3.87–3.70 (m, 8H), 3.07 (d, 2H, $J = 13.4$ Hz), 3.00 (d, 2H, $J = 13.4$ Hz), 1.80–1.98 (m, 8H), 0.90–1.06 (m, 12H); ^{13}C NMR (75 MHz, chloroform-*d*): δ 163.1, 156.5, 154.0, 151.8, 149.9, 146.2, 140.3, 136.4, 136.2, 135.9, 135.8, 134.9, 134.7, 132.0, 129.3, 128.9, 128.8 \times 2, 128.4, 128.3, 128.1 \times 2, 127.9, 124.7, 123.3, 122.0, 121.4, 116.8, 115.4, 76.7 \times 2, 76.6, 71.3, 31.1 \times 2, 23.3, 23.2 \times 2, 10.5, 10.4 \times 2; IR (ATR): ν 3340, 1664, 1540 cm^{-1} ; HRMS (ESI+): m/z $[\text{M} + \text{H}]^+$ calcd for $\text{C}_{61}\text{H}_{67}\text{N}_2\text{O}_7$ 939.4943, found 939.4943; Anal. calcd. for $\text{C}_{61}\text{H}_{66}\text{N}_2\text{O}_7$: C 78.01, H 7.08, N 2.98. Found: C 78.11, H 7.19, N 2.78.

Synthesis of 14

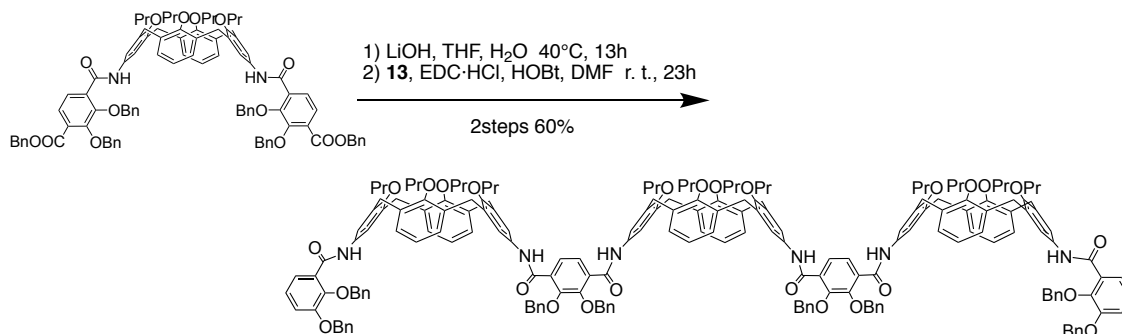


To a solution of 2,3-bis(benzyloxy)terephthalic acid (60.3 mg, 0.160 mmol), ethyl-3-(3-dimethylaminopropyl)carbodiimide hydrochloride (61.1 mg, 0.319 mmol), and 1-hydroxybenzotriazole (43.1 mg, 0.319 mmol) in dry DMF (30 mL) was added **13** (0.300 g, 0.319 mmol). After being stirred at room temperature for 8 h, the resultant mixture was poured in 1N aqueous hydrochloric acid. The aqueous layer was extracted with ethyl acetate. The organic layer was washed with brine, dried over anhydrous sodium sulfate, and concentrated in *vacuo*. The crude product was purified by column chromatography on silica gel (5% ethyl acetate–toluene) to give **14** as a white powder (0.273 g, 0.123 mmol) in 77% yield. M.p. 148–150 °C; $^1\text{H NMR}$ (300 MHz, chloroform-*d*): δ 9.89 (s, 2H), 9.66 (s, 2H), 8.08 (s, 2H), 7.84 (m, 2H), 7.28–7.54 (m, 30H), 7.17–7.20 (m, 4H), 7.01 (s, 8H), 6.33 (m, 4H), 6.21–6.28 (d, 8H), 5.29 (s, 4H), 5.19 (s, 4H), 5.17 (s, 4H), 4.41 (d, 4H, $J = 13.2$ Hz), 4.38 (d, 4H $J = 13.2$ Hz), 3.87–4.00 (m, 8H), 3.71 (t, 8H, $J = 6.9$ Hz), 3.05 (d, 4H, $J = 13.2$ Hz), 3.03 (d, 4H, $J = 13.2$ Hz), 1.82–2.03 (m, 16H), 1.09 (t, 12 H, $J = 7.4$ Hz), 0.91 (t, 6H, $J = 7.4$ Hz), 0.90 (t, 6H, $J = 7.4$ Hz); $^{13}\text{C NMR}$ (75 MHz, chloroform-*d*): δ 162.6, 161.4, 155.5, 154.6, 154.3, 151.9, 150.2, 146.6, 137.0, 136.8, 136.5, 136.2, 135.5, 133.5, 133.3, 132.2, 131.7, 130.9, 129.4, 129.2, 129.1 \times 2, 129.0, 128.9, 128.5, 127.9, 127.8, 127.7, 127.6, 127.2, 124.7, 123.6, 122.2, 120.7, 120.5, 117.3, 77.7, 77.4, 77.1, 71.5, 31.1, 23.6, 23.1 \times 2, 10.9, 10.1 \times 2; IR (ATR): ν 3346, 1671, 1538 cm^{-1} ; HRMS (ESI+): m/z $[\text{M} + \text{Na}]^+$ calcd for $\text{C}_{144}\text{H}_{146}\text{N}_4\text{O}_{18}\text{Na}$ 2242.0524, found 2242.0541; Anal. calcd. for $\text{C}_{144}\text{H}_{146}\text{N}_4\text{O}_{18}$: C 77.88, H 6.63, N 2.52. Found: C 77.74, H 6.63, N 2.30.

Synthesis of 15



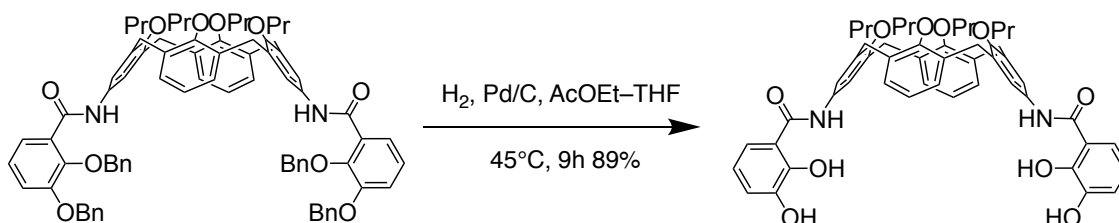
To a solution of 2,3-bis(benzyloxy)telephthalic acid monobenzyl ester (355 mg, 758 μ mol), ethyl-3-(3-dimethylaminopropyl)carbodiimide hydrochloride (145 mg, 758 μ mol), and 1-hydroxybenzotriazole (102 mg, 758 μ mol) in dry DMF (13 mL) was added **2** (236 mg, 379 μ mol). After being stirred at room temperature for 17 h, the resultant mixture was poured in 1N aqueous hydrochloric acid. The aqueous layer was extracted with ethyl acetate. The organic layer was washed with brine, dried over anhydrous sodium sulfate, and concentrated in *vacuo*. The crude product was purified by column chromatography on silica gel (10% ethyl acetate–hexane) to give **15** as a white solid (359 mg, 236 μ mol) in 63% yield. M.p. 168–170 °C; ^1H NMR (300 MHz, chloroform-*d*): δ 9.86 (s, 2H), 8.08 (d, 2H, $J = 8.5$ Hz), 7.71 (d, 2H, $J = 8.5$ Hz), 7.30–7.51 (m, 30H), 7.01 (s, 4H), 6.28 (t, 2H, $J = 7.5$ Hz), 6.17 (d, 4H, $J = 7.5$ Hz), 5.36 (s, 4H), 5.24 (s, 4H), 5.19 (s, 4H), 4.38 (d, 4H, $J = 13.1$ Hz), 3.90–4.03 (m, 4H), 3.69 (t, 4H, $J = 6.8$ Hz), 3.02 (d, 4H, $J = 13.1$ Hz), 1.82–2.03 (m, 8H), 1.11 (t, 6H, $J = 7.4$ Hz), 0.89 (t, 6H, $J = 7.4$ Hz); ^{13}C NMR (75 MHz, chloroform-*d*): δ 165.1, 161.4, 155.3, 154.7, 152.1, 151.4, 137.2, 136.7, 135.7, 135.6, 133.2, 131.7, 131.0, 129.9, 129.4, 129.3, 129.1, 128.8, 128.7 \times 2, 128.6, 128.5, 127.6, 126.7, 126.5, 122.1, 120.7, 77.4, 77.1, 76.9, 76.7, 67.4, 31.7, 31.0, 23.7, 23.1, 22.8, 14.3, 10.9, 10.0; IR (ATR): ν 3334, 1669, 1539 cm^{-1} ; HRMS (ESI+): m/z $[\text{M} + \text{Na}]^+$ calcd for $\text{C}_{98}\text{H}_{94}\text{N}_2\text{O}_{14}\text{Na}$ 1545.6597, found 1545.6608; Anal. calcd. for $\text{C}_{98}\text{H}_{94}\text{N}_2\text{O}_{14} \cdot 0.5\text{H}_2\text{O}$: C 76.79, H 6.25, N 1.83. Found: C 76.89, H 6.09, N 1.86.

Synthesis of **16**

To a solution of **15** (86.3 mg, 56.6 μ mol) in dry THF (5 mL) was added lithium hydroxide (9.21 mg, 0.219 mmol) in water (2 mL). After being stirred at 40 °C for 13 h, the resultant mixture was acidified with 1N aqueous hydrochloric acid. The aqueous layer was extracted with ethyl acetate. The combined organic layer was washed with brine, dried over anhydrous sodium sulfate, and concentrated in *vacuo*. The crude product was dissolved in dry DMF (13mL). Ethyl-3-(3-dimethylaminopropyl)carbodiimide hydrochloride (18.3 mg, 95.5 μ mol), 1-hydroxybenzotriazole (15.5 mg, 0.115 mmol), and **13** (78.9mg, 84.4 μ mol) was added to the solution. After being stirred at room temperature for 23 h, the resultant mixture was poured in 1N aqueous hydrochloric acid. The aqueous layer was extracted with ethyl acetate. The organic layer was washed with brine, dried over anhydrous sodium sulfate, and concentrated in *vacuo*. The crude product was purified by column chromatography on silica gel (20% ethyl acetate–hexane) to give **16** as a white powder (0.106 mg, 33.3 μ mol) in 60% yield. M.p. 184–186 °C; ¹H NMR (300 MHz, chloroform-*d*): δ 9.90 (s, 2H), 9.76 (s, 2H), 9.67 (s, 2H), 8.11 (m, 4H), 7.84 (t, 2H, *J* = 4.9 Hz), 7.29–7.56 (m, 40H), 7.13–7.22 (m, 4H), 7.07 (s, 4H), 7.02 (s, 4H), 7.00 (s, 4H), 6.14–6.37 (m, 18H), 5.33 (s, 4H), 5.31 (s, 4H), 5.19 (s, 4H), 5.17 (s, 4H), 4.31–4.47 (m, 12H), 3.95 (m, 12H), 3.71 (m, 12H), 2.94–3.12 (m, 12H), 1.83–2.03 (m, 24H), 1.03–1.16 (m, 18H), 0.84–0.96 (m, 18H); ¹³C NMR (75 MHz, chloroform-*d*): δ 162.4, 161.3, 155.4, 155.3, 154.5 \times 2, 154.1, 151.7, 150.1 \times 2, 146.4, 137.2, 137.0, 136.8, 136.7, 136.4, 136.0, 135.4, 133.4, 133.3, 133.2, 132.1, 131.7 \times 2, 131.0, 130.7, 129.2, 129.1 \times 2, 129.0, 128.9, 128.8, 128.7, 128.3, 127.9, 127.8, 127.7, 127.6, 124.7, 123.6, 122.2, 120.7, 120.5, 117.3, 77.7, 77.4, 77.1, 76.1, 71.5, 31.1, 23.7, 23.6, 23.1 \times 2, 11.0,

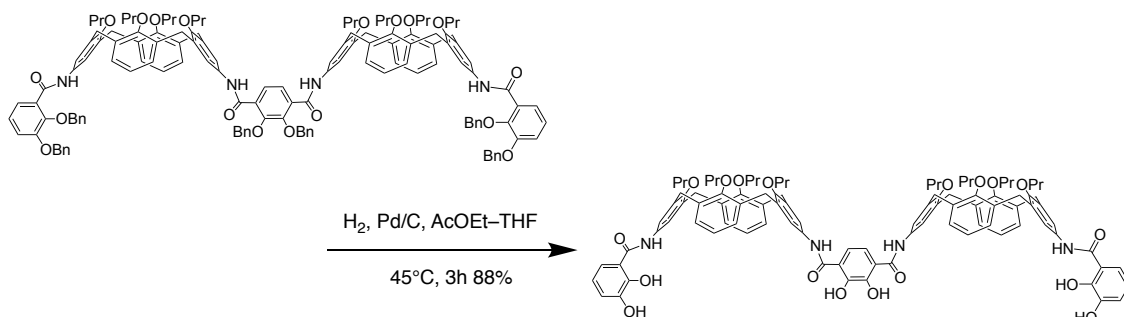
10.9, 10.1 \times 2; IR (ATR): ν 3340, 1667, 1534 cm^{-1} ; HRMS (ESI+): m/z $[\text{M} + \text{Na}]^+$ calcd for $\text{C}_{206}\text{H}_{210}\text{N}_6\text{O}_{26}\text{Na}$ 3206.5187, found 3206.5124; Anal. calcd. for $\text{C}_{206}\text{H}_{210}\text{N}_6\text{O}_{26}\cdot\text{H}_2\text{O}$: C 77.22, H 6.67, N 2.62. Found: C 77.34, H 6.91, N 2.62.

Synthesis of L1



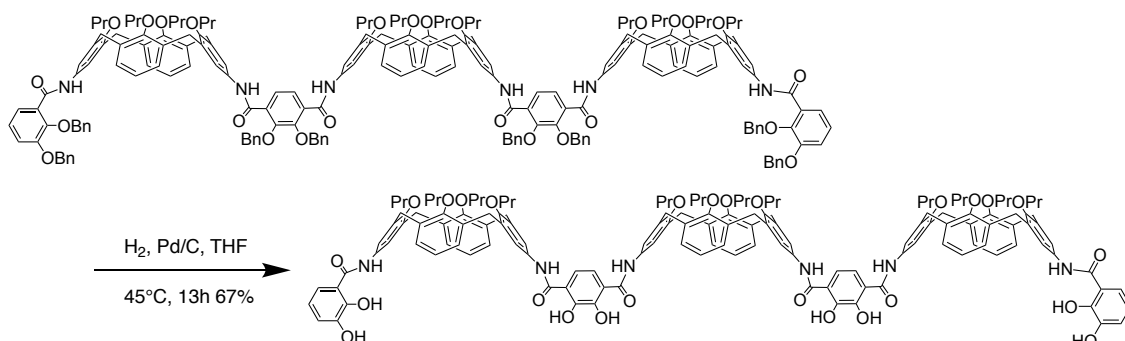
To a solution of **12** (0.310 g, 0.247 mmol) in ethyl acetate (5 mL) and tetrahydrofuran (15 mL) was added 10% Pd/C (240 mg). After being stirred at 45 °C for 9 h under H_2 atmosphere, the resultant mixture was filtered through a celite pad. The filtrate was concentrated in *vacuo*. The crude product was purified by GPC (chloroform) to give **L1** as a white powder (198 mg, 0.221 mmol) in 89% yield. M.p. 282–285 °C; ^1H NMR (300 MHz, chloroform-*d*): δ 12.42 (s, 2H), 7.60 (s, 2H), 6.97 (d, 4H, $J = 7.3$ Hz), 6.90 (d, 2H, $J = 7.8$ Hz), 6.84 (t, 2H, $J = 7.3$ Hz), 6.67 (d, 2H, $J = 7.8$ Hz), 6.59 (s, 4H), 6.45 (t, 2H, $J = 7.8$ Hz), 5.69 (s, 2H), 4.49 (d, 4H, $J = 13.8$ Hz), 3.98 (m, 4H), 3.76 (t, 4H, $J = 7.7$ Hz), 3.19 (d, 4H, $J = 13.8$ Hz), 1.81–2.04 (m, 8H), 1.06 (t, 6H, $J = 7.4$ Hz), 0.95 (t, 6H, $J = 7.4$ Hz); ^{13}C NMR (75 MHz, chloroform-*d*): δ 168.3, 157.3, 154.2, 149.2, 146.0, 135.8, 135.3, 130.3, 128.9, 122.6, 121.5, 118.8, 118.4, 115.9, 114.3, 77.2, 76.9, 31.2, 23.5, 23.2, 10.6, 10.2; IR (ATR): ν 3390, 1645, 1536 cm^{-1} ; HRMS (FAB+): m/z $[\text{M}]^+$ calcd for $\text{C}_{54}\text{H}_{58}\text{N}_2\text{O}_{10}$ 894.4091, found 894.4120; Anal. calcd. for $\text{C}_{54}\text{H}_{58}\text{N}_2\text{O}_{10}\cdot 0.3\text{H}_2\text{O}$: C 72.03, H 6.56, N 3.11. Found: C 72.06, H 6.38, N 3.11.

Synthesis of L2



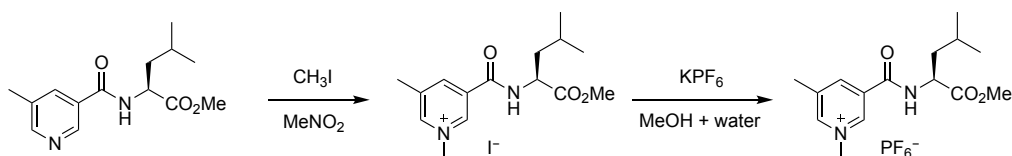
To a solution of **14** (0.266 g, 120 μmol) in ethyl acetate (3mL) and tetrahydrofuran (9 mL) was added 10% Pd/C (200 mg). After being stirred at 45 $^\circ\text{C}$ for 3 h under H_2 atmosphere, the resultant mixture was filtered through a celite pad. The filtrate was concentrated in *vacuo*. The crude product was purified by GPC (chloroform) to give **L2** as a white powder (178 mg, 106 μmol) in 88% yield. M.p. 242–243 $^\circ\text{C}$; ^1H NMR (300 MHz, chloroform-*d*): δ 12.23, (s, 2H), 11.68 (s, 2H), 7.74 (s, 2H), 7.63 (s, 2H), 7.14 (dd, 4H, $J = 7.4, 1.6$ Hz), 7.10 (dd, 4H, $J = 7.4, 1.6$ Hz), 6.91 (t, 4H, $J = 7.4$ Hz), 6.69 (d, 2H, $J = 8.0$ Hz), 6.62 (d, 2H, $J = 8.0$ Hz), 6.54 (s, 4H), 6.53 (s, 4H), 6.40 (t, 2H, $J = 8.0$ Hz), 6.26 (s, 2H), 5.92 (s, 2H), 4.49 (d, 8H, $J = 13.3$ Hz), 4.05 (m, 8H), 3.70 (t, 4H, $J = 6.8$ Hz), 3.69 (t, 4H, $J = 6.8$ Hz), 3.23 (d, 4H, $J = 13.3$ Hz), 3.18 (d, 4H, $J = 13.3$ Hz), 1.80–2.10 (m, 16H), 1.11 (t, 6H, $J = 7.4$ Hz), 1.10 (t, 6H, $J = 7.4$ Hz), 0.92 (t, 12H, $J = 7.4$ Hz); ^{13}C NMR (75 MHz, chloroform-*d*): δ 167.7, 167.1, 157.7, 153.4, 153.3, 150.4, 148.8, 145.4, 136.7, 136.4, 134.5, 134.3, 130.8, 130.6, 129.4, 129.0, 122.5, 121.7, 120.3, 118.8, 118.4, 116.8, 116.7, 114.7, 114.0, 77.4 \times 2, 77.3, 31.2 \times 2, 23.6, 23.1, 10.9, 10.0; IR (ATR): ν 3359, 1645, 1539 cm^{-1} ; HRMS (ESI+): m/z $[\text{M} + \text{Na}]^+$ calcd for $\text{C}_{102}\text{H}_{110}\text{N}_4\text{O}_{18}\text{Na}$ 1701.7707, found 1701.7682; Anal. calcd. for $\text{C}_{102}\text{H}_{110}\text{N}_4\text{O}_{18}\cdot 2\text{H}_2\text{O}$: C 71.39, H 6.70, N 3.26. Found: C 71.38, H 6.71, N 3.18.

Synthesis of L3



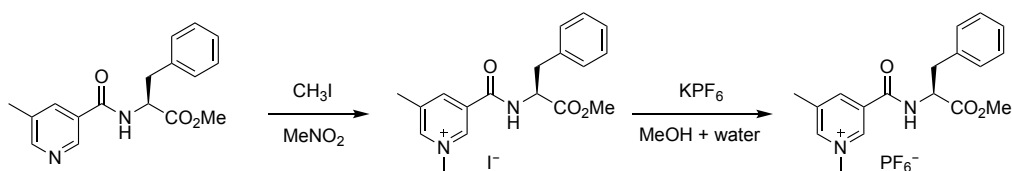
To a solution of **16** (81.6 mg, 25.6 μmol) in tetrahydrofuran (5 mL) was added 10% Pd/C (90 mg). After being stirred at 45 °C for 13 h under H_2 atmosphere, the resultant mixture was filtered through a celite pad. The filtrate was concentrated in *vacuo*. The crude product was purified by GPC (chloroform) to obtain **L3** as a white powder (42.4 mg, 17.2 μmol) in 67% yield. M.p. > 300 °C; ^1H NMR (300 MHz, $\text{THF-}d_8$): δ 12.50 (s, 2H), 11.7 (bs, 4H), 9.49 (s, 2H), 9.46 (s, 2H), 9.11 (s, 2H), 7.78 (s, 2H), 7.35 (s, 4H), 7.25 (s, 4H), 7.17 (s, 4H), 7.15 (s, 4H), 7.09 (dd, 2H, $J = 8.2, 1.2$ Hz), 6.84 (dd, 2H, $J = 8.2, 1.2$ Hz), 6.58 (d, 8H, $J = 7.6$ Hz), 6.53 (t, 2H, $J = 8.2$ Hz), 6.46 (t, 4H, $J = 7.4$ Hz), 6.44 (d, 4H, $J = 7.4$ Hz), 6.36 (t, 2H, $J = 7.4$ Hz), 4.53 (d, 4H, $J = 13.0$ Hz), 4.52 (d, 4H, $J = 13.0$ Hz), 4.51 (d, 4H, $J = 13.0$ Hz), 4.01 (m, 4H), 3.93 (t, 4H, $J = 7.6$ Hz), 3.92 (t, 4H, $J = 7.6$ Hz), 3.88 (t, 8H, $J = 7.4$ Hz), 3.81 (t, 4H, $J = 7.0$ Hz), 3.18 (d, 4H, $J = 13.0$ Hz), 3.16 (d, 8H, $J = 13.0$ Hz), 1.91–2.07 (m, 24H), 1.09 (t, 6H, $J = 7.5$ Hz), 1.05 (t, 12H, $J = 7.6$ Hz), 1.01 (t, 12H, $J = 7.6$ Hz), 0.99 (t, 6H, $J = 7.6$ Hz); ^{13}C NMR (75 MHz, $\text{THF-}d_8$): δ 168.5, 166.0, 156.2, 155.8, 154.1, 153.8, 153.7, 150.0, 149.3 $\times 2$, 146.8, 136.2, 135.5, 135.4, 134.3 $\times 2$, 133.6, 132.3, 132.1, 128.0 $\times 2$, 127.8, 122.0, 121.5, 121.3, 121.2, 119.0, 118.4, 117.8, 116.4, 115.3, 76.8, 76.7, 76.6, 31.1, 23.3, 23.2, 23.2 $\times 2$, 23.1, 10.0, 9.8, 9.7 $\times 2$, 9.6; IR (ATR): ν 3360, 1652, 1539 cm^{-1} ; HRMS (ESI+): m/z $[\text{M} + \text{Na}]^+$ calcd for $\text{C}_{150}\text{H}_{162}\text{N}_6\text{O}_{26}\text{Na}$ 2486.1431, found 2486.1447; Anal. calcd. for $\text{C}_{150}\text{H}_{162}\text{N}_6\text{O}_{26}\cdot 3\text{H}_2\text{O}$: C 71.52, H 6.72, N 3.34. Found: C 71.46, H 6.79, N 3.31.

Synthesis of (S)-7



To a solution of methyl (5-methylnicotinoyl)-(*S*)-leucinate (0.509 g, 2.07 mmol) in nitromethane (5.0 mL) was added iodomethane (0.19 mL, 3.1 mmol). After being stirred in a sealed tube at 80 °C for 5 h, the solvent was removed in *vacuo*. The residue was dissolved in methanol (14 mL), water (6 mL), and potassium hexafluorophosphate (1.16 g, 6.30 mmol) was added to the solution. After being stirred at room temperature for 30 min, the suspension was concentrated in *vacuo*. The residue was dissolved in chloroform, and the organic layer was washed with water. The organic layer was concentrated in *vacuo* to afford (*S*)-7 as yellow oil (0.578 g, 1.36 mmol) in 66% yield. (*R*)-7 was synthesized by the similar method. ¹H NMR (300 MHz, chloroform-*d*): δ 8.86 (s, 1H), 8.65 (s, 1H), 8.56 (s, 1H), 7.28 (br, 1H), 4.71 (m, 1H), 4.40 (s, 3H), 3.75 (s, 3H), 2.61 (s, 3H), 1.72-1.82 (m, 3H), 0.97 (d, 3H, *J* = 6.4 Hz), 0.95 (d, 3H, *J* = 6.4 Hz); ¹³C NMR (75 MHz, chloroform-*d*): δ 172.7, 161.7, 146.9, 144.5, 141.4, 140.5, 133.9, 52.6, 52.2, 48.9, 40.1, 24.9, 22.8, 21.6, 18.4; ¹⁹F NMR (282 MHz, chloroform-*d*): δ -74.7 (d, *J* = 713 Hz); IR (ATR): ν 3411, 1743, 1635, 1544 cm⁻¹; HRMS (ESI⁺): *m/z* [M]⁺ calcd for C₁₅H₂₃N₂O₃ 279.1703, found 279.1707; (*S*)-7 [α]²⁵_D = -13.4 cm³ g⁻¹ dm⁻¹ (c 0.01 g cm⁻³); (*R*)-7 [α]²⁵_D = +13.8 cm³ g⁻¹ dm⁻¹ (c 0.01 g cm⁻³).

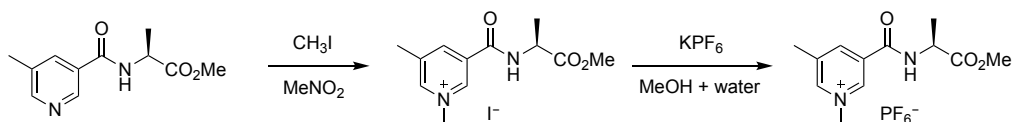
Synthesis of (S)-8



To a solution of methyl (5-methylnicotinoyl)-(*S*)-phenylalaninate (0.513 g, 1.72 mmol) in nitromethane (5 mL) was added iodomethane (0.16 mL, 2.6 mmol). After being stirred in a sealed tube at 80 °C for 9 h, the solvent was removed in *vacuo*. The residue was

dissolved in methanol (8 mL), water (5 mL) and potassium hexafluorophosphate (0.861 g, 4.68 mmol) was added to the solution. After being stirred at room temperature for 30 min, the suspension was concentrated in *vacuo*. The residue was dissolved in chloroform, and the organic layer was washed with water. The organic layer was concentrated in *vacuo* to afford (*S*)-**8** as yellow oil (0.542 g, 1.18 mmol) in 69% yield. (*R*)-**8** was synthesized by the similar method. ¹H NMR (300 MHz, acetone-*d*₆): δ 9.23 (s, 1H), 9.06 (s, 1H), 8.82 (s, 1H), 8.51 (d, 1H, *J* = 7.5 Hz), 7.19-7.33 (m, 5H), 4.96 (m, 1H), 4.61 (s, 3H), 3.71 (s, 3H), 3.30 (ABX, 1H, *J* = 13.9, 5.6 Hz), 3.16 (ABX, 1H, *J* = 13.9, 8.8 Hz), 2.65 (s, 3H); ¹³C NMR (75 MHz, acetone-*d*₆): δ 172.0, 162.3, 148.1, 144.5, 143.8, 140.4, 137.8, 134.1, 130.1, 129.4, 127.7, 55.6, 52.7, 49.3, 37.9, 18.4; ¹⁹F NMR (282 MHz, acetone-*d*₆): δ -75.2 (d, *J* = 708 Hz); IR (ATR): ν 3407, 1739, 1635, 1539 cm⁻¹; HRMS (ESI+): *m/z* [M]⁺ calcd for C₁₈H₂₁N₂O₃ 313.1547, found 313.1548; (*S*)-**8** [α]²⁵_D = -27.4 cm³ g⁻¹ dm⁻¹ (c 0.01 g cm⁻³); (*R*)-**8** [α]²⁵_D = 27.6 cm³ g⁻¹ dm⁻¹ (c 0.01 g cm⁻³).

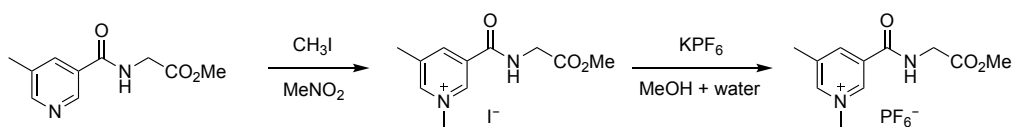
Synthesis of (*S*)-**9**



To a solution of methyl (5-methylnicotinoyl)-(*S*)-alaninate (0.657 g, 2.96 mmol) in nitromethane (5 mL) was added iodomethane (0.28 mL, 4.5 mmol). After being stirred in a sealed tube at 80 °C for 9 h, the solvent was removed in *vacuo*. The residue was dissolved in methanol (8 mL), water (5 mL), and potassium hexafluorophosphate (1.29 g, 7.02 mmol) was added to the solution. After being stirred at room temperature for 30 min, the suspension was concentrated in *vacuo*. The precipitates were washed with water to afford (*S*)-**9** as colorless crystal (0.282 g, 0.738 mmol) in 25% yield. (*R*)-**9** was synthesized by the similar method. M.p. 157–159 °C; ¹H NMR (300 MHz, methanol-*d*₄): δ 9.16 (s, 1H), 8.91 (s, 1H), 8.79 (s, 1H), 4.65 (q, 1H, *J* = 7.3 Hz), 4.42 (s, 3H), 3.75 (s, 3H), 2.62 (s, 3H), 1.53 (d, 3H, *J* = 7.3 Hz); ¹³C NMR (75 MHz, acetone-*d*₆): δ 173.1, 162.2, 148.0, 144.5, 143.8, 140.4, 134.2, 52.6, 49.9, 49.3, 18.4, 17.4; ¹⁹F NMR (282 MHz, acetone-*d*₆): δ -72.80 (d, *J* = 708 Hz); IR (ATR): ν 3417, 1739, 1635, 1539 cm⁻¹; HRMS (ESI+): *m/z* [M]⁺ calcd for C₁₂H₂₇N₂O₃ 237.1234, found 237.1233; (*S*)-**9**

$[\alpha]_{\text{D}}^{25} = -5.0 \text{ cm}^3 \text{ g}^{-1} \text{ dm}^{-1}$ (c 0.01 g cm⁻³); (*R*)-**9** $[\alpha]_{\text{D}}^{25} = 5.2 \text{ cm}^3 \text{ g}^{-1} \text{ dm}^{-1}$ (c 0.01 g cm⁻³).

Synthesis of **10**



To a solution of methyl (5-methylnicotinoyl)glycinate (0.417 g, 2.00 mmol) in nitromethane (5 mL) was added iodomethane (0.187 mL, 3.00 mmol). After being stirred in a sealed tube at 80 °C for 9 h, the solvent was removed in *vacuo*. The residue was dissolved in methanol (8 mL), water (5 mL), and potassium hexafluorophosphate (1.29 g, 7.02 mmol) was added to the solution. The residue was dissolved in methanol (10 mL), water (5 mL) and potassium hexafluorophosphate (1.26 g, 6.84 mmol) was added to the solution. After being stirred at room temperature for 30 min, the suspension was concentrated in *vacuo*. The aqueous layer was extracted with ethyl acetate. The organic layer was concentrated in *vacuo* to afford **10** as yellow oil (64.4 mg, 0.175 mmol) in 9% yield. ¹H NMR (300 MHz, acetone-*d*₆): δ 9.28 (s, 1H), 9.08 (s, 1H), 8.88 (s, 1H), 8.61 (br, 1H), 4.64 (s, 3H), 4.22 (d, 2H, *J* = 5.9 Hz), 3.72 (s, 3H), 2.67 (s, 3H); ¹³C NMR (75 MHz, acetone-*d*₆): δ 170.2, 162.7, 148.1, 144.4, 143.7, 140.5, 134.2, 52.4, 49.3, 42.2, 18.4; ¹⁹F NMR (282 MHz, acetone-*d*₆): δ -75.3 (d, *J* = 708 Hz); IR (ATR): ν 3433, 1743, 1635, 1550 cm⁻¹; HRMS (ESI+): *m/z* [M]⁺ calcd for C₁₁H₁₅N₂O₃ 223.1077, found 223.1075.

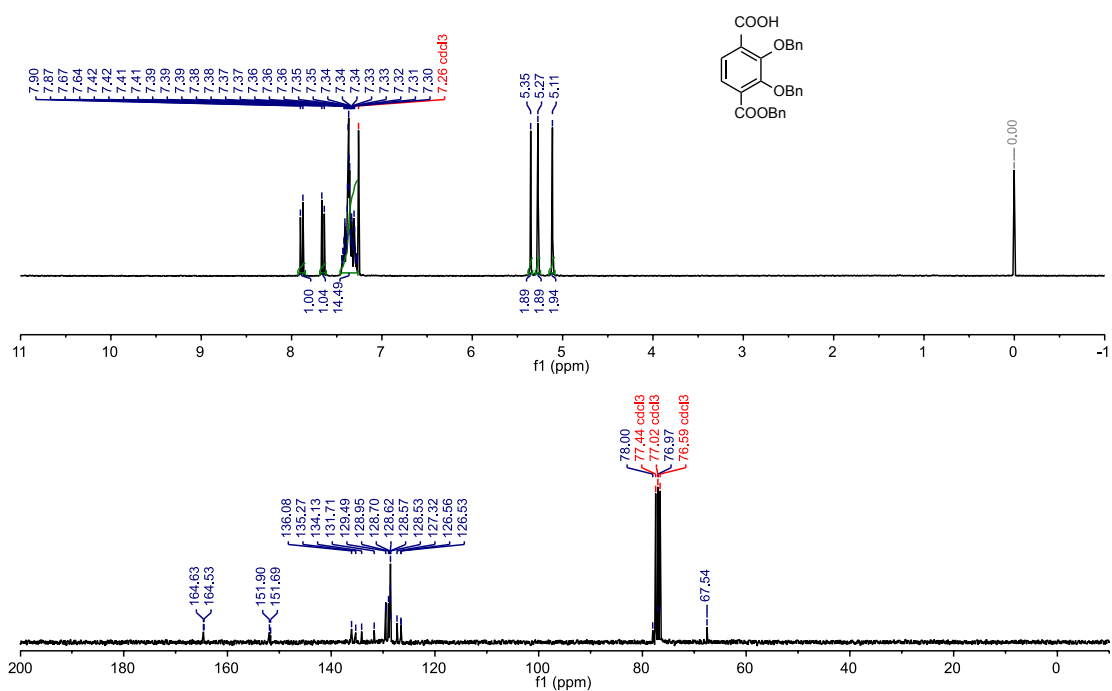


Figure 3-4-1. ^1H NMR spectrum (300 MHz, chloroform- d_1 , 293 K) and ^{13}C NMR spectrum (75 Hz, chloroform- d_1 , 293 K) of 2,3-bis(benzyloxy)tephthalic acid monobenzyl ester.

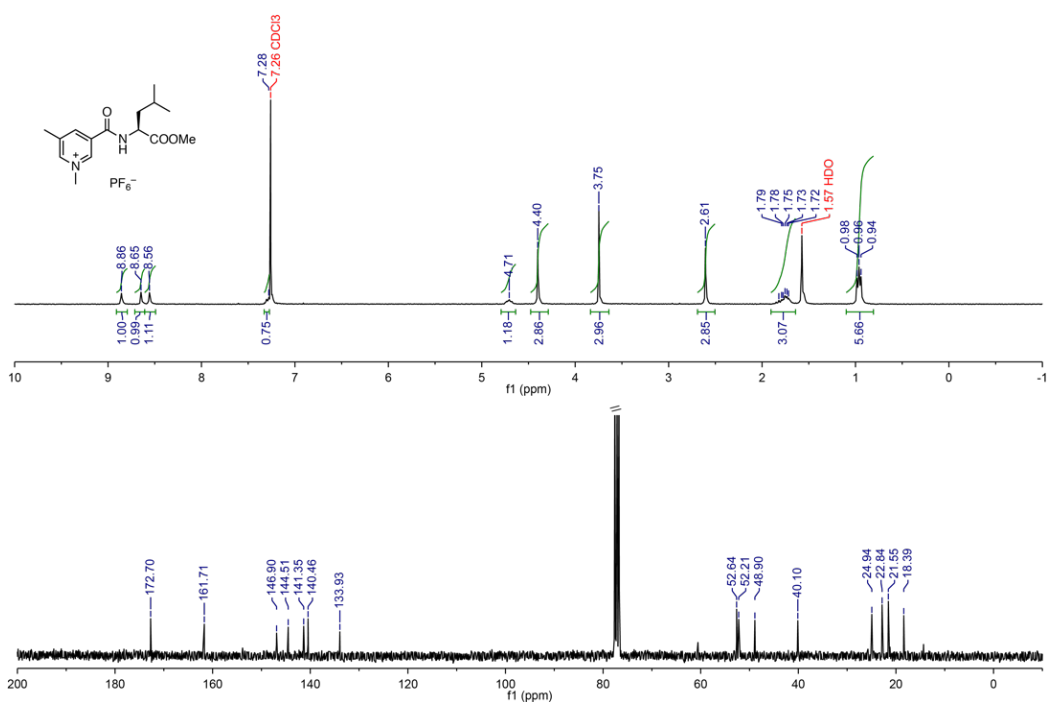


Figure 3-4-2. ^1H NMR spectrum (300 MHz, chloroform- d_1 , 293 K) and ^{13}C NMR spectrum (75 Hz, chloroform- d_1 , 293 K) of (*R*)-7.

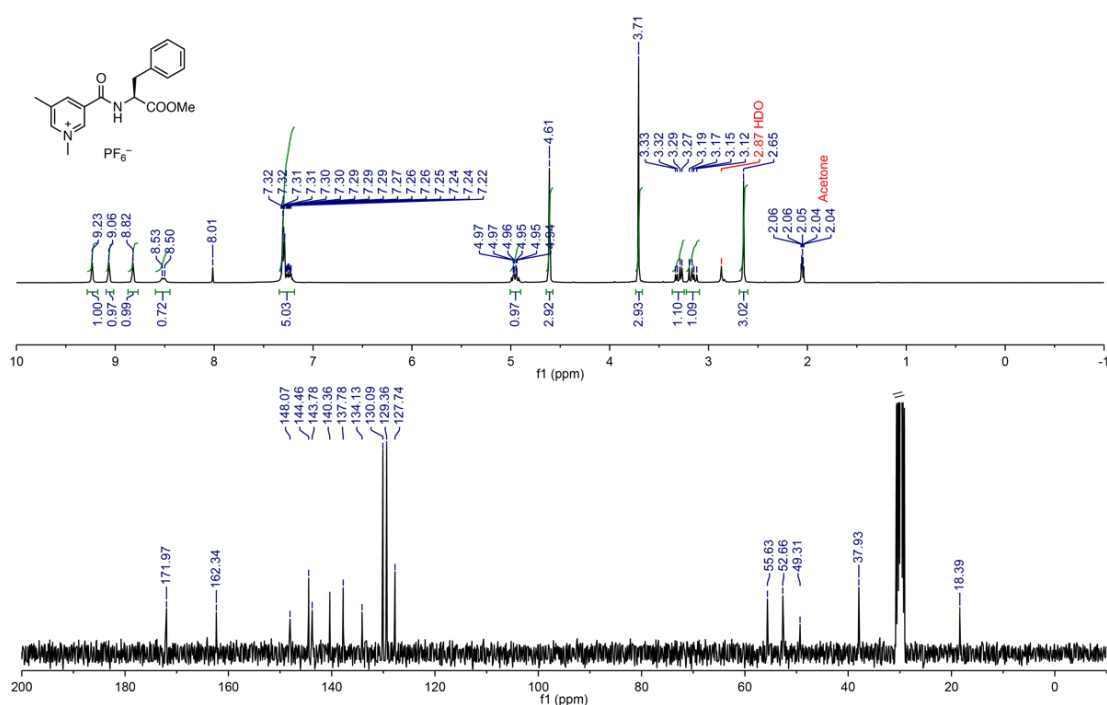


Figure 3-4-3. ^1H NMR spectrum (300 MHz, acetone- d_6 , 293 K) and ^{13}C NMR spectrum (75 Hz, acetone- d_6 , 293 K) of (*R*)-**8**. The singlet signal at $\delta=8.01$ ppm in the ^1H NMR originates from CHCl_3 .

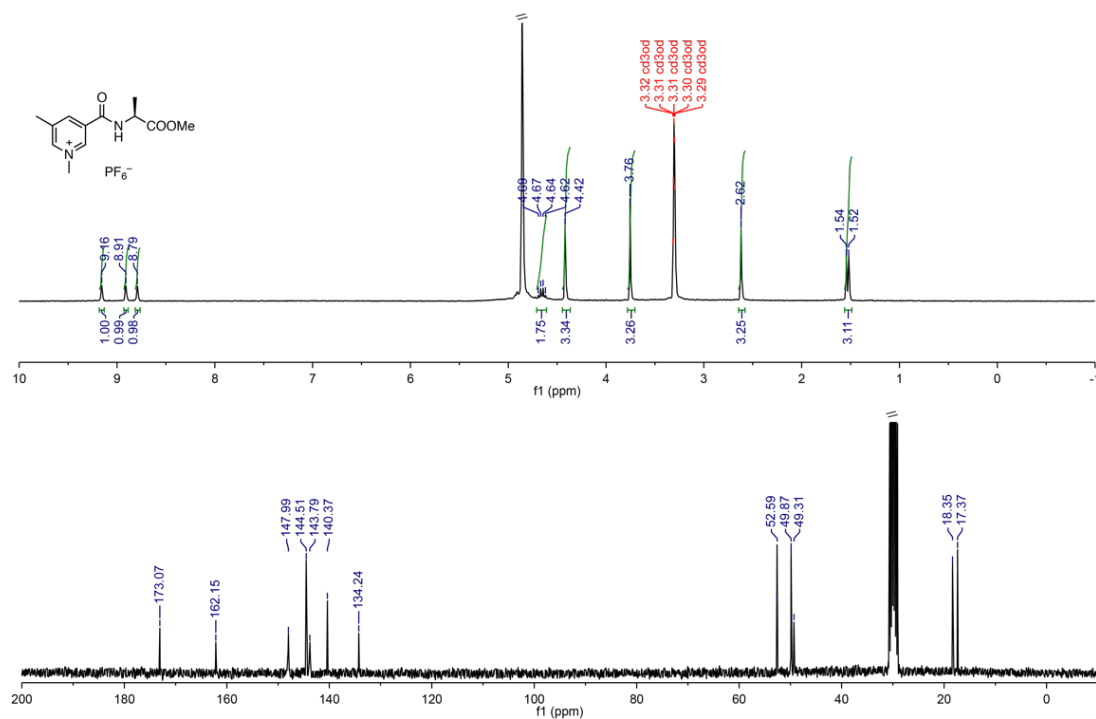


Figure 3-4-4. ^1H NMR spectrum (300 MHz, methanol- d_4 , 293 K) and ^{13}C NMR spectrum (75 Hz, acetone- d_6 , 293 K) of (*R*)-**9**.

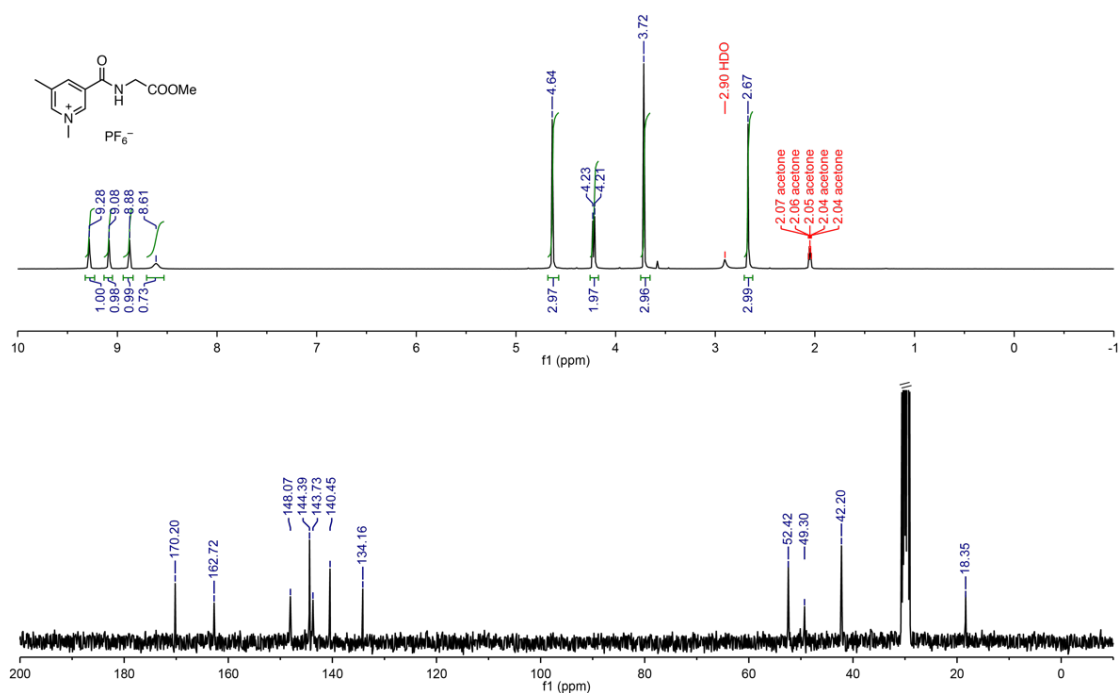


Figure 3-4-5. ^1H NMR spectrum (300 MHz, acetone- d_6 , 293 K) and ^{13}C NMR spectrum (75 Hz, acetone- d_6 , 293 K) of **10**.

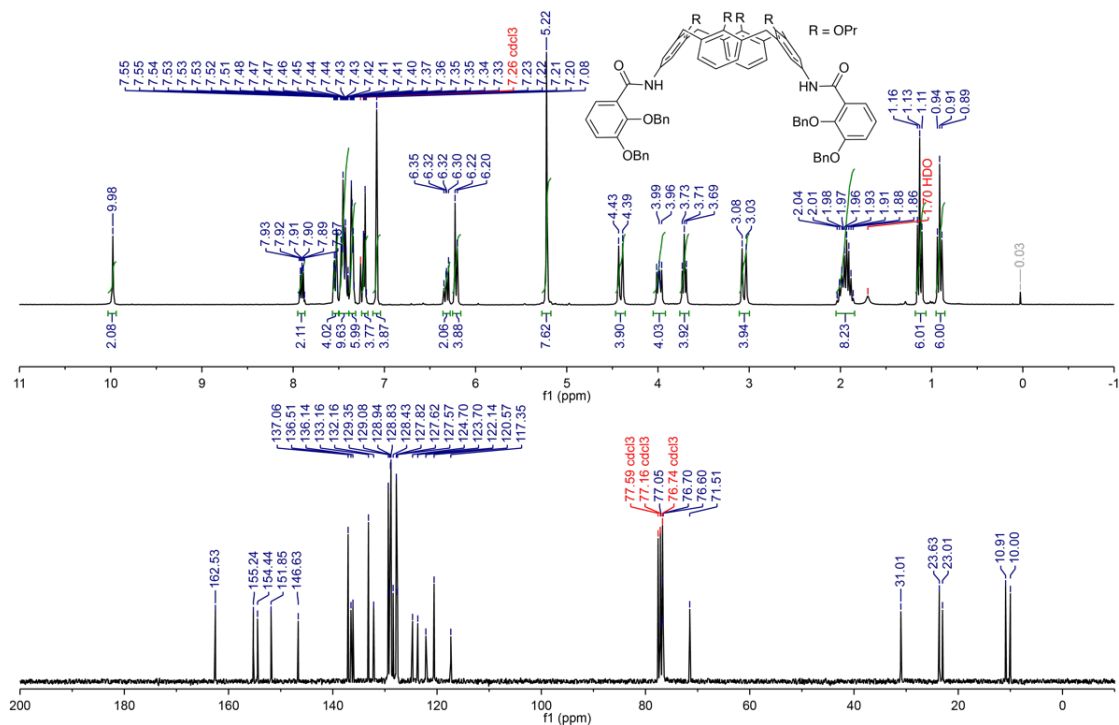


Figure 3-4-6. ^1H NMR spectrum (300 MHz, chloroform- d_1 , 293 K) and ^{13}C NMR spectrum (75 Hz, chloroform- d_1 , 293 K) of **12**.

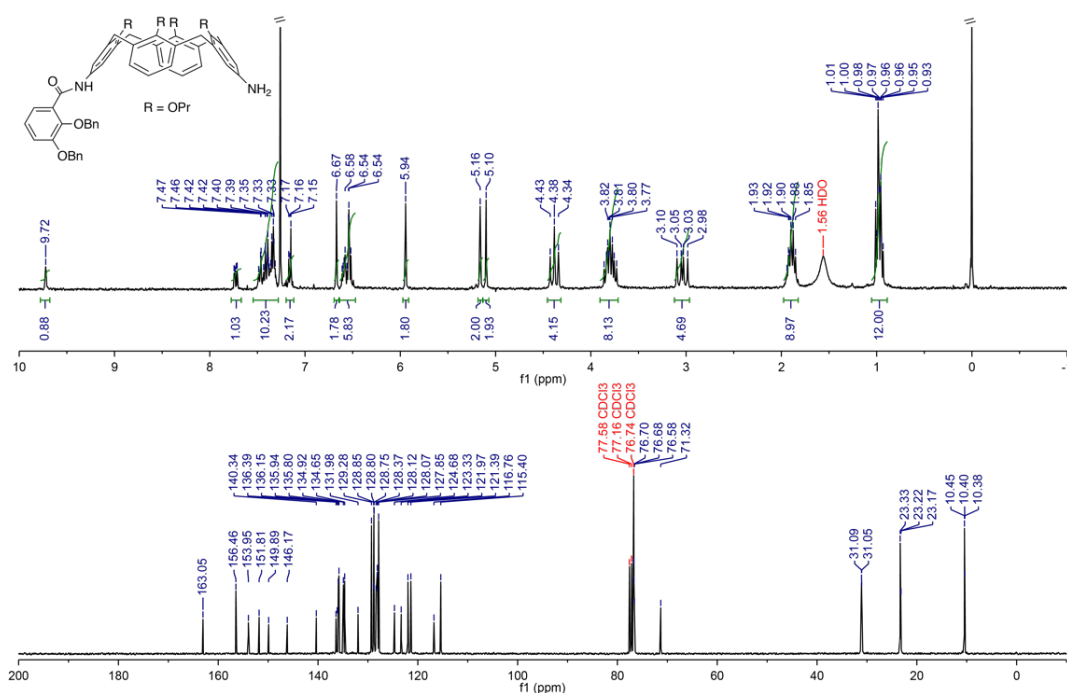


Figure 3-4-7. ^1H NMR spectrum (300 MHz, chloroform- d_1 , 293 K) and ^{13}C NMR spectrum (75 Hz, chloroform- d_1 , 293 K) of **13**.

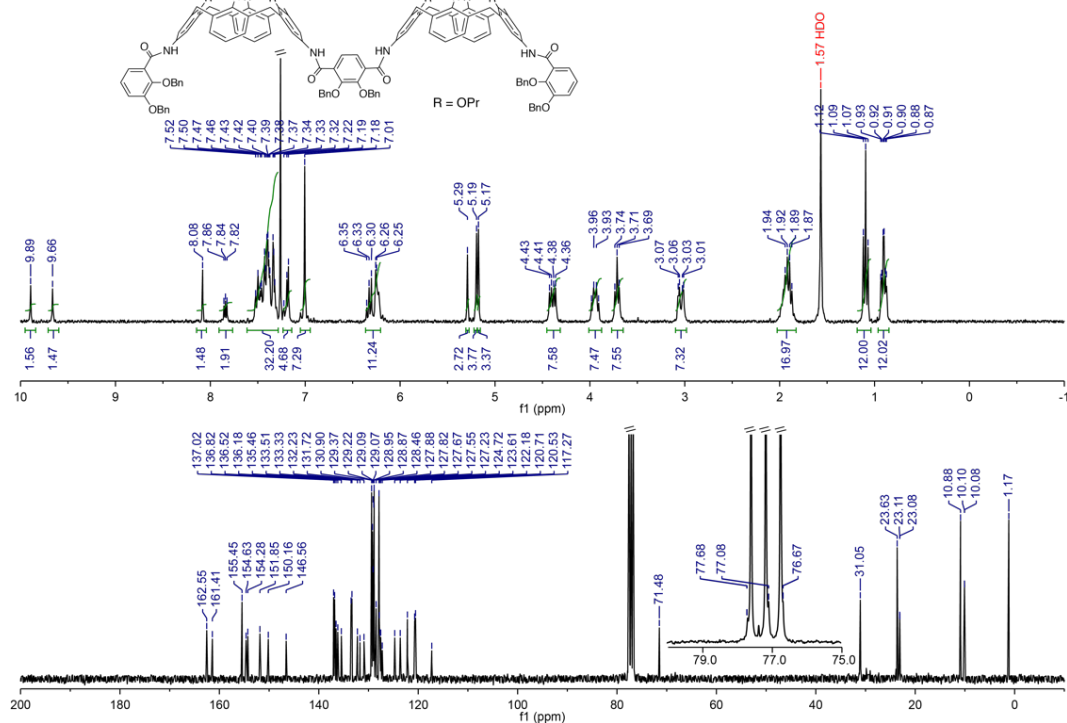


Figure 3-4-8. ^1H NMR spectrum (300 MHz, chloroform- d_1 , 293 K) and ^{13}C NMR spectrum (75 Hz, chloroform- d_1 , 293 K) of **14**.

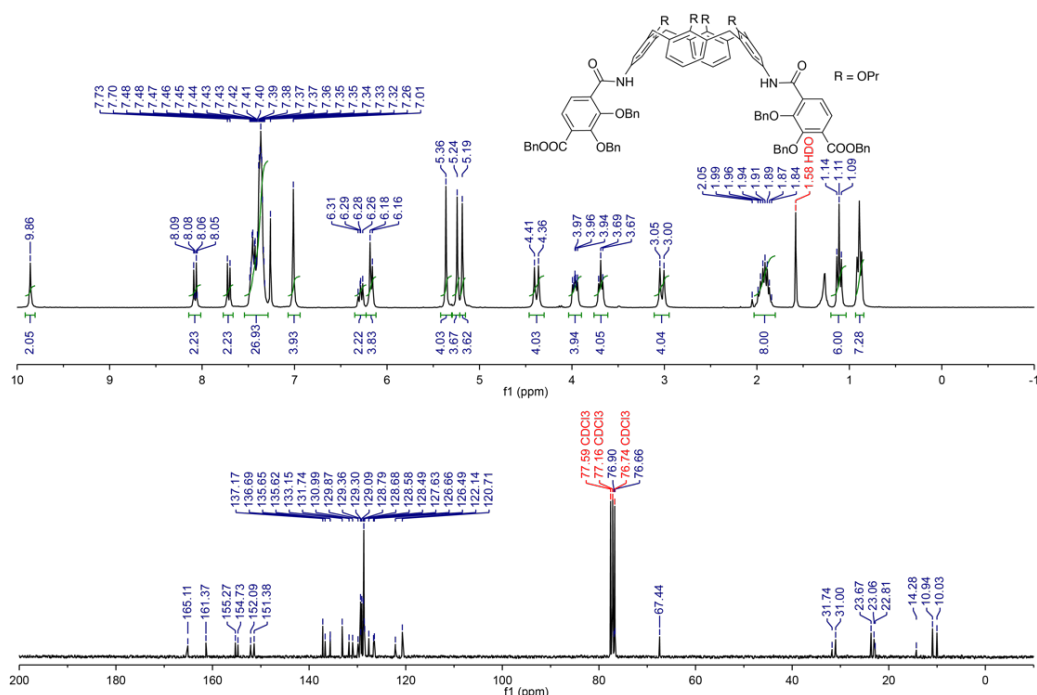


Figure 3-4-9. ^1H NMR spectrum (300 MHz, chloroform- d_1 , 293 K) and ^{13}C NMR spectrum (75 Hz, chloroform- d_1 , 293 K) of **15**.

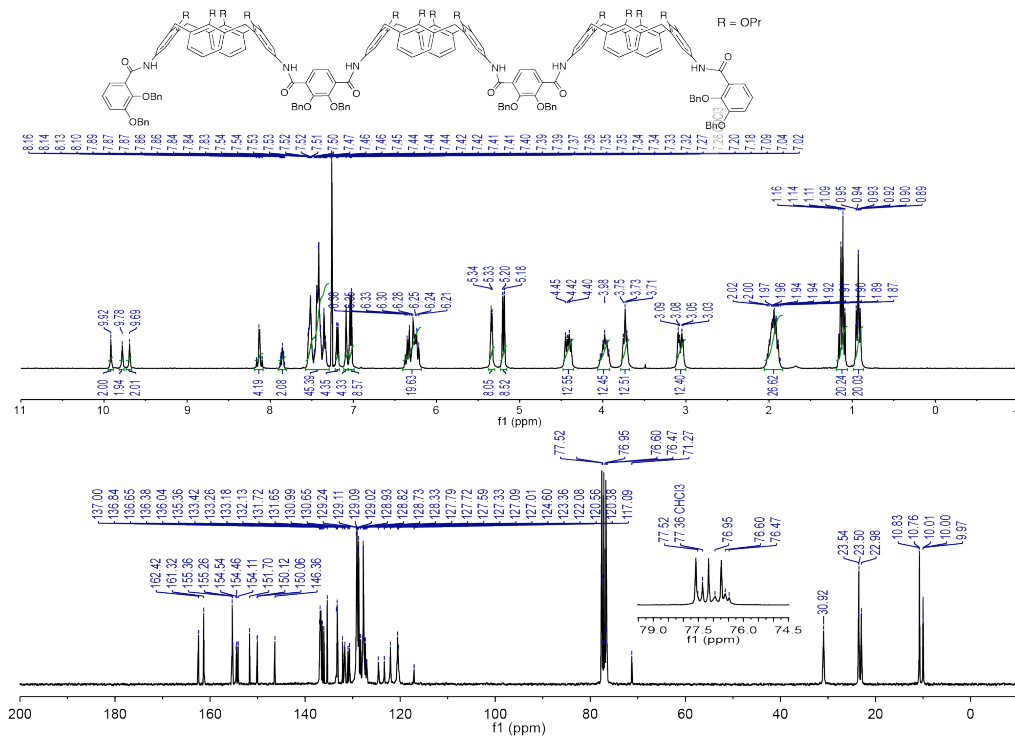


Figure 3-4-10. ^1H NMR spectrum (300 MHz, chloroform- d_1 , 293 K) and ^{13}C NMR spectrum (75 Hz, chloroform- d_1 , 293 K) of **16**.

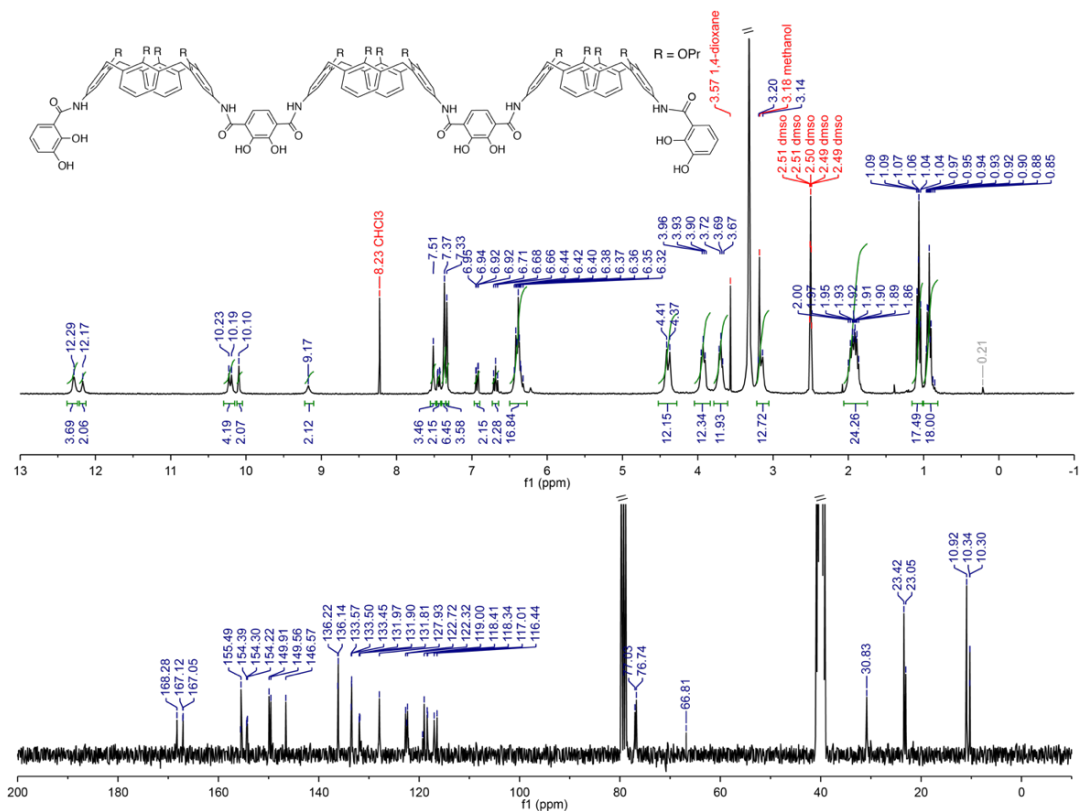


Figure 3-4-13. ¹H NMR spectrum (300 MHz, 40% DMSO-*d*₆-chloroform-*d*₁, 293 K) and ¹³C NMR spectrum (75 MHz, 40% DMSO-*d*₆-chloroform-*d*₁, 293 K) of L3.

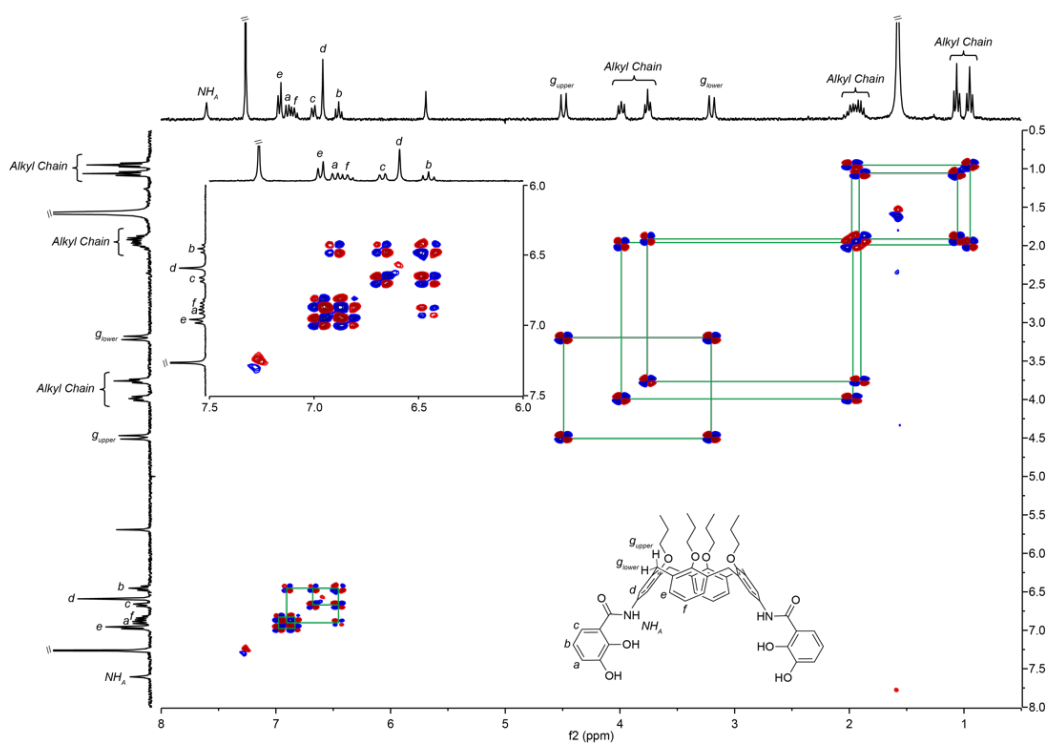


Figure 3-4-14. Selected region of DQF-COSY spectrum (300 MHz, chloroform- d_1 , 293 K) of L1.

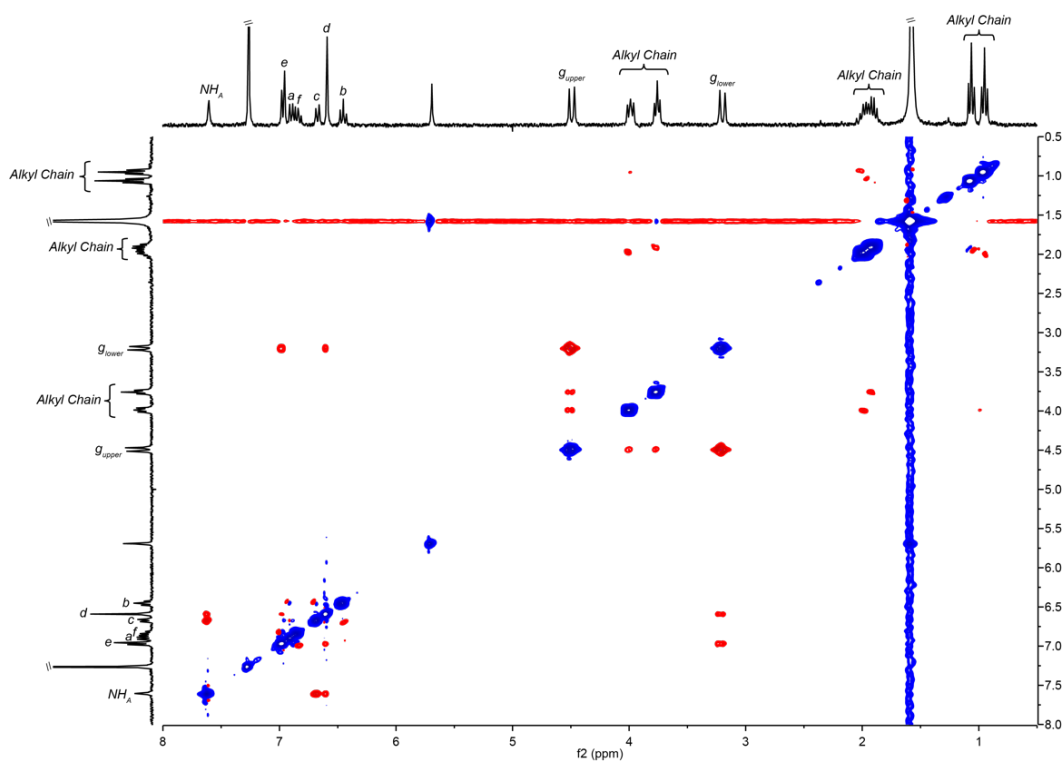


Figure 3-4-15. Selected region of NOESY spectrum (300 MHz, chloroform- d_1 , 293 K) of L1. Mixing time = 400 ms.

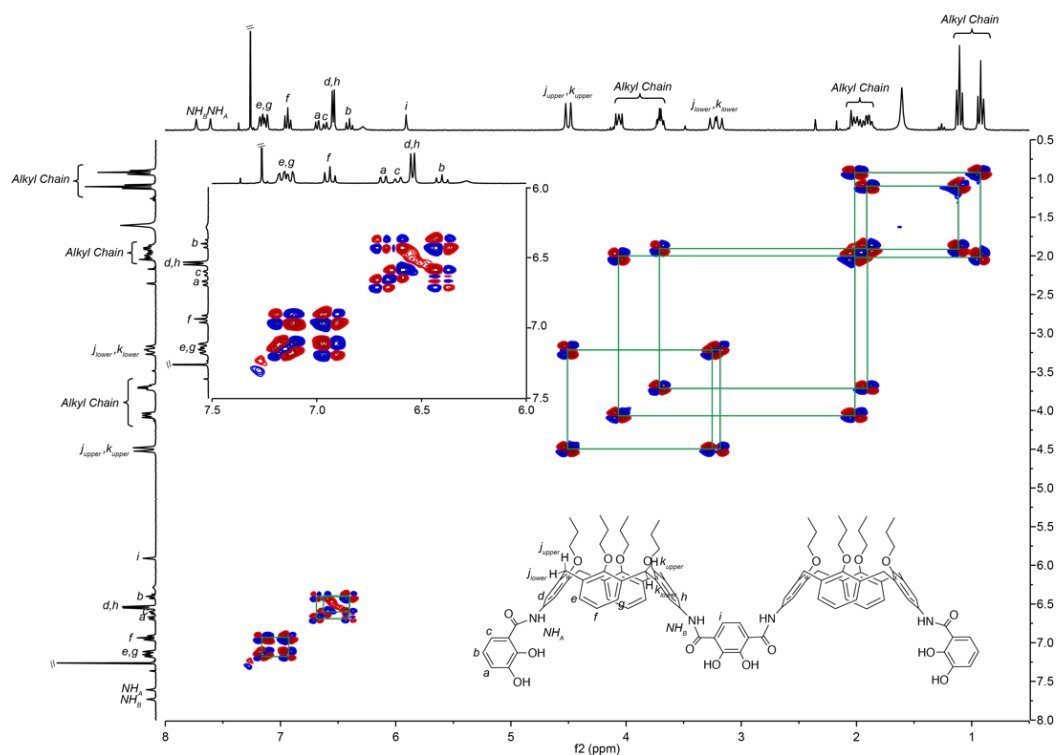


Figure 3-4-16. Selected region of DQF-COSY spectrum (300 MHz, chloroform- d_1 , 293 K) of L2.

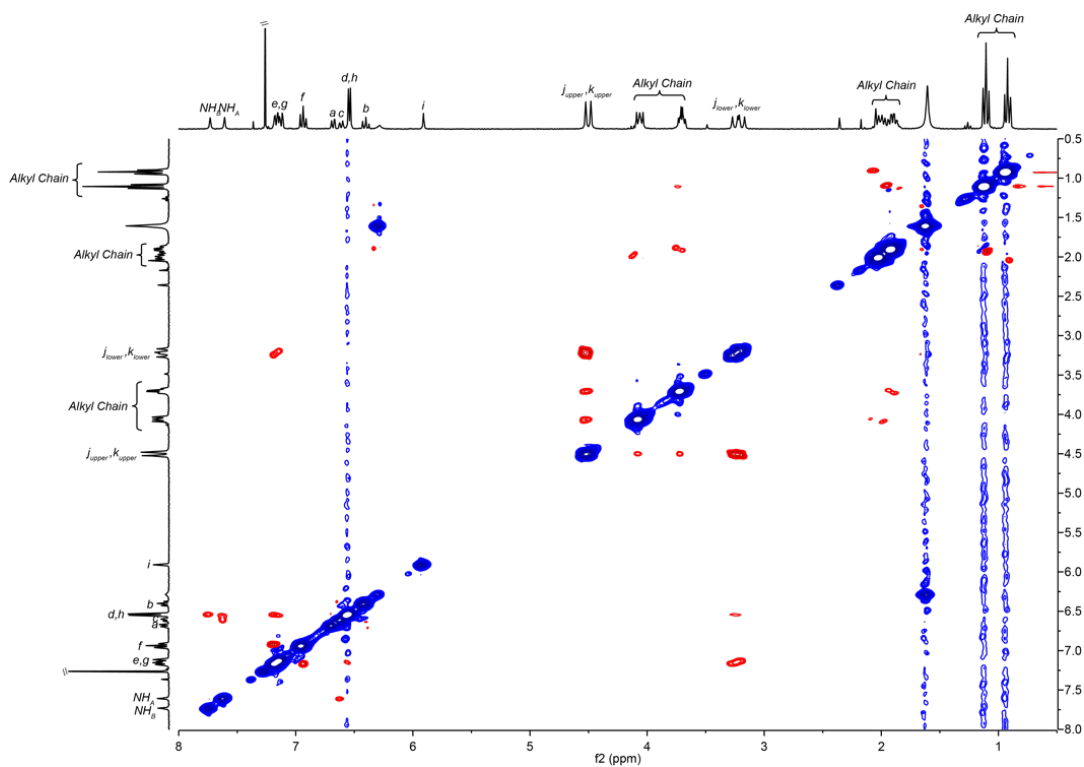


Figure 3-4-17. Selected region of NOESY spectrum (300 MHz, chloroform- d_1 , 293 K) of L2. Mixing time = 400 ms.

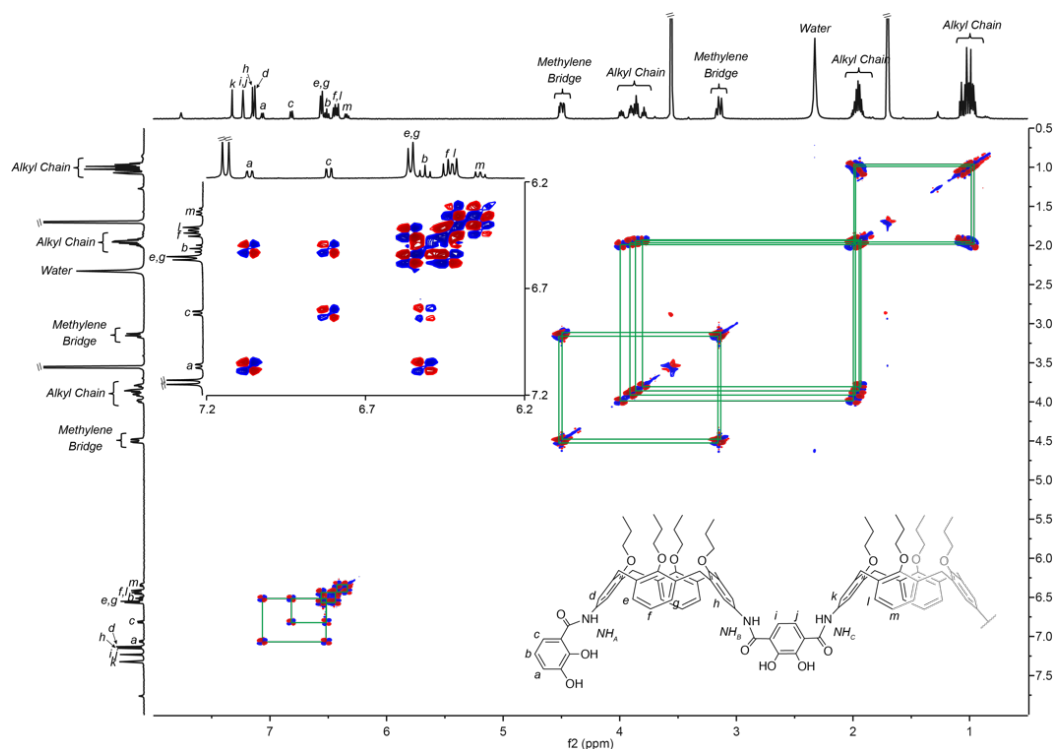


Figure 3-4-18. Selected region of DQF-COSY spectrum (500 MHz, THF- d_8 , 323K) of L3.

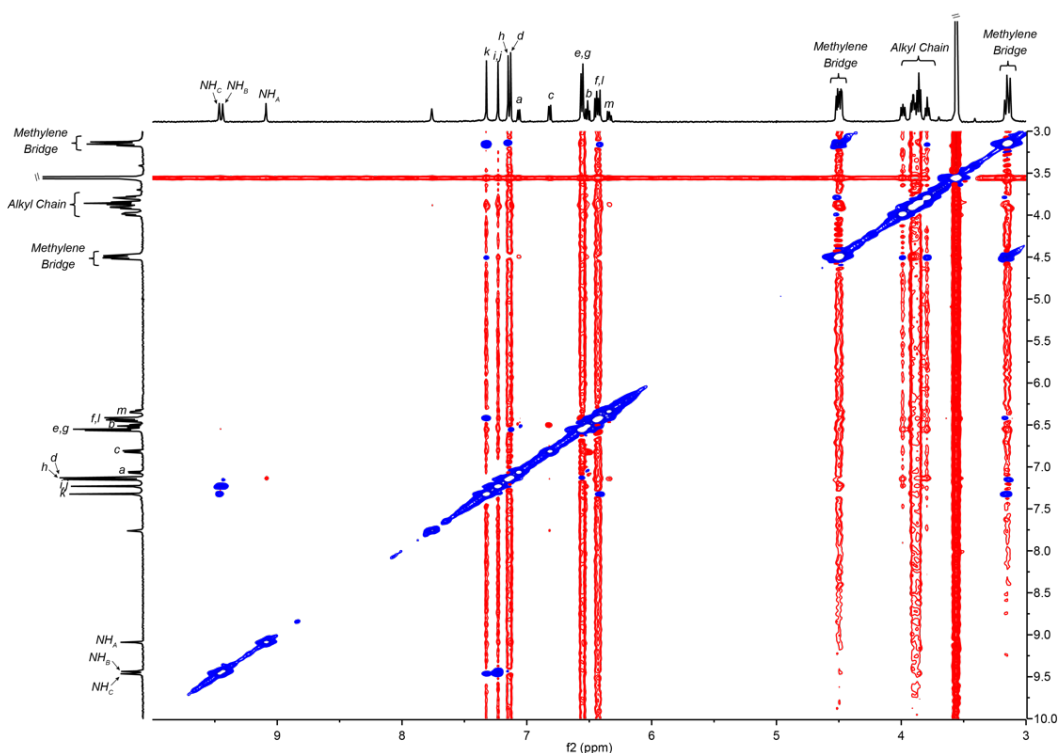


Figure 3-4-19. Selected region of NOESY spectrum (500 MHz, THF- d_8 , 323 K) of L3. Mixing time = 500 ms.

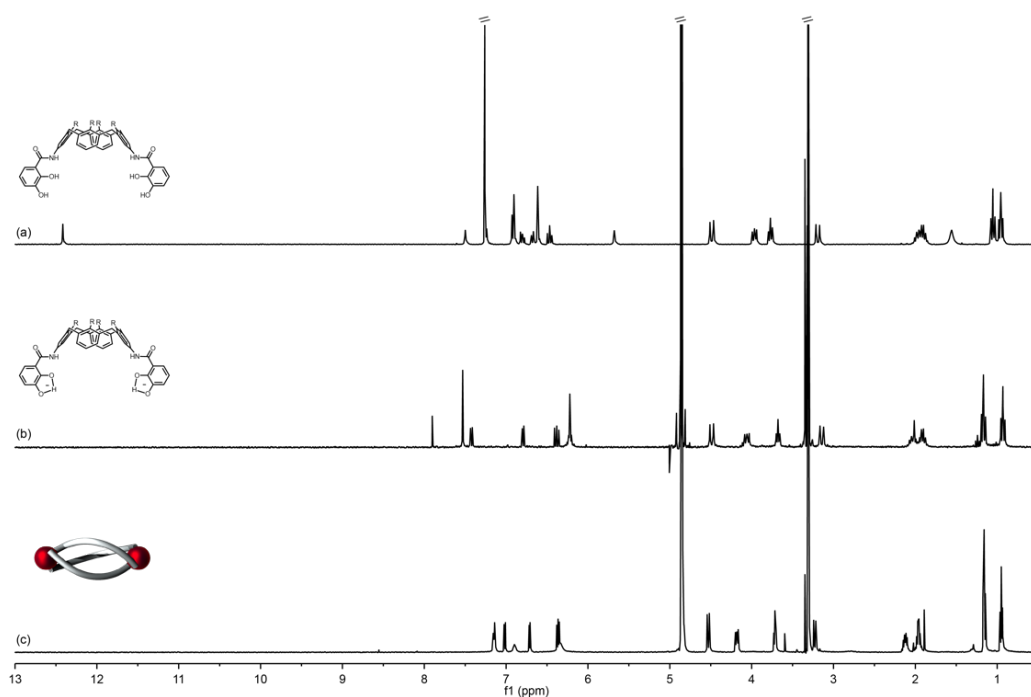


Figure 3-4-20. The formation of 4b. (a) L1 in chloroform- d_1 , (b) $\text{K}_2\text{L1}$ in methanol- d_4 , and (c) 4b in methanol- d_4 .

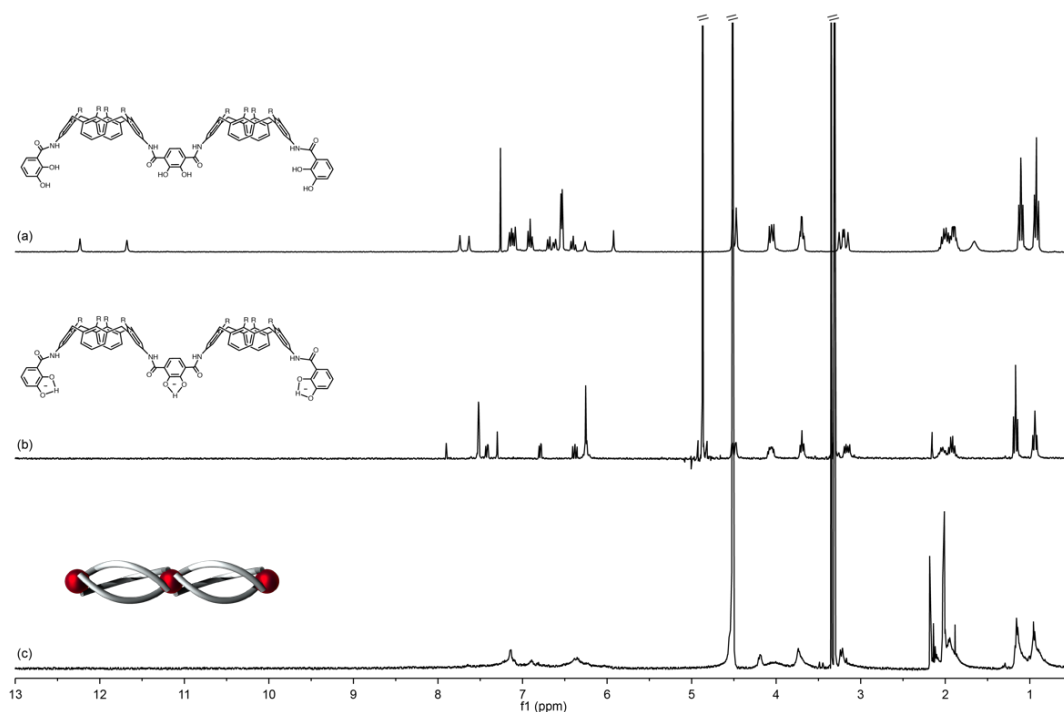


Figure 3-4-21. The formation of the metallohelicite 5b. (a) L2 in chloroform- d_1 , (b) $\text{K}_3\text{L2}$ in methanol- d_4 , and (c) 5b in methanol- d_4 .

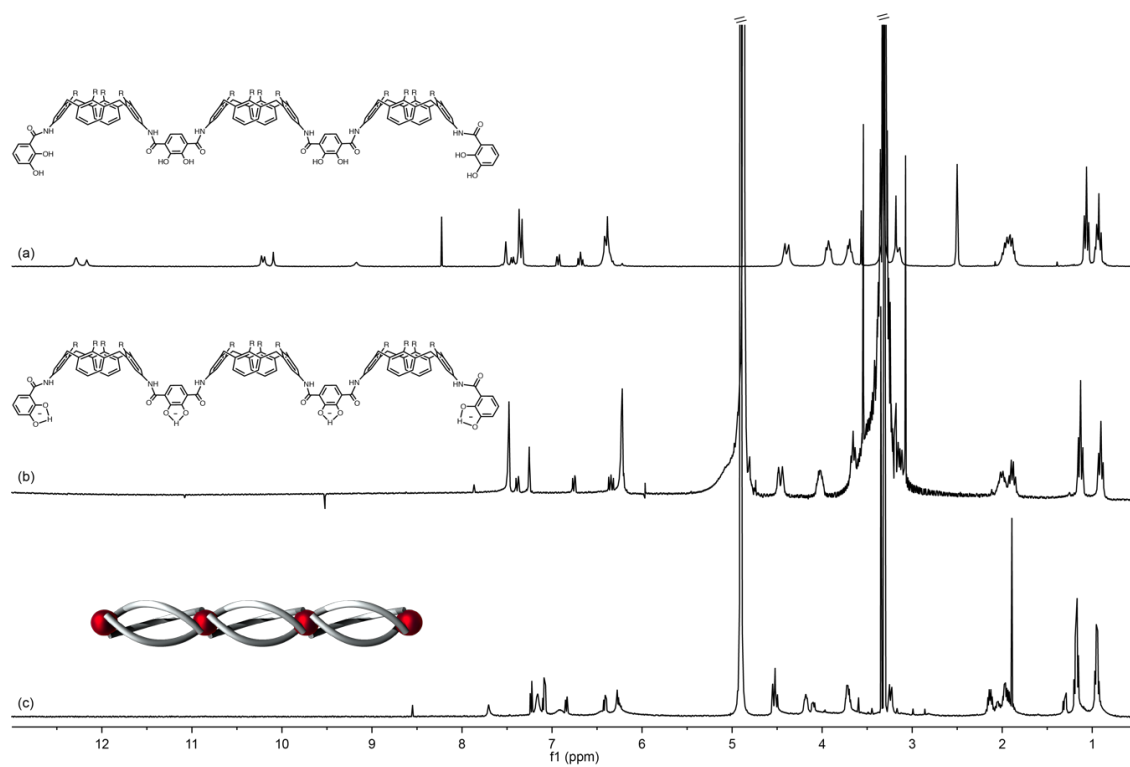


Figure 3-4-22. The formation of the metallosupramolecular assembly **6b**. (a) **L3** in 40% DMSO-*d*₆-chloroform-*d*₁, (b) **K₄L3** in methanol-*d*₄, and (c) **6b** in methanol-*d*₄.

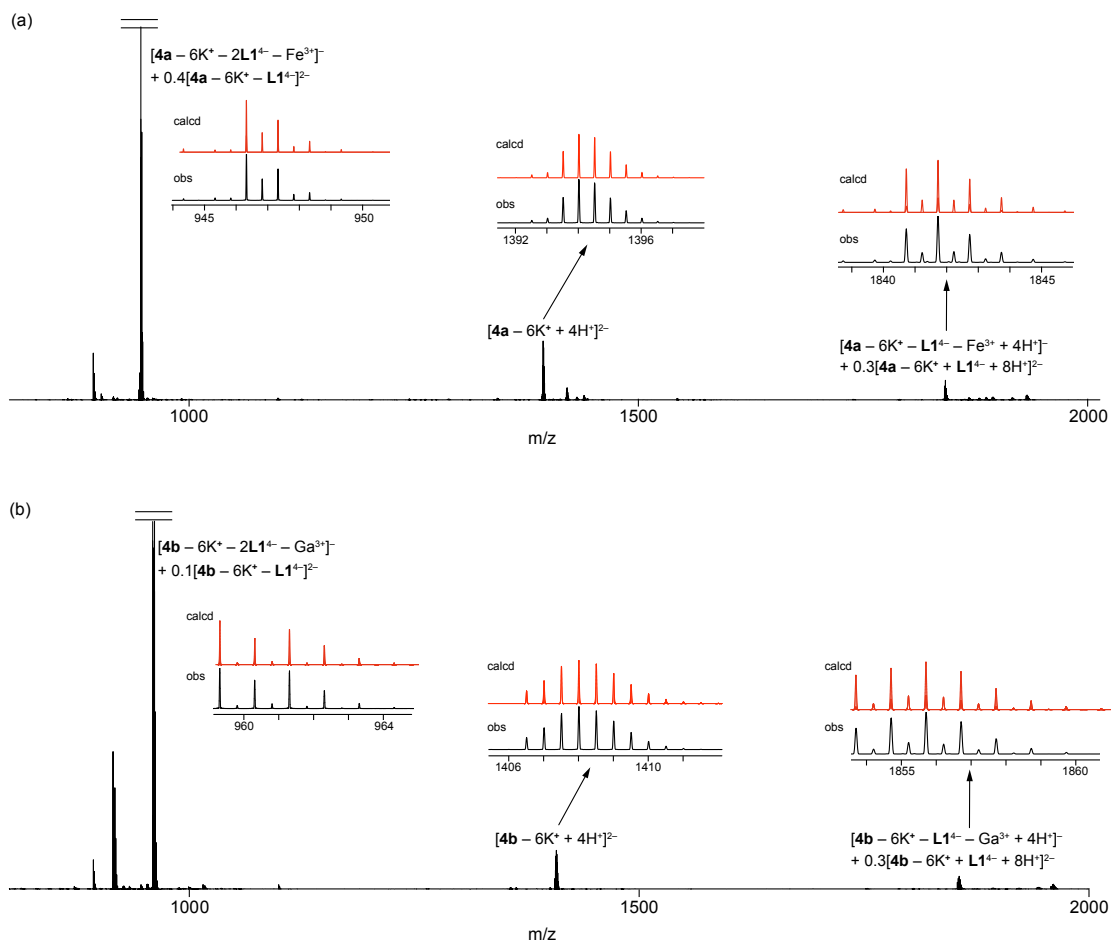


Figure 3-4-23. ESI-MS spectra (negative ion mode) of (a) **4a** and (b) **4b**. Insets in (a) and (b): observed (bottom, black) and calculated (top, red) isotope pattern of (a) **4a** and (b) **4b**.

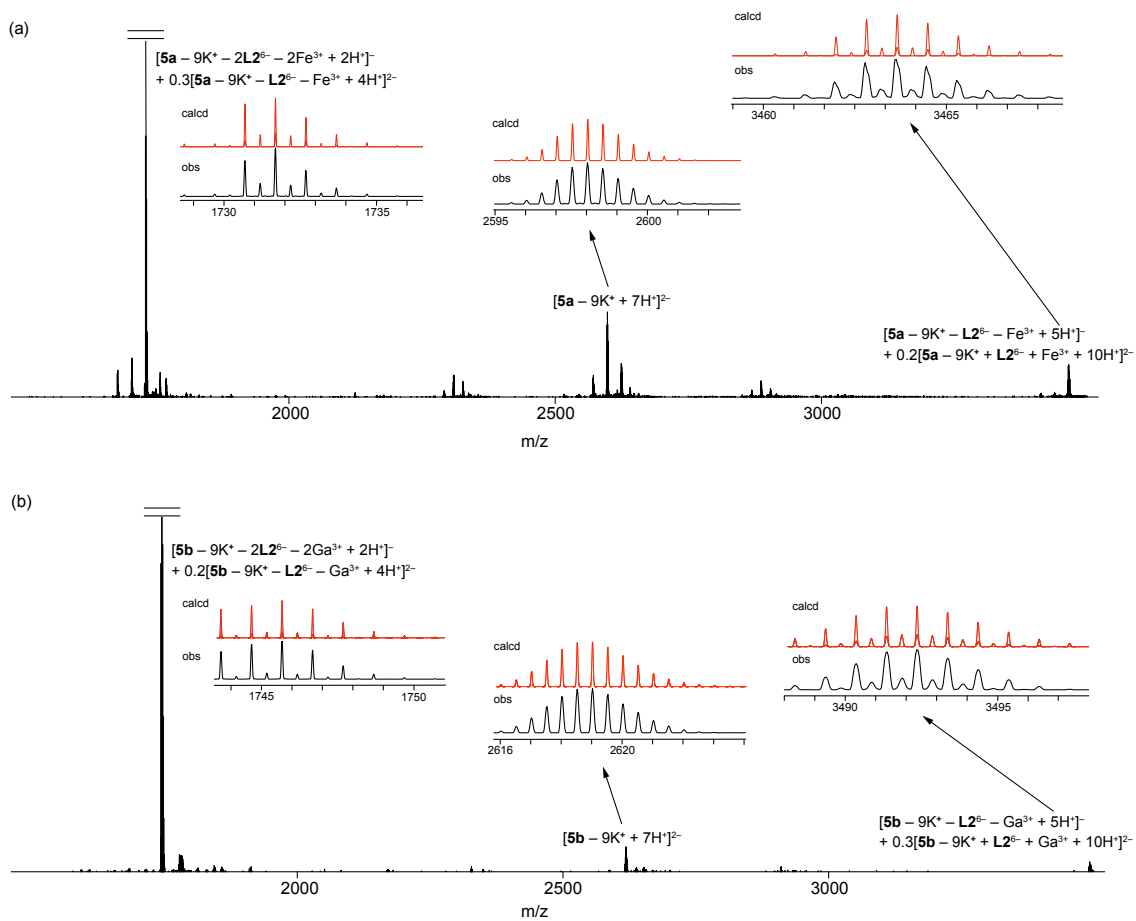


Figure 3-4-24. ESI-MS spectra (negative ion mode) of (a) **5a** and (b) **5b**. Insets in (a) and (b): observed (bottom, black) and calculated (top, red) isotope pattern of (a) **5a** and (b) **5b**.

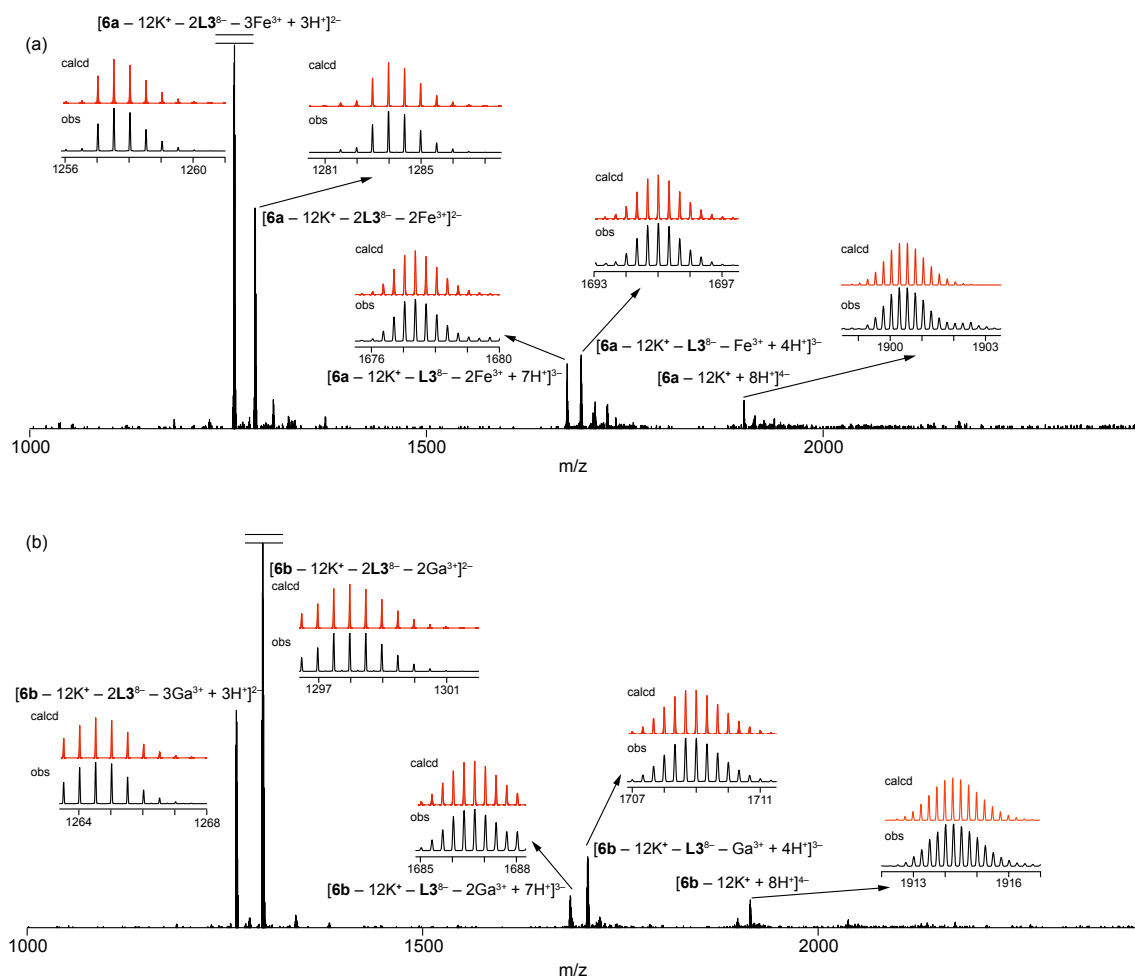


Figure 3-4-25. ESI-MS spectra (negative ion mode) of (a) **6a** and (b) **6b**. Insets in (a) and (b): observed (bottom, black) and calculated (top, red) isotope pattern of (a) **6a** and (b) **6b**.

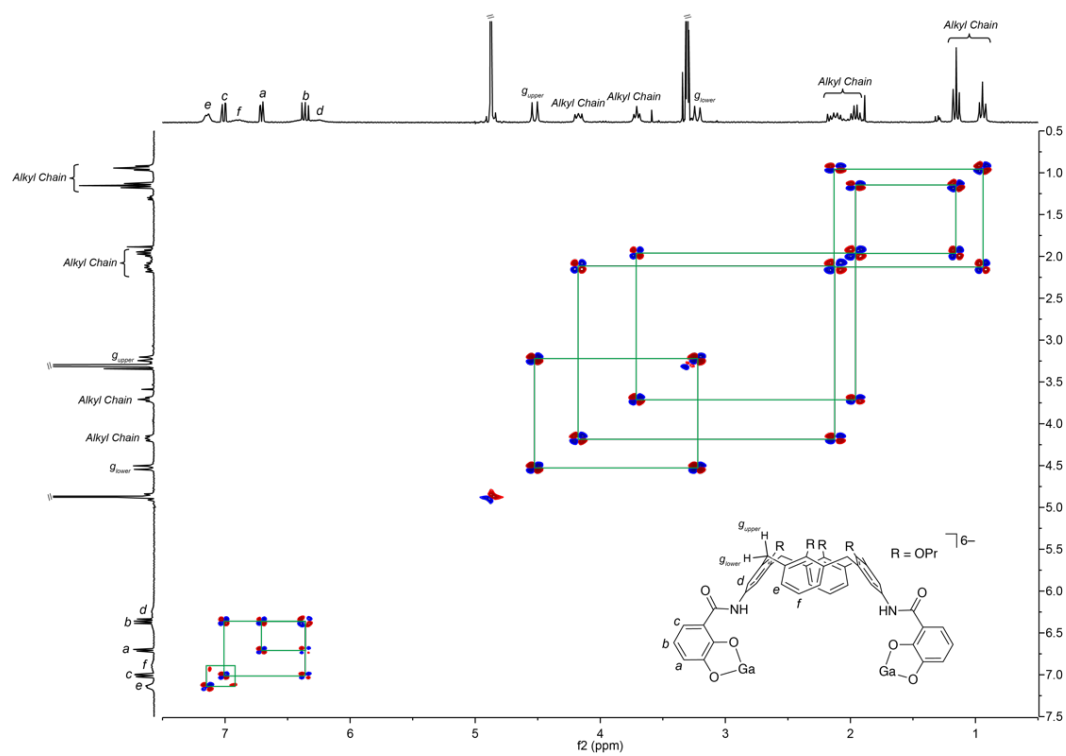


Figure 3-4-26. Selected region of DQF-COSY spectrum (300 MHz, methanol- d_4 , 293 K) of **4b**.

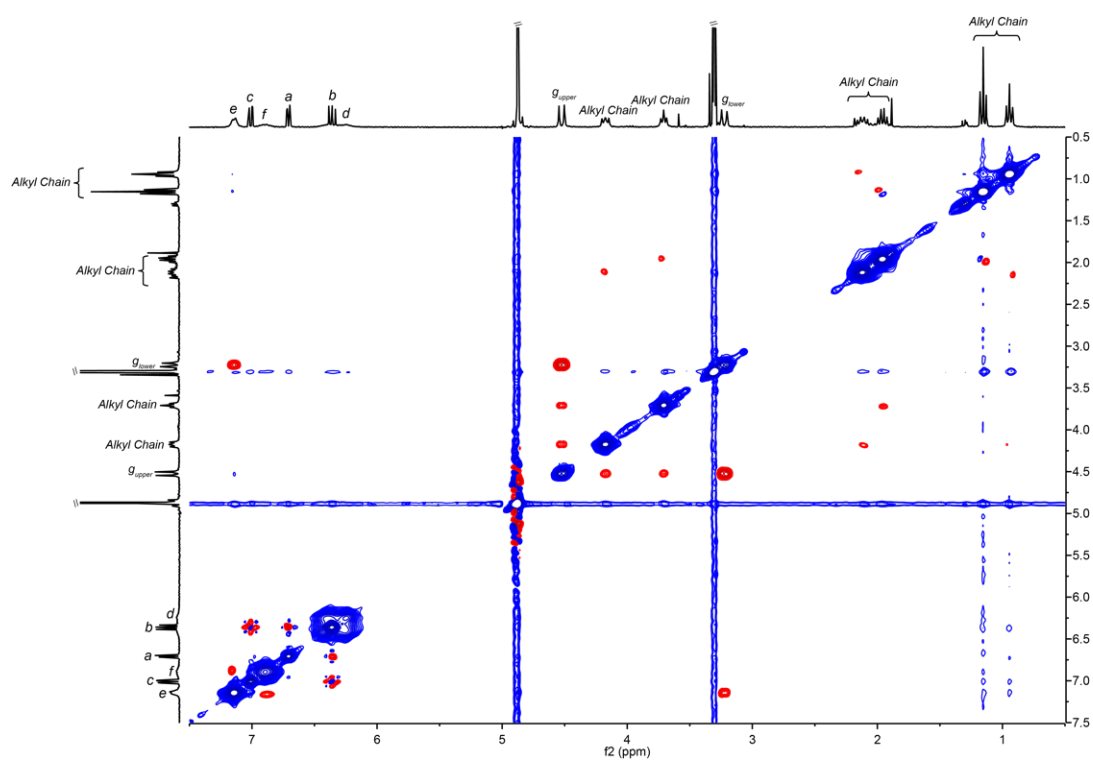


Figure 3-4-27. Selected region of NOESY spectrum (300 MHz, methanol- d_4 , 293 K) of **4b**. Mixing time = 400 ms.

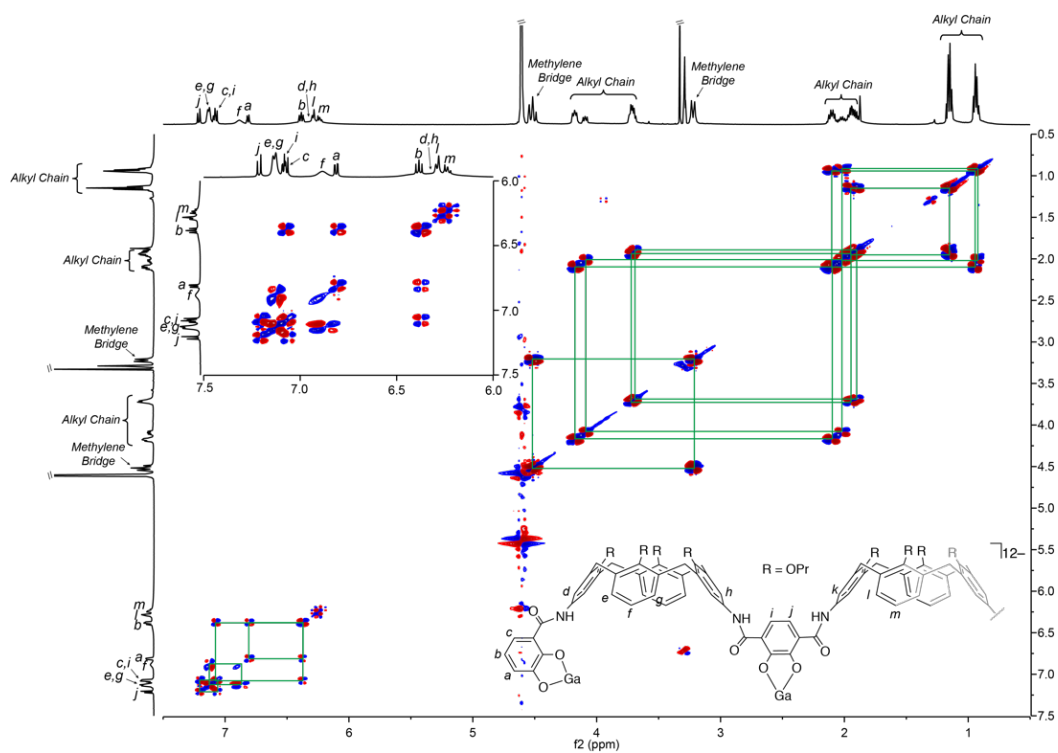


Figure 3-4-28. Selected region of DQF-COSY spectrum (500 MHz, methanol- d_4 , 323 K) of **6b**.

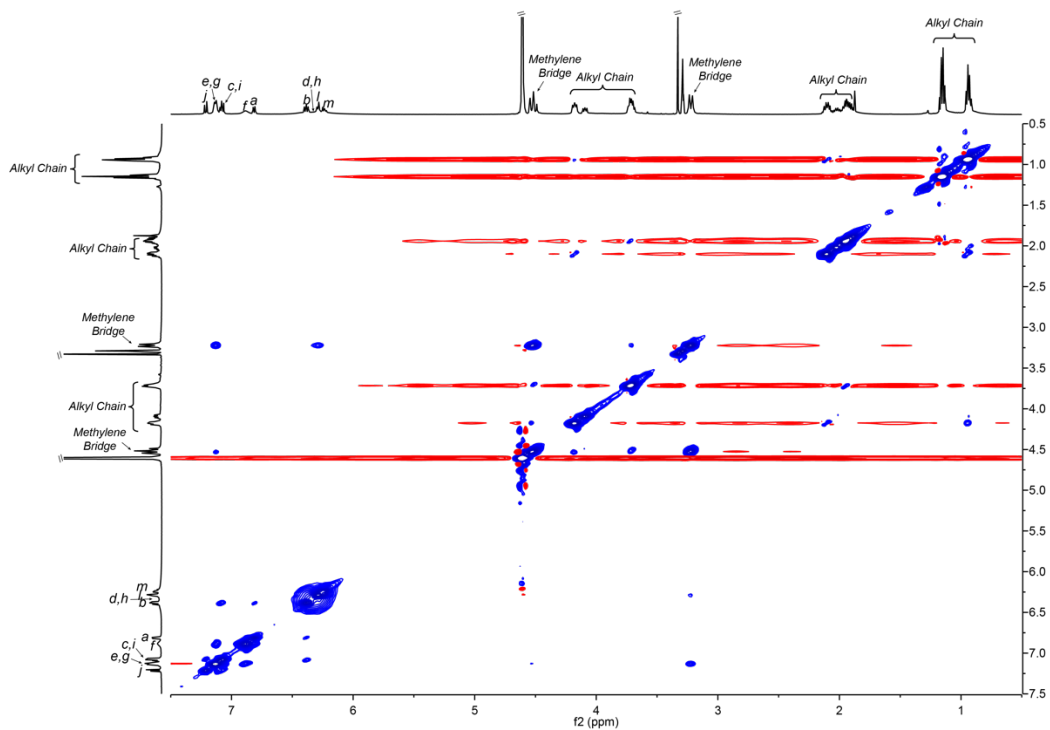


Figure 3-4-29. Selected region of NOESY spectrum (500 MHz, methanol- d_4 , 323 K) of **6b**. Mixing time = 600 ms.

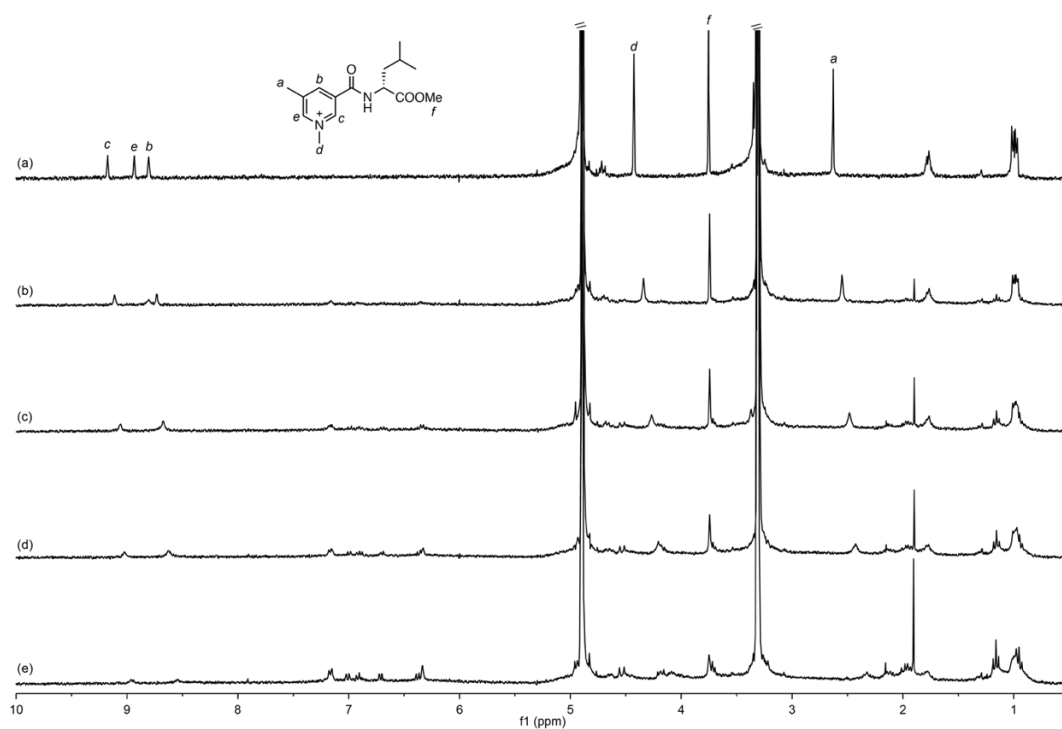


Figure 3-4-31. ^1H NMR (300 MHz, methanol- d_4 , 293 K) titration of (R) -7 ($1.0 \times 10^{-3} \text{ mol L}^{-1}$) with **4b** (a–e: 0, 1.0×10^{-4} , 2×10^{-4} , 3.0×10^{-4} , $5.0 \times 10^{-4} \text{ mol L}^{-1}$).

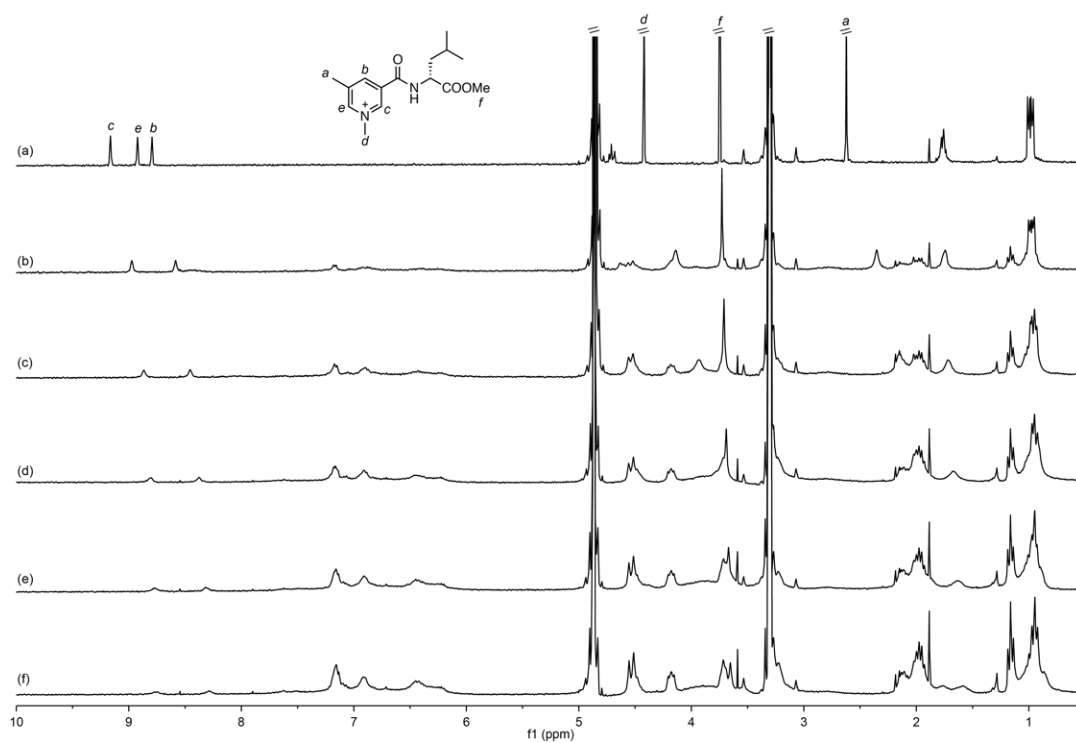


Figure 3-4-32. ^1H NMR (300 MHz, methanol- d_4 , 293 K) titration of (R) -7 ($1.0 \times 10^{-3} \text{ mol L}^{-1}$) with **5b** (a–f: 0, 1.0×10^{-4} , 2×10^{-4} , 3.0×10^{-4} , 4.0×10^{-4} , $5.0 \times 10^{-4} \text{ mol L}^{-1}$).

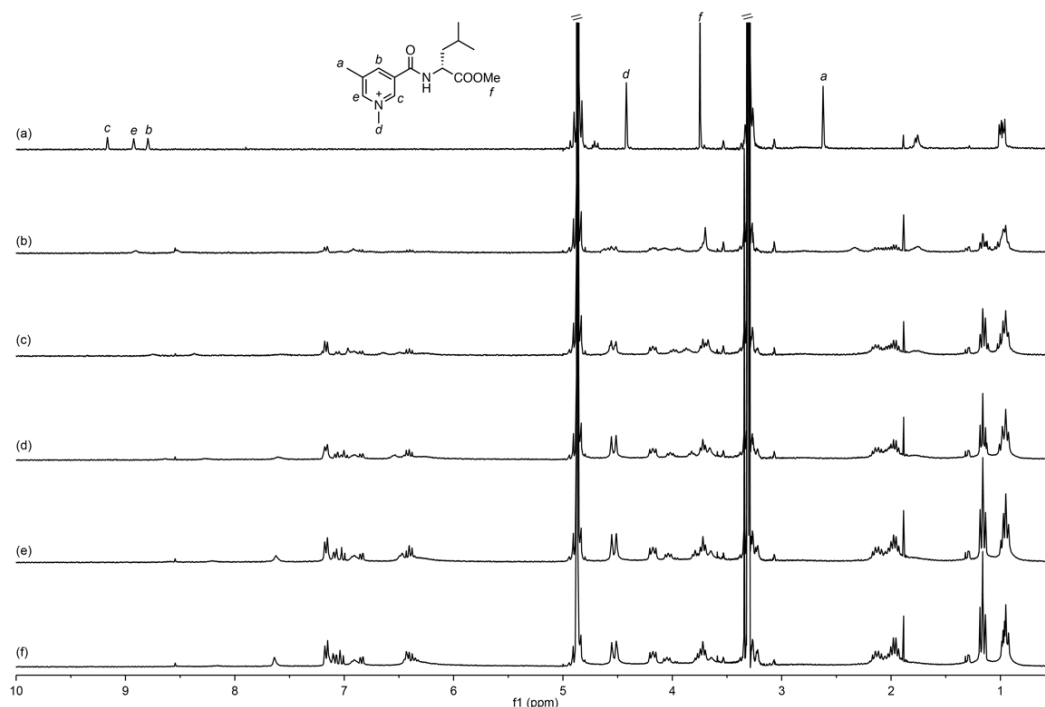


Figure 3-4-33. ^1H NMR (300 MHz, methanol- d_4 , 293 K) titration of (*R*)-**7** (1.0×10^{-3} mol L^{-1}) with **6b** (a–f: 0, 1.0×10^{-4} , 2×10^{-4} , 3.0×10^{-4} , 4.0×10^{-4} , 5.0×10^{-4} mol L^{-1}).

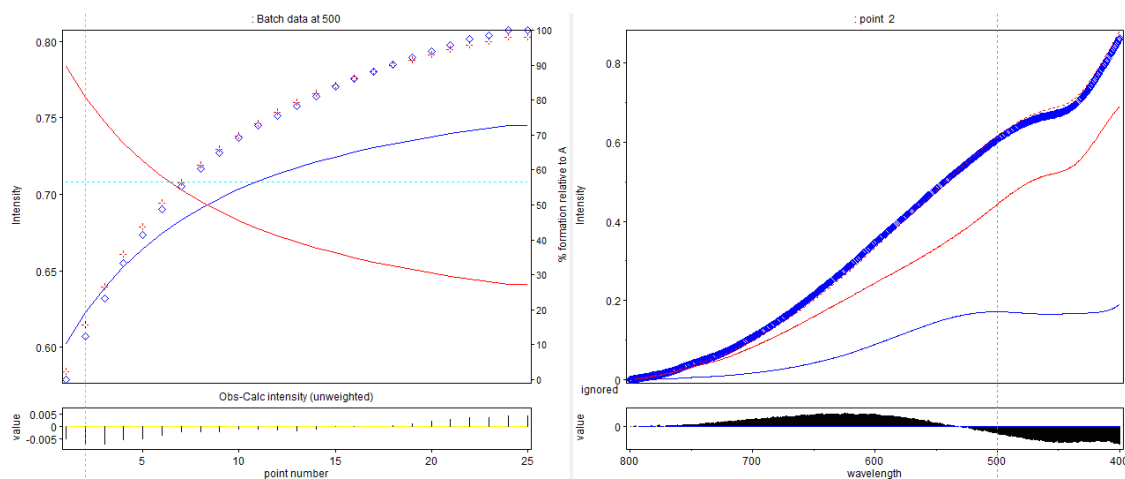


Figure 3-4-34. Non-linear least square fitting of the titration data ($\lambda = 500$ nm) of **4a** and (*R*)-**7** in methanol. **4a** = 1.0×10^{-4} mol L^{-1} . The red crosses and the blue diamonds in the left graph denote the observed and calculated intensity at $\lambda = 500$ nm, respectively. The residues are shown in the bottom of the graph. The red and blue lines in the graphs denote free **4a** and (*R*)-**7** \rightleftharpoons **4a**, respectively.

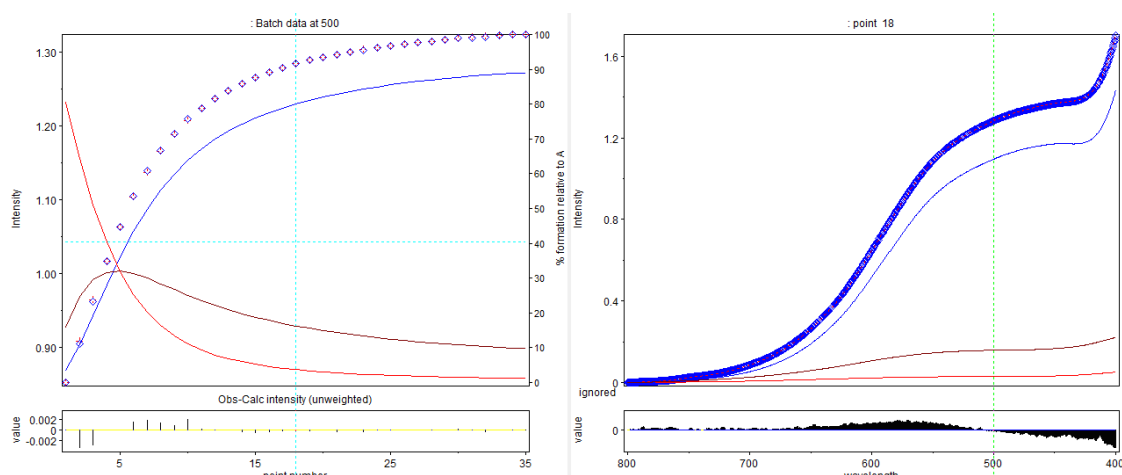


Figure 3-4-35. Non-linear least square fitting of the titration data ($\lambda = 500$ nm) of **5a** and (R)-7 in methanol. **5a** = 1.0×10^{-4} mol L $^{-1}$. The red crosses and the blue diamonds in the left graph denote the observed and calculated intensity at $\lambda = 500$ nm, respectively. The residues are shown in the bottom of the graph. The red, brown, and blue lines in the graphs denote free **5a**, (R)-7 \subset **5a**, and {(R)-7} $_2 \subset$ **5a**, respectively.

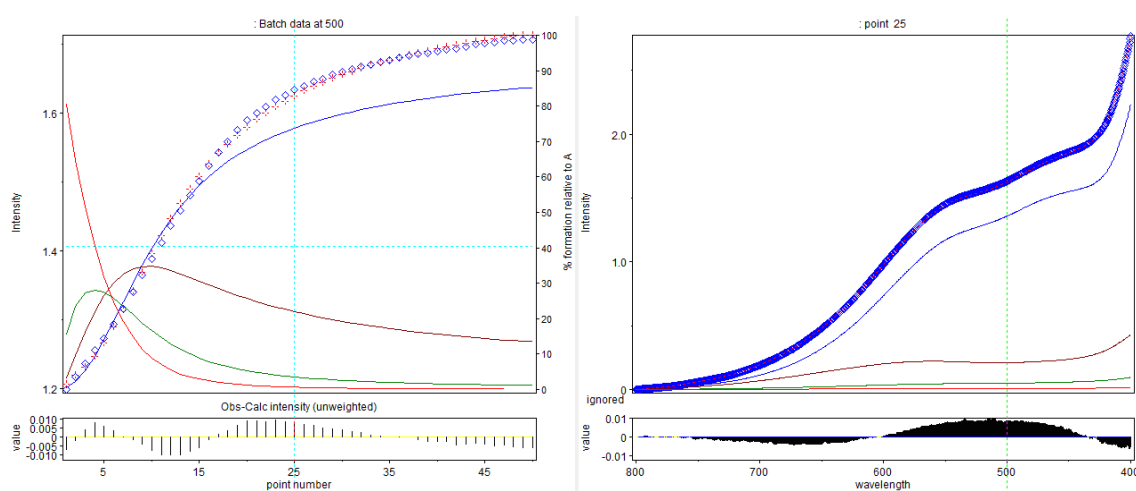


Figure 3-4-36. Non-linear least square fitting of the titration data ($\lambda = 500$ nm) of **6a** and (R)-7 in methanol. **6a** = 1.0×10^{-4} mol L $^{-1}$. The red crosses and the blue diamonds in the left graph denote the observed and calculated intensity at $\lambda = 500$ nm, respectively. The residues are shown in the bottom of the graph. The red, green, brown, and blue lines in the graphs denote free **6a**, (R)-7 \subset **6a**, {(R)-7} $_2 \subset$ **6a**, and {(R)-7} $_3 \subset$ **6a**, respectively.

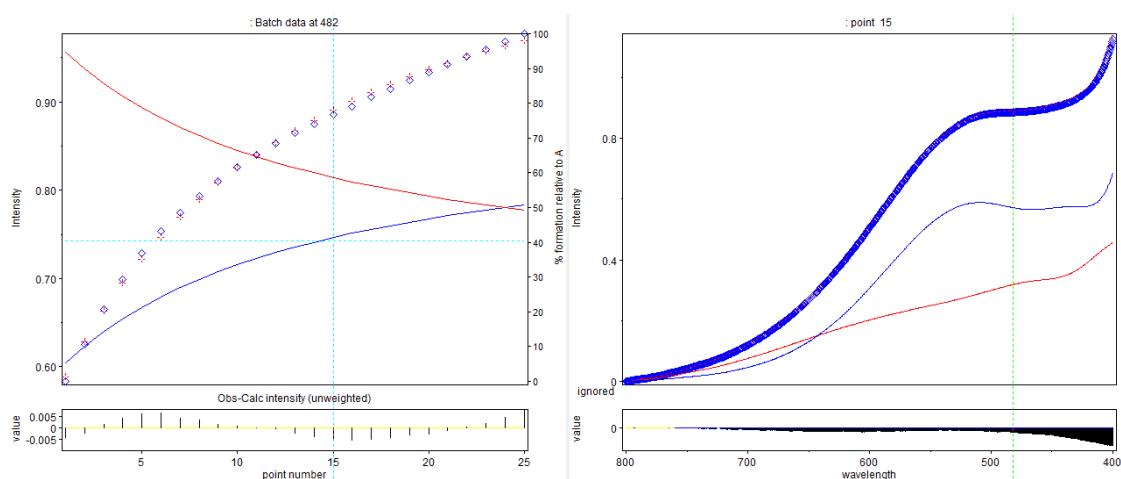


Figure 3-4-37. Non-linear least square fitting of the titration data ($\lambda = 482$ nm) of **4a** and (*R*)-**8** in methanol. **4a** = 1.0×10^{-4} mol L $^{-1}$. The red crosses and the blue diamonds in the left graph denote the observed and calculated intensity at $\lambda = 482$ nm, respectively. The residues are shown in the bottom of the graph. The red and blue lines in the graphs denote free **4a** and (*R*)-**8**⊂**4a**, respectively.

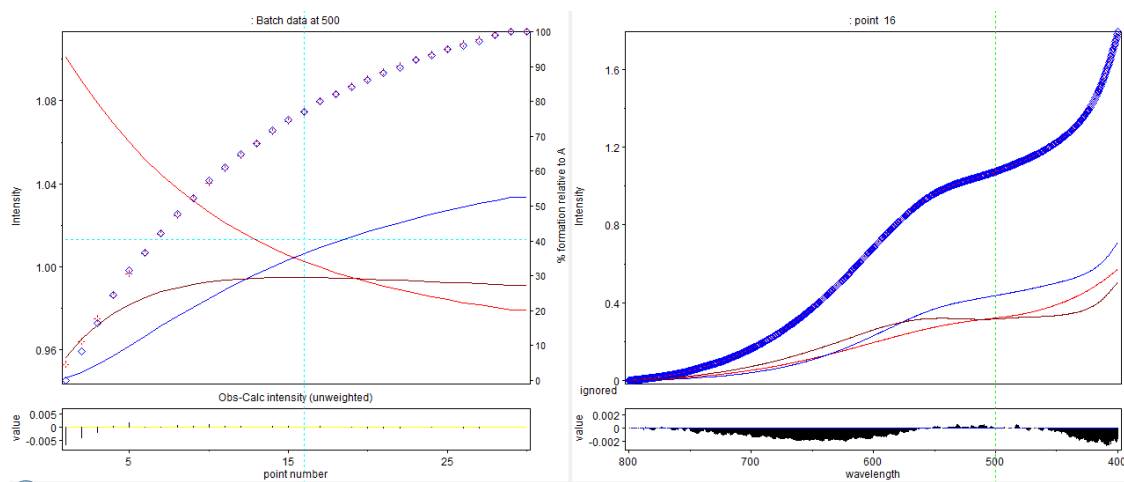


Figure 3-4-38. Non-linear least square fitting of the titration data ($\lambda = 500$ nm) of **5a** and (*R*)-**8** in methanol. **5a** = 1.0×10^{-4} mol L $^{-1}$. The red crosses and the blue diamonds in the left graph denote the observed and calculated intensity at $\lambda = 500$ nm, respectively. The residues are shown in the bottom of the graph. The red, brown, and blue lines in the graphs denote free **5a**, (*R*)-**8**⊂**5a**, and $\{(R)\text{-}8\}_2 \subset \mathbf{5a}$, respectively.

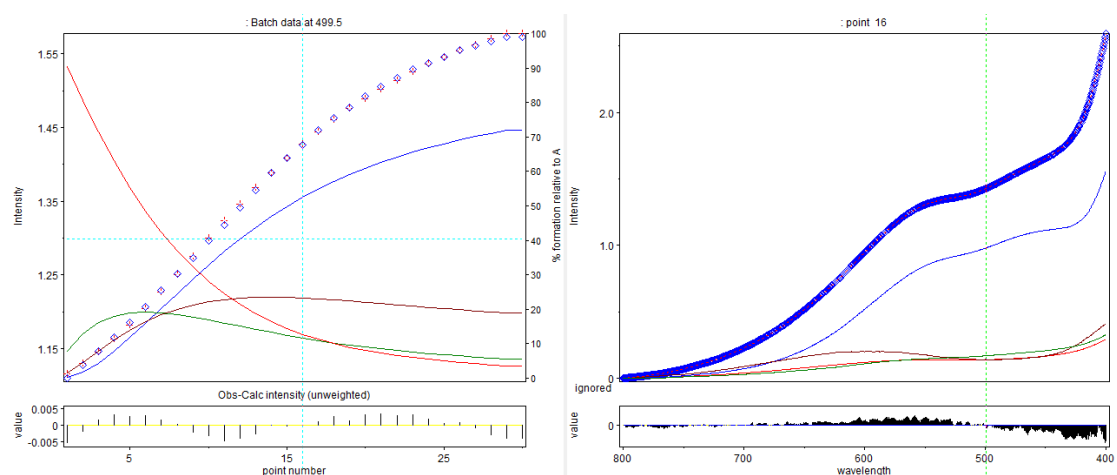


Figure 3-4-39. Non-linear least square fitting of the titration data ($\lambda = 499 \text{ nm}$) of **6a** and $(R)\text{-8}$ in methanol. $6a = 1.0 \times 10^{-4} \text{ mol L}^{-1}$. The red crosses and the blue diamonds in the left graph denote the observed and calculated intensity at $\lambda = 499 \text{ nm}$, respectively. The residues are shown in the bottom of the graph. The red, green, brown, and blue lines in the graphs denote free **6a**, $(R)\text{-8} \subset 6a$, $\{(R)\text{-8}\}_2 \subset 6a$, and $\{(R)\text{-8}\}_3 \subset 6a$, respectively.

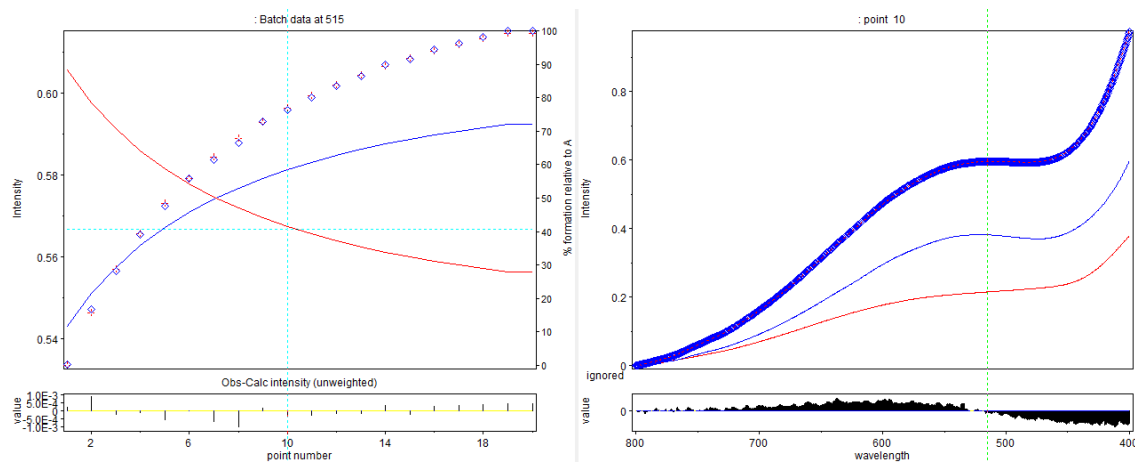


Figure 3-4-40. Non-linear least square fitting of the titration data ($\lambda = 515 \text{ nm}$) of **4a** and $(R)\text{-9}$ in methanol. $4a = 1.0 \times 10^{-4} \text{ mol L}^{-1}$. The red crosses and the blue diamonds in the left graph denote the observed and calculated intensity at $\lambda = 515 \text{ nm}$, respectively. The residues are shown in the bottom of the graph. The residues are shown in the bottom of the graph. The red and blue lines in the graphs denote free **4a** and $(R)\text{-9} \subset 4a$, respectively.

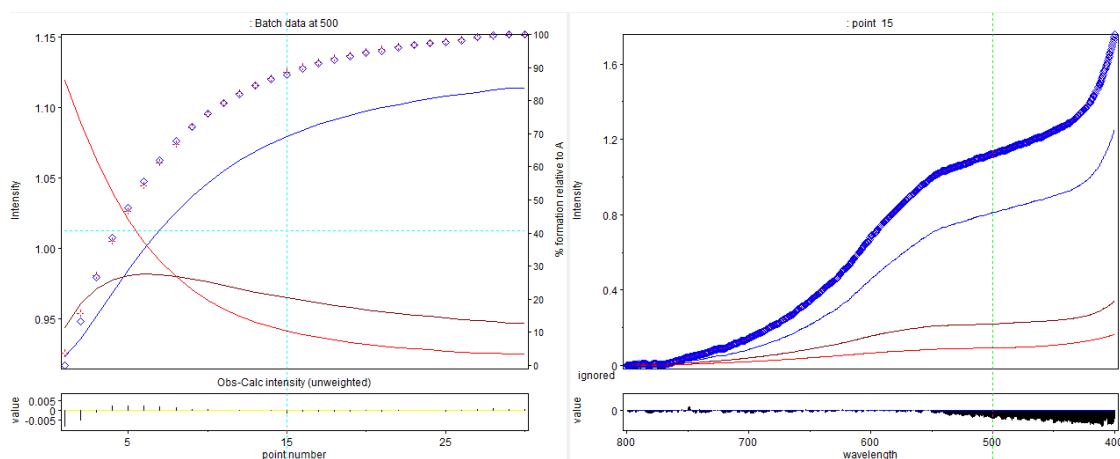


Figure 3-4-41. Non-linear least square fitting of the titration data ($\lambda = 500$ nm) of **5a** and (R) -**9** in methanol. **5a** = 1.0×10^{-4} mol L $^{-1}$. The red crosses and the blue diamonds in the left graph denote the observed and calculated intensity at $\lambda = 500$ nm, respectively. The residues are shown in the bottom of the graph. The red, brown, and blue lines in the graphs denote free **5a**, (R) -**9** \subset **5a**, and $\{(R)$ -**9** $\}_2\subset$ **5a**, respectively.

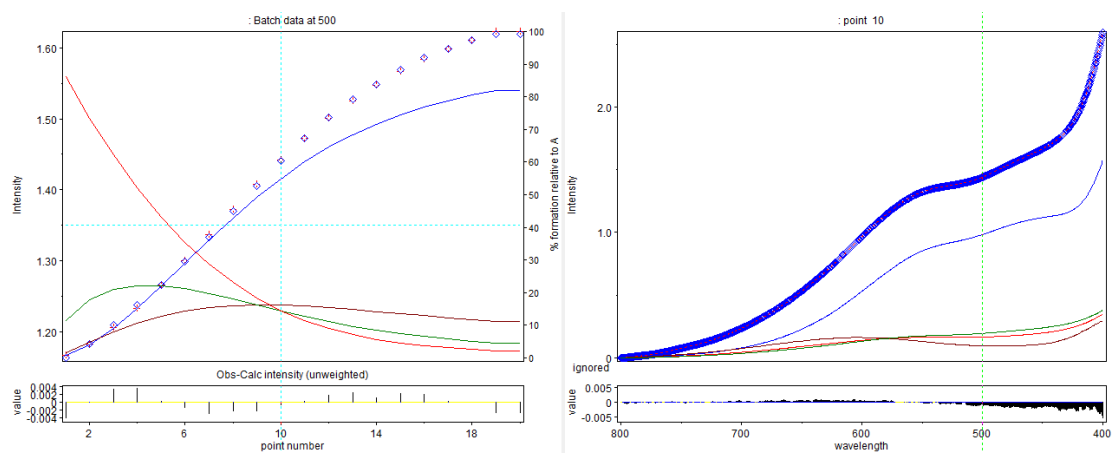


Figure 3-4-42. Non-linear least square fitting of the titration data ($\lambda = 500$ nm) of **6a** and (R) -**9** in methanol. **6a** = 1.0×10^{-4} mol L $^{-1}$. The red crosses and the blue diamonds in the left graph denote the observed and calculated intensity at $\lambda = 500$ nm, respectively. The residues are shown in the bottom of the graph. The red, green, brown, and blue lines in the graphs denote free **6a**, (R) -**9** \subset **6a**, $\{(R)$ -**9** $\}_2\subset$ **6a**, and $\{(R)$ -**9** $\}_3\subset$ **6a**, respectively.

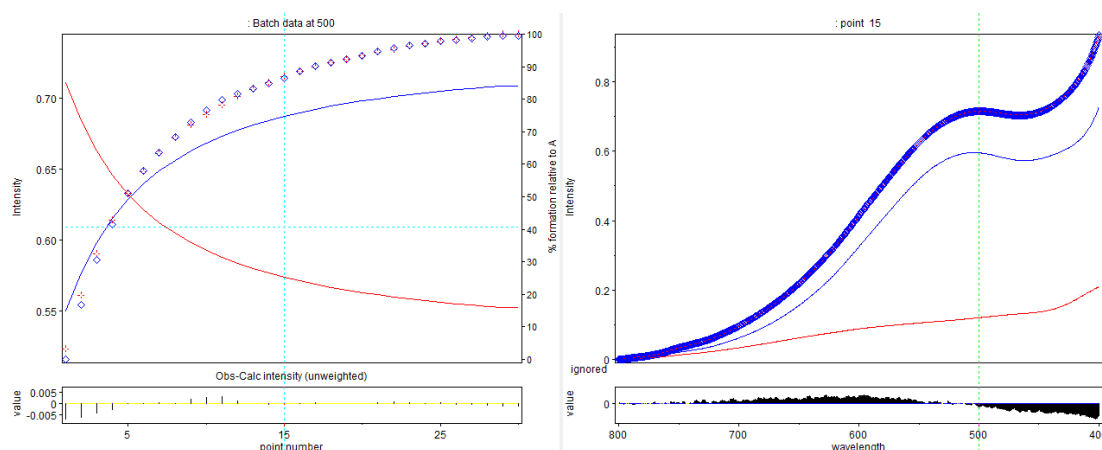


Figure 3-4-43. Non-linear least square fitting of the titration data ($\lambda = 500$ nm) of **4a** and **10** in methanol. **4a** = 1.0×10^{-4} mol L $^{-1}$. The red crosses and the blue diamonds in the left graph denote the observed and calculated intensity at $\lambda = 500$ nm, respectively. The residues are shown in the bottom of the graph. The red and blue lines in the graphs denote free **4a** and **10** \subset **4a**, respectively.

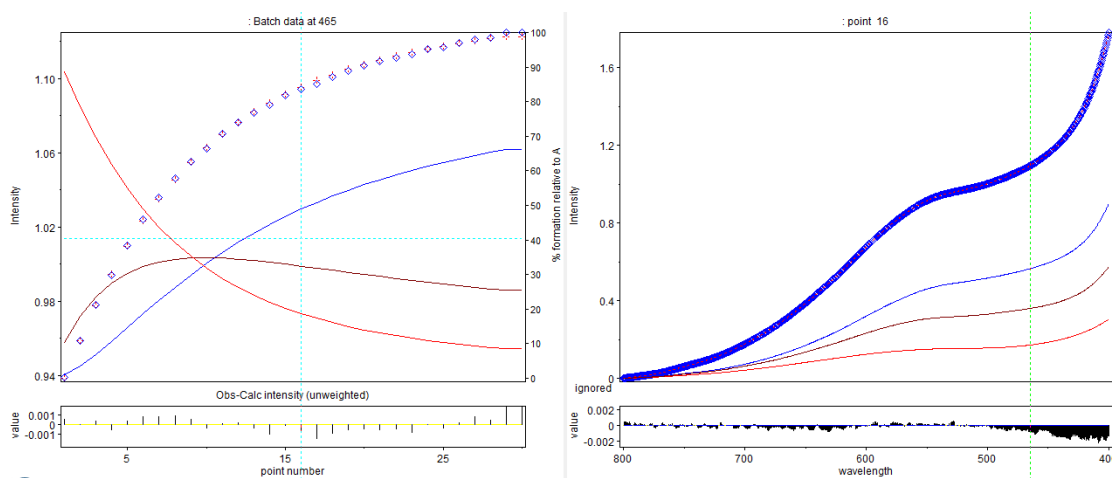


Figure 3-4-44. Non-linear least square fitting of the titration data ($\lambda = 465$ nm) of **5a** and **10** in methanol. **5a** = 1.0×10^{-4} mol L $^{-1}$. The red crosses and the blue diamonds in the left graph denote the observed and calculated intensity at $\lambda = 465$ nm, respectively. The residues are shown in the bottom of the graph. The red, brown, and blue lines in the graphs denote free **5a**, **10** \subset **5a**, and **(10) $_2$** \subset **5a**, respectively.

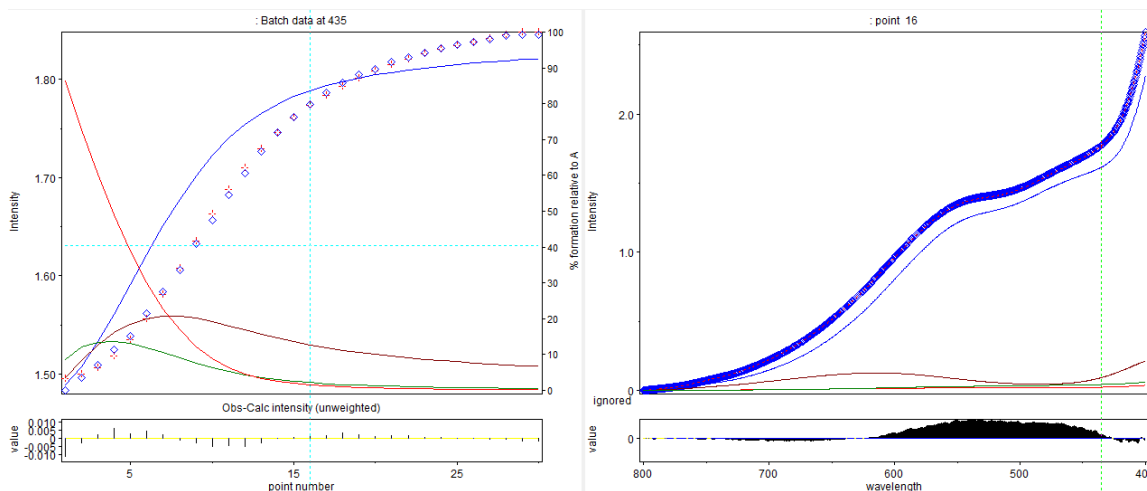


Figure 3-4-45. Non-linear least square fitting of the titration data ($\lambda = 435$ nm) of **6a** and **10** in methanol. **6a** = 1.0×10^{-4} mol L $^{-1}$. The red crosses and the blue diamonds in the left graph denote the observed and calculated intensity at $\lambda = 435$ nm, respectively. The residues are shown in the bottom of the graph. The red, green, brown, and blue lines in the graphs denote free **6a**, **10** \subset **6a**, **(10)** $_2$ \subset **6a**, and **(10)** $_3$ \subset **6a**, respectively.

Table 3-4-2. Normalized ICD intensities and molecular circular dichroisms ($\Delta\epsilon / \text{L mol}^{-1} \text{cm}^{-1}$) of helicates **4a–6a** (1.0×10^{-4} mol L $^{-1}$) in the presence of guests **7** at 298 K in methanol. The total concentrations of the (*R*)- and (*S*)-guests were maintained to be 1.0×10^{-2} mol L $^{-1}$.

7	Normalized ICD ($\Delta\epsilon / \text{L mol}^{-1} \text{cm}^{-1}$)		
	4a	5a	6a
<i>ee</i> / %			
0	0.000 (0.00)	0.000 (0.00)	0.000 (0.00)
20	0.146 (−1.37)	0.314 (1.53)	0.372 (−0.798)
40	0.341 (−3.21)	0.479 (2.33)	0.590 (−1.27)
60	0.579 (−5.45)	0.658 (3.20)	0.730 (−1.57)
80	0.746 (−7.02)	0.849 (4.13)	0.917 (−1.97)
100	1.00 (−9.41)	1.00 (4.86)	1.00 (−2.15)

ICD intensities were observed at 365, 439.5, and 569.5 nm for **4a**, **5a**, and **6a**, respectively.

Table 3-4-3. Normalized ICD intensities and molecular circular dichroisms ($\Delta\epsilon / \text{L mol}^{-1} \text{cm}^{-1}$) of helicates **4a–6a** ($1.0 \times 10^{-4} \text{ mol L}^{-1}$) in the presence of guests **8** at 298 K in methanol. The total concentrations of the (*R*)- and (*S*)-guests were maintained to be $1.0 \times 10^{-2} \text{ mol L}^{-1}$.

8	Normalized ICD ($\Delta\epsilon / \text{L mol}^{-1} \text{cm}^{-1}$)		
<i>ee</i> / %	4a	5a	6a
0	0.000 (0.00)	0.000 (0.00)	0.000 (0.00)
20	0.256 (0.720)	0.526 (15.0)	0.587 (−0.994)
40	0.471 (1.32)	0.733 (21.0)	0.901 (−1.53)
60	0.675 (1.90)	0.880 (25.2)	0.893 (−1.51)
80	0.803 (2.26)	0.954 (27.3)	0.951 (−1.61)
100	1.00 (2.81)	1.00 (28.6)	1.00 (−1.69)

ICD intensities were observed at 553.5, 366, and 465 nm for **4a**, **5a**, and **6a**, respectively.

Table 3-4-4. Normalized ICD intensities and molecular circular dichroisms ($\Delta\epsilon / \text{L mol}^{-1} \text{cm}^{-1}$) of helicates **4a–6a** ($1.0 \times 10^{-4} \text{ mol L}^{-1}$) in the presence of guests **9** at 298 K in methanol. The total concentrations of the (*R*)- and (*S*)-guests were maintained to be $1.0 \times 10^{-2} \text{ mol L}^{-1}$.

9	Normalized ICD ($\Delta\epsilon / \text{L mol}^{-1} \text{cm}^{-1}$)		
<i>ee</i> / %	4a	5a	6a
0	0.000 (0.00)	0.000 (0.00)	0.000 (0.00)
20	0.170 (0.695)	0.450 (2.95)	0.642 (−0.612)
40	0.394 (1.61)	0.642 (4.21)	0.927 (−0.883)
60	0.624 (2.56)	0.828 (5.43)	0.953 (−0.908)
80	0.851 (3.49)	0.925 (6.07)	0.981 (−0.935)
100	1.00 (4.10)	1.00 (6.56)	1.00 (−0.953)

ICD intensities were observed at 529, 460, and 454 nm for **4a**, **5a**, and **6a**, respectively.

3-5 References

- [1] R. A. Hegstrom, D. K. Kondepudi, *Sci. Am.* **1990**, 262, 108-115.
- [2] A. Klug, *Angew. Chem. Int. Ed. Engl.* **1983**, 22, 565-582.
- [3] K. C. Holmes, D. Popp, W. Gebhard, W. Kabsch, *Nature* **1990**, 347, 44-49.
- [4] J. D. Watson, F. H. C. Crick, *Nature* **1953**, 171, 737-738.
- [5] L. Pauling, R. B. Corey, H. R. Branson, *Proc. Natl. Acad. Sci. USA* **1951**, 37, 205-211.
- [6] a) M. Liu, L. Zhang, T. Wang, *Chem. Rev.* **2015**, 115, 7304-7397; b) E. Yashima, N. Ousaka, D. Taura, K. Shimomura, T. Ikai, K. Maeda, *Chem. Rev.* **2016**, 116, 13752-13990.
- [7] a) J.-M. Lehn, *Supramolecular Chemistry: Concepts and Perspectives*, VCH, Weinheim, **1995**; b) M. A. Mateos-Timoneda, M. Crego-Calama, D. N. Reinhoudt, *Chem. Soc. Rev.* **2004**, 33, 363-372; c) E. Yashima, K. Maeda, Y. Furusho, *Acc. Chem. Res.* **2008**, 41, 1166-1180; d) Q. Jin, L. Zhang, H. Cao, T. Wang, X. Zhu, J. Jiang, M. Liu, *Langmuir* **2011**, 27, 13847-13853; e) M. M. Safont-Sempere, G. Fernández, F. Würthner, *Chem. Rev.* **2011**, 111, 5784-5814; f) J. Kumar, T. Nakashima, H. Tsumatori, T. Kawai, *J. Phys. Chem. Lett.* **2014**, 5, 316-321.
- [8] a) N. Kimizuka, T. Kawasaki, K. Hirata, T. Kunitake, *J. Am. Chem. Soc.* **1995**, 117, 6360-6361; b) J. H. K. K. Hirschberg, L. Brunsveld, A. Ramzi, J. A. J. M. Vekemans, R. P. Sijbesma, E. W. Meijer, *Nature* **2000**, 407, 167-170; c) M. Reggelin, M. Schultz, M. Holbach, *Angew. Chem. Int. Ed.* **2002**, 41, 1614-1617; d) P. Jonkheijm, F. J. M. Hoeben, R. Kleppinger, J. van Herrikhuyzen, A. P. H. J. Schenning, E. W. Meijer, *J. Am. Chem. Soc.* **2003**, 125, 15941-15949; e) M. M. J. Smulders, A. P. H. J. Schenning, E. W. Meijer, *J. Am. Chem. Soc.* **2008**, 130, 606-611; f) T. Yamamoto, M. Suginome, *Angew. Chem. Int. Ed.* **2009**, 48, 539-542; g) S. Yagai, H. Aonuma, Y. Kikkawa, S. Kubota, T. Karatsu, A. Kitamura, S. Mahesh, A. Ajayaghosh, *Chem. Eur. J.* **2010**, 16, 8652-8661; h) F. Würthner, T. E. Kaiser, C. R. Saha-Möller, *Angew. Chem. Int. Ed.* **2011**, 50, 3376-3410; i) R. P. Megens, G. Roelfes, *Chem. Eur. J.* **2011**, 17, 8514-8523; j) P. A. Korevaar, S. J. George, A. J. Markvoort, M. M. J. Smulders, P. A. J. Hilbers, A. P. H. J. Schenning, T. F. A. De Greef, E. W. Meijer, *Nature* **2012**, 481, 492-496; k) T. Miyabe, H. Iida, A. Ohnishi, E. Yashima, *Chem. Sci.* **2012**, 3, 863-867; l) S. I. Stupp, L. C. Palmer, *Chem. Mater.* **2014**, 26, 507-518; m) Y. Akai,

- L. Konnert, T. Yamamoto, M. Suginome, *Chem. Commun.* **2015**, 51, 7211-7214; n) H. Wang, N. Li, Z. Yan, J. Zhang, X. Wan, *RSC Adv.* **2015**, 5, 2882-2890; o) Y. Yoshinaga, T. Yamamoto, M. Suginome, *ACS Macro Lett.* **2017**, 6, 705-710.
- [9] a) D. M. Bassani, J.-M. Lehn, G. Baum, D. Fenske, *Angew. Chem. Int. Ed. Engl.* **1997**, 36, 1845-1847; b) O. Mamula, A. von Zelewsky, T. Bark, G. Bernardinelli, *Angew. Chem. Int. Ed.* **1999**, 38, 2945-2948; c) V. Berl, I. Huc, R. G. Khoury, J.-M. Lehn, *Chem. Eur. J.* **2001**, 7, 2810-2820; d) X.-M. Chen, G.-F. Liu, *Chem. Eur. J.* **2002**, 8, 4811-4817; e) Y. Tanaka, H. Katagiri, Y. Furusho, E. Yashima, *Angew. Chem. Int. Ed.* **2005**, 44, 3867-3870; f) H. Goto, H. Katagiri, Y. Furusho, E. Yashima, *J. Am. Chem. Soc.* **2006**, 128, 7176-7178; g) D. Haldar, C. Schmuck, *Chem. Soc. Rev.* **2009**, 38, 363-371; h) S. Li, C. Jia, B. Wu, Q. Luo, X. Huang, Z. Yang, Q.-S. Li, X.-J. Yang, *Angew. Chem. Int. Ed.* **2011**, 50, 5721-5724; i) B. Wu, S. Li, Y. Lei, H. Hu, N. D. S. Amadeu, C. Janiak, J. S. Mathieson, D.-L. Long, L. Cronin, X.-J. Yang, *Chem. Eur. J.* **2015**, 21, 2588-2593; j) C. Jia, W. Zuo, D. Yang, Y. Chen, L. Cao, R. Custelcean, J. Hostaš, P. Hobza, R. Glaser, Y.-Y. Wang, X.-J. Yang, B. Wu, *Nat. Commun.* **2017**, 8, 938.
- [10] a) J.-M. Lehn, A. Rigault, J. Siegel, J. Harrowfield, B. Chevrier, D. Moras, *Proc. Natl. Acad. Sci. USA* **1987**, 84, 2565-2569; b) A. Pfeil, J.-M. Lehn, *J. Chem. Soc. Chem. Commun.* **1992**, 838-840; c) B. Hasenknopf, J.-M. Lehn, G. Baum, D. Fenske, *Proc. Natl. Acad. Sci. USA* **1996**, 93, 1397-1400; d) A. Marquis-Rigault, A. Dupont-Gervais, A. Van Dorsselaer, J.-M. Lehn, *Chem. Eur. J.* **1996**, 2, 1395-1398; e) V. C. M. Smith, J.-M. Lehn, *Chem. Commun.* **1996**, 2733-2734; f) A. Marquis, V. Smith, J. Harrowfield, J.-M. Lehn, H. Herschbach, R. Sanvito, E. Leize-Wagner, A. Van Dorsselaer, *Chem. Eur. J.* **2006**, 12, 5632-5641.
- [11] a) C. A. Schalley, A. Lützen, M. Albrecht, *Chem. Eur. J.* **2004**, 10, 1072-1080; b) C. R. K. Glasson, L. F. Lindoy, G. V. Meehan, *Coord. Chem. Rev.* **2008**, 252, 940-963; c) S. E. Howson, P. Scott, *Dalton Trans.* **2011**, 40, 10268-10277; d) M. Albrecht, *Chem. Rev.* **2001**, 101, 3457-3497.
- [12] a) E. C. Constable, R. Chotalia, *J. Chem. Soc. Chem. Commun.* **1992**, 64-66; b) C. Provent, S. Hewage, G. Brand, G. Bernardinelli, L. J. Charbonnière, A. F. Williams, *Angew. Chem. Int. Ed. Engl.* **1997**, 36, 1287-1289; c) D. A. McMorran, P. J. Steel, *Angew. Chem. Int. Ed.* **1998**, 37, 3295-3297; d) C. R. Rice, S. Wörl, J. C. Jeffery, R. L. Paul, M. D. Ward, *Chem. Commun.* **2000**, 1529-1530; e) P. K. Bowyer, V. C. Cook,

- N. Gharib-Naseri, P. A. Gugger, A. D. Rae, G. F. Swiegers, A. C. Willis, J. Zank, S. B. Wild, *Proc. Natl. Acad. Sci. USA* **2002**, *99*, 4877-4882; f) V. Maurizot, G. Linti, I. Huc, *Chem. Commun.* **2004**, 924-925; g) M. Bera, G. Aromí, W. T. Wong, D. Ray, *Chem. Commun.* **2006**, 671-673; h) W. Chen, X. Tang, W. Dou, B. Wang, L. Guo, Z. Ju, W. Liu, *Chem. Eur. J.* **2017**, *23*, 9804-9811; i) S. Naskar, C. Dalal, P. Ghosh, *Chem. Commun.* **2017**, *53*, 2487-2490; j) E. C. Constable, T. Kulke, M. Neuburger, M. Zehnder, *Chem. Commun.* **1997**, 489-490; k) J. S. Fleming, K. L. V. Mann, S. M. Couchman, J. C. Jeffery, J. A. McCleverty, M. D. Ward, *J. Chem. Soc. Dalton Trans.* **1998**, 2047-2052; l) V. Amendola, L. Fabbrizzi, L. Gianelli, C. Maggi, C. Mangano, P. Pallavicini, M. Zema, *Inorg. Chem.* **2001**, *40*, 3579-3587; m) R. Annunziata, M. Benaglia, A. Famulari, L. Raimondi, *Magn. Reson. Chem.* **2001**, *39*, 341-354; n) W. Schuh, H. Kopacka, K. Wurst, P. Peringer, *Chem. Commun.* **2001**, 2186-2187.
- [13] a) B. Kersting, M. Meyer, R. E. Powers, K. N. Raymond, *J. Am. Chem. Soc.* **1996**, *118*, 7221-7222; b) B. Kersting, J. R. Telford, M. Meyer, K. N. Raymond, *J. Am. Chem. Soc.* **1996**, *118*, 5712-5721; c) D. L. Caulder, K. N. Raymond, *Angew. Chem. Int. Ed. Engl.* **1997**, *36*, 1440-1442; d) M. Meyer, B. Kersting, R. E. Powers, K. N. Raymond, *Inorg. Chem.* **1997**, *36*, 5179-5191.
- [14] E. J. Enemark, T. D. P. Stack, *Angew. Chem. Int. Ed. Engl.* **1995**, *34*, 996-998.
- [15] a) M. Albrecht, S. Kotila, *Angew. Chem. Int. Ed. Engl.* **1995**, *34*, 2134-2137; b) I. Janser, M. Albrecht, K. Hunger, S. Burk, K. Rissanen, *Eur. J. Inorg. Chem.* **2006**, 244-251; c) M. Albrecht, E. Isaak, H. Shigemitsu, V. Moha, G. Raabe, R. Fröhlich, *Dalton Trans.* **2014**, *43*, 14636-14643; d) D. Van Craen, M. Albrecht, G. Raabe, F. Pan, K. Rissanen, *Chem. Eur. J.* **2016**, *22*, 3255-3258.
- [16] a) H. V. Huynh, C. S. Isfort, W. W. Seidel, T. Lügger, R. Fröhlich, O. Kataeva, F. E. Hahn, *Chem. Eur. J.* **2002**, *8*, 1327-1335; b) F. E. Hahn, C. S. Isfort, T. Pape, *Angew. Chem. Int. Ed.* **2004**, *43*, 4807-4810; c) C. S. Isfort, T. Kreickmann, T. Pape, R. Fröhlich, F. E. Hahn, *Chem. Eur. J.* **2007**, *13*, 2344-2357; d) F. E. Hahn, M. Offermann, C. S. Isfort, T. Pape, R. Fröhlich, *Angew. Chem. Int. Ed.* **2008**, *47*, 6794-6797.
- [17] a) R. M. Yeh, M. Ziegler, D. W. Johnson, A. J. Terpin, K. N. Raymond, *Inorg. Chem.* **2001**, *40*, 2216-2217; b) R. M. Yeh, K. N. Raymond, *Inorg. Chem.* **2006**, *45*, 1130-1139.

- [18] a) D. Zare, Y. Suffren, H. Nozary, A. Hauser, C. Piguet, *Angew. Chem. Int. Ed.* **2017**, *56*, 14612-14617; b) J. L. Greenfield, F. J. Rizzuto, I. Goldberga, J. R. Nitschke, *Angew. Chem. Int. Ed.* **2017**, *56*, 7541-7545; c) F. Cui, S. Li, C. Jia, J. S. Mathieson, L. Cronin, X.-J. Yang, B. Wu, *Inorg. Chem.* **2012**, *51*, 179-187; d) U. Kiehne, T. Weilandt, A. Lützen, *Org. Lett.* **2007**, *9*, 1283-1286; e) C. J. Baylies, T. Riis-Johannessen, L. P. Harding, J. C. Jeffery, R. Moon, C. R. Rice, M. Whitehead, *Angew. Chem. Int. Ed.* **2005**, *44*, 6909-6912; f) A. Lützen, M. Hapke, J. Griep-Raming, D. Haase, W. Saak, *Angew. Chem. Int. Ed.* **2002**, *41*, 2086-2089; g) M. Greenwald, D. Wessely, E. Katz, I. Willner, Y. Cohen, *J. Org. Chem.* **2000**, *65*, 1050-1058; h) N. Fatin-Rouge, S. Blanc, E. Leize, A. Van Dorsselaer, P. Baret, J.-L. Pierre, A.-M. Albrecht-Gary, *Inorg. Chem.* **2000**, *39*, 5771-5778; i) M. Greenwald, D. Wessely, I. Goldberg, Y. Cohen, *New J. Chem.* **1999**, *23*, 337-344; j) J. J. Jodry, J. Lacour, *Chem. Eur. J.* **2000**, *6*, 4297-4304; k) G. Baum, E. C. Constable, D. Fenske, T. Kulke, *Chem. Commun.* **1997**, 2043-2044.
- [19] a) S.-Y. Chang, H.-Y. Jang, K.-S. Jeong, *Chem. Eur. J.* **2004**, *10*, 4358-4366; b) S. Freye, J. Hey, A. Torras-Galán, D. Stalke, R. Herbst-Irmer, M. John, G. H. Clever, *Angew. Chem. Int. Ed.* **2012**, *51*, 2191-2194; c) O. Gidron, M. Jirásek, M. Wörle, F. Diederich, *Chem. Eur. J.* **2016**, *22*, 16172-16177; d) W. J. Ramsay, T. K. Ronson, J. K. Clegg, J. R. Nitschke, *Angew. Chem. Int. Ed.* **2013**, *52*, 13439-13443.
- [20] T. Haino, H. Shio, R. Takano, Y. Fukazawa, *Chem. Commun.* **2009**, 2481-2483.
- [21] A. M. A. van Wageningen, E. Snip, W. Verboom, D. N. Reinhoudt, H. Boerrigter, *Liebigs Ann./Recl.* **1997**, 2235-2245.
- [22] a) S. Salama, J. D. Stong, J. B. Neilands, T. G. Spiro, *Biochemistry* **1978**, *17*, 3781-3785; b) T. B. Karpishin, M. S. Gebhard, E. I. Solomon, K. N. Raymond, *J. Am. Chem. Soc.* **1991**, *113*, 2977-2984.
- [23] a) Y. Cohen, L. Avram, L. Frish, *Angew. Chem. Int. Ed.* **2005**, *44*, 520-554; b) A. S. Altieri, D. P. Hinton, R. A. Byrd, *J. Am. Chem. Soc.* **1995**, *117*, 7566-7567.
- [24] a) L. Avram, Y. Cohen, *Chem. Soc. Rev.* **2015**, *44*, 586-602; b) A. Macchioni, G. Ciancaleoni, C. Zuccaccia, D. Zuccaccia, *Chem. Soc. Rev.* **2008**, *37*, 479-489.
- [25] a) H.-C. Chen and S.-H. Chen, *J. Phys. Chem.* **1984**, *88*, 5118-5121. b) N. D. Favera, L. Guenee, G. Bernardinelli, C. Piguet, *Dalton Trans.* **2009**, 7625-7638; c) B. M. Schulze, D. L. Watkins, J. Zhang, I. Ghiviriga, R. K. Castellano, *Org. Biomol. Chem.* **2014**, *12*, 7932-7936.

- [26] a) F. Mohamadi, N. G. J. Richards, W. C. Guida, R. Liskamp, M. Lipton, C. Caufield, G. Chang, T. Hendrickson, W. C. Still, *J. Comput. Chem.* **1990**, *11*, 440-467; b) S. J. Weiner, P. A. Kollman, D. A. Case, U. C. Singh, C. Ghio, G. Alagona, S. Profeta, Jr., P. Weiner, *J. Am. Chem. Soc.* **1984**, *106*, 765-784.
- [27] a) M. Albrecht, S. Mirtschin, M. de Groot, I. Janser, J. Runsink, G. Raabe, M. Kogej, C. A. Schalley, R. Fröhlich, *J. Am. Chem. Soc.* **2005**, *127*, 10371-10387; b) A. Marquis-Rigault, A. Dupont-Gervais, P. N. W. Baxter, A. Van Dorsselaer, J.-M. Lehn, *Inorg. Chem.* **1996**, *35*, 2307-2310.
- [28] I. Kolossváry, W. C. Guida, *J. Am. Chem. Soc.* **1996**, *118*, 5011-5019.
- [29] a) A. Braibanti, G. Ostacoli, P. Paoletti, L. D. Pettit, S. Sammartano, *Pure Appl. Chem.* **1987**, *59*, 1721-1728; b) K. A. Connors, *Binding Constants: The Measurements of Molecular Complex Stability*, Wiley, New York, **1987**; c) P. Gans, A. Sabatini, A. Vacca, *Talanta* **1996**, *43*, 1739-1753; d) P. Gans, A. Sabatini, A. Vacca, *Ann. Chim.* **1999**, *89*, 45-49.
- [30] a) H. J. Hogben, J. K. Sprafke, M. Hoffmann, M. Pawlicki, H. L. Anderson, *J. Am. Chem. Soc.* **2011**, *133*, 20962-20969; b) C.-H. Lee, H. Yoon, P. Kim, S. Cho, D. Kim, W.-D. Jang, *Chem. Commun.* **2011**, *47*, 4246-4248; c) J. Wang, D.-T. Pham, T. W. Kee, S. N. Clifton, X. Guo, P. Clements, S. F. Lincoln, R. K. Prud'homme, C. J. Easton, *Macromolecules* **2011**, *44*, 9782-9791; d) S. Brahma, S. A. Iqbal, A. Dhamija, S. P. Rath, *Inorg. Chem.* **2014**, *53*, 2381-2395; e) D. Shimoyama, H. Yamada, T. Ikeda, R. Sekiya, T. Haino, *Eur. J. Org. Chem.* **2016**, 3300-3303; f) P. Mondal, S. Sarkar, S. P. Rath, *Chem. Eur. J.* **2017**, *23*, 7093-7103; g) L. K. S. von Krbek, A. J. Achazi, S. Schoder, M. Gaedke, T. Biberger, B. Paulus, C. A. Schalley, *Chem. Eur. J.* **2017**, *23*, 2877-2883; h) Y.-L. Ma, H. Ke, A. Valkonen, K. Rissanen, W. Jiang, *Angew. Chem. Int. Ed.* **2018**, *57*, 709-713.
- [31] T. B. Karpishin, T. D. P. Stack, K. N. Raymond, *J. Am. Chem. Soc.* **1993**, *115*, 6115-6125.
- [32] a) J. van Gestel, *Macromolecules* **2004**, *37*, 3894-3898; b) J. van Gestel, *J. Phys. Chem. B* **2006**, *110*, 4365-4370.
- [33] a) M. M. Green, J.-W. Park, T. Sato, A. Teramoto, S. Lifson, R. L. B. Selinger, J. V. Selinger, *Angew. Chem. Int. Ed.* **1999**, *38*, 3138-3154; b) A. R. A. Palmans, E. W. Meijer, *Angew. Chem. Int. Ed.* **2007**, *46*, 8948-8968.

- [34] a) M. M. Green, N. C. Peterson, T. Sato, A. Teramoto, R. Cook, S. Lifson, *Science* **1995**, *268*, 1860-1866; b) R. Nonokawa, E. Yashima, *J. Am. Chem. Soc.* **2003**, *125*, 1278-1283; c) B. Isare, M. Linares, L. Zargarian, S. Femandjian, M. Miura, S. Motohashi, N. Vanthuynne, R. Lazzaroni, L. Bouteiller, *Chem. Eur. J.* **2010**, *16*, 173-177; d) M. M. J. Smulders, I. A. W. Filot, J. M. A. Leenders, P. van der Schoot, A. R. A. Palmans, A. P. H. J. Schenning, E. W. Meijer, *J. Am. Chem. Soc.* **2010**, *132*, 611-619; e) T. Kim, T. Mori, T. Aida, D. Miyajima, *Chem. Sci.* **2016**, *7*, 6689-6694; f) Y. Tsunoda, M. Takatsuka, R. Sekiya, T. Haino, *Angew. Chem. Int. Ed.* **2017**, *56*, 2613-2618.

Acknowledgements

The author is especially grateful to Professor Takeharu Haino, Hiroshima University, for his helpful guidance, constructive discussion, encouragement, and full support of the present study.

The author expresses sincere gratitude to Associate Professor Ryo Sekiya, Hiroshima University, for his helpful instruction, general discussion, encouragement, and full support of the present study.

The author is grateful to Assistant Professor Toshiaki Ikeda, Tokai University, for his helpful instruction, advice, encouragement, kind support, and suggestion of the present study.

The author is grateful to Assistant Professor Takehiro Hirao, Hiroshima University, for his helpful instruction, advice, encouragement, and suggestion of the present study.

The author is grateful to Prof. Takayuki Ichikawa, Advanced Materials Division, the Natural Science Center for Basic Research and Development (N-BARD), Hiroshima University, for their kind permission to measure and analyze the adsorption-desorption isotherm of apohost in chapter 2 of this work.

The author is grateful to Ms. Tomoko Amimoto, N-BARD, Hiroshima University, for the measurement of MS spectra and discussion of measurement.

The author is grateful to Ms. Naomi Kawata, N-BARD, Hiroshima University, for the measurement of single-crystal XRD analysis and discussion of measurement.

The author thanks Mr. Hitoshi Fujitaka, N-BARD, Hiroshima University, for the measurement of NMR spectra.

The author thanks Dr. Makoto Maeda, N-BARD, Hiroshima University, for the measurement of Scanning Electron Microscopy.

The author thanks Dr. Yutaka Mouri, N-BARD, Hiroshima University, for the measurement of elemental analysis.

The author thanks Dr. Yasunori Kajiki, Mr. Tetsuya Masuda, Mr. Tatsuya Iijima, Ms. Yuko Ueda, Mr. Yoshinori Oi, Mr. Susumu Katayama, Ms. Yuko Hirai, Mr. Kanashi Kinjo, Ms. Midori Takayama, Ms. Kaori Misaka, Ms. Hitomi Yamada, Mr. Taisuke Imamura, Mr. Wataru Tada, Mr. Yuta Tsunoda, Mr. Masaru Hirano, Mr. Yusuke Morisaka, Mr. Hiroaki Adachi, Mr. Yuichiro Uemura, Mr. Yu Sasaki, Mr. Kohei Nadamoto, Mr. Hiroaki Kudo, Mr. Daisuke Shimoyama, Ms. Kaho Suzuki, Ms. Mei Takatsuka, Mr. Kyohei

Hirano, Mr. Xiaosheng Liang, Mr. Shun Kohno, Mr. Takeshi Maehara, Mr. Kei Maruyama, Ms. Mai Sota, Ms. Natsumi Nitta, Mr. Naoyuki Hisano, Ms. Mahoko Hiyoshi, Mr. Kairi Yamato, Mr. Lai Nang Duy, Mr. Yoshiki Iwabe, Mr. Shohei Nishitani, Ms. Naoka Fujii, Ms. Haruna Fujimoto, Mr. Atsushi Oyama, Mr. Yudai Ono, Mr. Kentaro Harada, Mr. Satoshi Fukuta, Organic Stereochemistry Groups of Hiroshima University, for their support through this work.

Finally, the author thanks those not specially mentioned who contributed to this work.

**Molecular Recognition of Supramolecular
Assemblies Based on Calix[4]arenes.**

Department of Chemistry, Graduate School of Science

Hiroshima University

January, 2019

Yutaro Yamasaki

公表論文

- (1) Hexameric Assembly of 5,17-Di-Substituted Calix[4]arene in the Solid State.

Yutaro Yamasaki, Ryo Sekiya, and Takeharu Haino.

CrystEngComm **2017**, *19*, 6744-6751.

- (2) Majority-Rules Effect and Allostery in Molecular Recognition of Calix[4]arene-Based Triple-Stranded Metallohelicates.

Yutaro Yamasaki, Hidemi Shio, Tomoko Amimoto, Ryo Sekiya, and Takeharu Haino.

Chemistry – A European Journal **2018**, *24*, 8558-8568.

参考論文

- (1) Head-to-tail Polymeric Columnar Structure of Calix[4]arene Possessing Catechol Arms in the Solid State.
Ryo Sekiya, Yutaro Yamasaki, Susumu Katayama, Hidemi Shio, and Takeharu Haino.
CrystEngComm **2013**, 15, 8404-8407.

- (2) Guest induced head-to-tail columnar assembly of 5,17-Difunctionalized Calix[4]arene.
Ryo Sekiya, Yutaro Yamasaki, Wataru Tada, Hidemi Shio, and Takeharu Haino.
CrystEngComm **2014**, 16, 6023-6032.

- (3) Induced-Fit Molecular Recognition of Alkyl Chains in *p*-*tert*-Butylcalix[5]arene in the Solid State.
Yasunori Kajiki, Ryo Sekiya, Yutaro Yamasaki, Yuichiro Uemura, and Takeharu Haino.
Bulletin of the Chemical Society of Japan **2016**, 89, 220-225.

